



Role of CD4⁺ T lymphocytes in cardiac wound healing and remodeling after experimental myocardial infarction in mice

Die Bedeutung von CD4⁺ T-Lymphozyten für die kardiale Wundheilung und Remodeling nach experimentellem Herzinfarkt im Mausmodell

Doctoral thesis for a doctoral degree
at the Graduate School of Life Sciences,
Julius-Maximilians-Universität Würzburg,
Section Infection and Immunity

submitted by

Johannes Weirather

from

Memmingen

Würzburg, 2014



Submitted on:

Office stamp

Members of the *Promotionskomitee*:

Chairperson: Prof. Dr. Thomas Hünig

Primary Supervisor: Prof. Dr. Stefan Frantz

Supervisor (Second): PD Dr. Ingolf Berberich

Supervisor (Third): PD Dr. Thomas Kerkau

Date of Public Defence:

Date of Receipt of Certificates:

Table of contents

1	Summary	1
2	Zusammenfassung	3
3	Introduction	5
3.1	Innate immunity	5
3.2	Adaptive immunity	6
3.2.1	Development of CD4 ⁺ and CD8 ⁺ αβ T lymphocytes	6
3.2.2	Antigen-presenting cells and T cell activation	8
3.2.3	T cell subsets	11
3.2.3.1	Conventional T cells	11
3.2.3.2	Regulatory CD4 ⁺ T cells	13
3.2.3.2.1	Development of thymus-derived Foxp3 ⁺ T _{reg} cells	13
3.2.3.2.2	Forkhead box protein 3 (Foxp3)	14
3.2.3.2.3	Induced regulatory CD4 ⁺ T cells	15
3.2.3.2.4	Immuno-regulation by T _{reg} cells	16
3.3	Postinfarction healing and remodeling	18
3.3.1	The relevance of innate immunity in wound healing after MI	19
3.3.1.1	Neutrophils	19
3.3.1.2	Mononuclear cells	20
3.3.1.2.1	Monocytes	21
3.3.1.2.2	Macrophages	22
3.3.2	Activation of adaptive immunity after MI	23
3.4	Aim of the study	26
4	Methods and Materials	27
4.1	Materials	27
4.1.1	Fine chemicals and reagents	27
4.1.2	Antibodies	28
4.1.3	Buffers and solutions	29
4.1.4	Ready for use kits and solutions	31
4.1.5	TaqMan probes	32
4.1.6	Antibodies, ligands, and fine chemicals for cell culture	32
4.1.7	Enzymes	33
4.1.8	Animals	33
4.1.9	Consumables	33
4.1.10	Instruments	34
4.1.11	Electronic data processing	35
4.2	Methods	36
4.2.1	<i>In vivo</i> experiments	36
4.2.1.1	Surgeries	36
4.2.1.2	T _{reg} cell depletion in DEREK mice	36
4.2.1.3	Antibody-mediated depletion of Foxp3 ⁺ CD4 ⁺ T _{reg} cells	36
4.2.1.4	T _{reg} cell activation <i>in vivo</i>	37
4.2.1.5	IL-2/ anti-IL-2 monoclonal antibody (mAb) complex treatment	37
4.2.1.6	Echocardiography	37
4.2.2	Organ preparation	38
4.2.3	Cell culture	39

4.2.4	Immunological methods.....	39
4.2.4.1	Flow cytometry.....	39
4.2.4.2	Fluorescence-activated cell sorting (FACS).....	40
4.2.4.3	Enzyme-linked Immunosorbent Assay (ELISA).....	40
4.2.4.4	Magnetic cell separation (MACS).....	41
4.2.5	Molecular biology.....	41
4.2.5.1	RNA isolation.....	41
4.2.5.2	RNA quantification.....	42
4.2.5.2.1	Fluorometric RNA quantification.....	42
4.2.5.2.2	Bioanalyzer measurement.....	42
4.2.5.3	DNA digestion.....	42
4.2.5.4	Reverse transcription of RNA.....	42
4.2.5.5	Real-time (RT) polymerase chain reaction (PCR).....	43
4.2.5.6	RNA <i>in vitro</i> transcription.....	44
4.2.6	Protein biochemistry.....	45
4.2.6.1	Protein extraction and assessment of protein concentration.....	45
4.2.6.2	Electrophoretic protein separation (SDS-PAGE).....	45
4.2.6.3	Sample preparation for SDS-PAGE.....	46
4.2.6.4	Western blot and protein detection.....	46
4.2.6.5	Membrane stripping.....	47
4.2.7	Optical imaging.....	47
4.2.7.1	Immuno-/ histochemical stainings on paraffin sections.....	47
4.2.7.1.1	Preparation of paraffin sections.....	47
4.2.7.1.2	Picrosirius red staining.....	48
4.2.7.1.3	Ladewig staining.....	48
4.2.7.1.4	Alpha smooth muscle actin staining.....	48
4.2.7.2	Immunofluorescence staining of Foxp3.....	49
4.2.7.3	Image acquisition.....	49
4.2.8	Infarct size determination.....	49
4.2.9	Evaluation of collagen content in the scar.....	50
4.2.10	Statistics.....	50
5	Results.....	51
5.1	Both conventional and Foxp3 ⁺ regulatory CD4 ⁺ T lymphocytes become activated in response to MI.....	51
5.2	CD4 ⁺ T Lymphocytes infiltrate the myocardium after MI.....	53
5.3	Survival and wound healing are impaired in MHC class II-deficient mice.....	54
5.4	Survival and wound healing are impaired in OT-II mice.....	56
5.5	Activation of conventional and regulatory CD4 ⁺ T cells in response to MI depends on antigen recognition.....	58
5.6	Specific diphtheria toxin-induced T _{reg} cell ablation in DEREK mice leads to increased infarct size and deteriorated cardiac function.....	59
5.7	T _{reg} cell ablation in DEREK mice leads to an accumulation of both inflammatory myeloid and T cells in the infarct zone.....	63
5.8	Anti-CD25 antibody-mediated T _{reg} cell depletion prior to MI leads to impaired survival, aggravated remodeling and increased recruitment of inflammatory myeloid cells.....	67

5.9	CD28-SA administration leads to enhanced T _{reg} cell recruitment into the infarct zone, associated with increased survival and improved scar tissue formation	70
5.10	Therapeutic T _{reg} cell activation induces an M2-like macrophage polarization in the healing myocardium.....	76
5.11	T _{reg} cell-derived cytokines drive M2 polarization in monocytic cells <i>in vitro</i>	78
5.12	Therapeutic T _{reg} cell activation by IL-2/ anti-IL-2 monoclonal antibody complexes provokes M2-like macrophage differentiation and accelerates scar tissue formation	83
6	Discussion	86
6.1	Antigen-dependant CD4 ⁺ T cell activation post-MI	86
6.2	CD4 ⁺ T cells facilitate healing post-MI	88
6.3	T _{reg} cell depletion deteriorates postinfarction healing due to an impaired macrophage M2 polarization.....	89
6.4	Therapeutic T _{reg} cell activation improves postinfarction wound healing by enhancing an M2-like macrophage polarization	92
6.5	Molecular mediators improving wound healing after therapeutic T _{reg} cell activation	94
6.6	Implications for the treatment of patients with MI.....	95
7	References	98
8	Appendix	116
8.1	Abbreviations.....	116
8.2	Acknowledgements.....	118
8.3	Publications	119
8.4	Oral presentations	120
8.5	Poster presentations.....	120
8.6	<i>Curriculum Vitae</i>	121
8.7	Affidavit.....	122

1 Summary

Cardiac healing after myocardial infarction (MI) represents the cardinal prerequisite for proper replacement of the irreversibly injured myocardium. In contrast to innate immunity, the functional role of adaptive immunity in postinfarction healing has not been systematically addressed. The present study focused on the influence of CD4⁺ T lymphocytes on wound healing and cardiac remodeling after experimental myocardial infarction in mice. Both conventional and Foxp3⁺ regulatory CD4⁺ T cells (T_{reg} cells) became activated in heart draining lymph nodes after MI and accumulated in the infarcted myocardium. T cell activation was strictly antigen-dependant as T cell receptor-transgenic OT-II mice in which CD4⁺ T cells exhibit a highly limited T cell receptor repertoire did not expand in heart-draining lymph nodes post-MI. Both OT-II and major histocompatibility complex class II-deficient mice lacking a CD4⁺ T cell compartment showed a fatal clinical postinfarction outcome characterized by disturbed scar tissue construction that resulted in impaired survival due to a prevalence of left-ventricular ruptures.

To assess the contribution of anti-inflammatory T_{reg} cells on wound healing after MI, the T_{reg} cell compartment was depleted using DEREK mice that specifically express the human diphtheria toxin receptor in Foxp3-positive cells, resulting in T_{reg} cell ablation after diphtheria toxin administration. In a parallel line of experiments, a second model of anti-CD25 antibody-mediated T_{reg} cell immuno-depletion was used. T_{reg} cell ablation prior to MI resulted in adverse postinfarction left-ventricular dilatation associated with cardiac deterioration. Mechanistically, T_{reg} cell depletion resulted in an increased recruitment of pro-inflammatory neutrophils and Ly-6C^{high} monocytes into the healing myocardium. Furthermore, T_{reg} cell-ablated mice exhibited an adverse activation of conventional non-regulatory CD4⁺ and CD8⁺ T cells that showed a reinforced infiltration into the infarct zone. Increased synthesis of TNF α and IFN γ by conventional CD4⁺ and CD8⁺ T cells in hearts of T_{reg} cell-depleted mice provoked an M1-like macrophage polarization characterized by heightened expression of healing-compromising induced NO synthase, in line with a reduced synthesis of healing-promoting transglutaminase factor XIII (FXIII), osteopontin (OPN) and transforming growth factor beta 1 (TGF β 1).

Therapeutic T_{reg} cell activation by a superagonistic anti-CD28 monoclonal antibody stimulated T_{reg} cell accumulation in the infarct zone and led to an increased

expression of mediators inducing an M2-like macrophage polarization state, i.e. interleukin-10, interleukin-13 and TGF β 1. M2-like macrophage differentiation in the healing infarct was associated with heightened expression of scar-forming pro-collagens as well as scar-stabilizing FXIII and OPN, resulting in improved survival due to a reduced incidence of left-ventricular ruptures. Therapeutic T_{reg} cell activation and the induction of a beneficial M2-like macrophage polarization was further achieved by employing a treatment modality of high clinical potential, i.e. by therapeutic administration of IL-2/ anti-IL-2 monoclonal antibody complexes. The findings of the present study suggest that therapeutic T_{reg} cell activation and the resulting improvement of healing may represent a suitable strategy to attenuate adverse infarct expansion, left-ventricular remodeling, or infarct ruptures in patients with MI.

2 Zusammenfassung

Die kardiale Wundheilung nach einem Herzinfarkt ist unabdingbare Voraussetzung um das unwideruflich beschädigte Myokard zu ersetzen. Im Gegensatz zur Rolle der angeborenen Immunität ist zur Bedeutung der adaptiven Immunität für die kardiale Wundheilung nur wenig bekannt. Im Fokus der Studie stand deshalb die Rolle von CD4⁺ T-Zellen bei der Wundheilung und kardialem Remodeling nach einem experimentellen Herzinfarkt im Mausmodell. Sowohl konventionelle, als auch Foxp3-positive regulatorische CD4⁺ T Zellen (T_{reg}-Zellen) wurden im Lymphknoten infarzierter Tiere aktiviert und akkumulierten im Infarktareal. Die Aktivierung von CD4⁺ T Zellen nach MI setzte die Erkennung von Selbstantigenen voraus, da OT-II Tiere, die ein stark eingeschränktes T-Zell-Rezeptor-Repertoire aufweisen, keine T-Zell-Aktivierung zeigten. Sowohl OT-II Tiere, als auch Haupthistokompatibilitätskomplex Klasse II Knock-out Mäuse, die kein CD4⁺ T-Zell Kompartiment aufweisen, zeigten einen fatalen klinischen Phänotyp, welcher durch eine gestörte Narbenbildung und damit verbunden einem verstärkten Auftreten linksventrikulärer Rupturen verbunden war.

Um den Einfluss anti-inflammatorischer T_{reg}-Zellen auf die kardiale Wundheilung nach Herzinfarkt zu untersuchen, wurde das T_{reg}-Zell Kompartiment vor MI Induktion depletiert. Hierzu wurden DEREK Mäuse verwendet, in denen Foxp3-positive Zellen den humanen Diphtherietoxin-Rezeptor exprimieren, sodass nach nach Diphterietoxin-Applikation die T_{reg}-Zellen spezifisch depletiert werden. In einer dazu parallel verlaufenden Versuchsreihe wurden die T_{reg}-Zellen mittels anti-CD25 monoklonaler Antikörper depletiert. Die Depletion des T_{reg}-Zell Kompartiments 2 Tage vor MI Induktion bewirkte ein verschlechtertes links-ventrikuläres Remodeling und damit einhergehend eine signifikante Verschlechterung der Herzfunktion. Mechanistisch führte die T_{reg}-Zell Depletion zu einer verstärkten Rekrutierung pro-inflammatorischer Ly-6C^{high} Monozyten und neutrophilen Granulozyten ins Infarktareal. Die Depletion von T_{reg}-Zellen war weiterhin mit einer adversen Aktivierung konventioneller CD4⁺ und CD8⁺ T-Zellen assoziiert, die eine verstärkte Infiltration ins infarzierte Myokard zeigten. Die erhöhte Synthese von TNF α und IFN γ in konventionellen T-Zellen führte zu einer M1-Makrophagen Polarisierung, welche durch eine verstärkte Expression der induzierbaren NO Synthase charakterisiert war. Weiterhin exprimierten diese M1 Makrophagen signifikant weniger der für eine

geordnete Heilung essentiellen Faktoren Osteopontin, Transglutaminase Faktor XIII und *transforming growth factor beta 1* (TGF β 1).

Im Gegensatz zu den Depletionsversuchen führte die therapeutische Aktivierung der T_{reg}-Zellen durch einen superagonistischen anti-CD28 monoklonalen Antikörper zu einer verstärkten Rekrutierung von T_{reg}-Zellen ins Infarktareal und bewirkte eine erhöhte Synthese von Interleukin (IL)-10, IL-13 sowie TGF β 1. Die damit einhergehende M2 Makrophagenpolarisierung im Infarktareal war mit einer verstärkten Narbenbildung sowie der Synthese von Osteopontin und Transglutaminase Faktor XIII verbunden, welche sich stabilisierend auf die Narbenbildung auswirken. Folgerichtig zeigten die behandelten Tiere ein verbessertes Überleben aufgrund einer signifikant verringerten Inzidenz linksventrikulärer Rupturen. Alternativ zum superagonistischen anti-CD28 monoklonalen Antikörper wurde ein weiterer klinisch relevanter Ansatz zur therapeutischen Aktivierung von T_{reg}-Zellen verfolgt. Durch die Applikation von IL-2/anti-IL-2 Antikörper-Komplexen konnte ebenfalls eine M2 Makrophagenpolarisierung hervorgerufen werden, die mit einer verstärkten Narbenbildung einherging. Die Ergebnisse der vorliegenden Studie deuten darauf hin, dass eine therapeutische Aktivierung von T_{reg}-Zellen bei Infarktpatienten und die dadurch hervorgerufene Verbesserung der Wundheilung potentiell einen geeigneten Ansatz darstellt, durch welchen adverses linksventrikuläres Remodeling sowie Infarktrupturen verhindert werden können.

3 Introduction

Myocardial infarction (MI) is an acute, life-threatening event and represents one of the most frequent causes of morbidity and mortality in the industrial nations. The disease accounts for 30% of deaths worldwide and costs global economy estimated U.S. \$863 billion per year¹. In most instances of ischemic cardiac injury, thrombus formation after rupture of a vulnerable atherosclerotic plaque causes the occlusion of a coronary artery. The interruption of blood supply to a part of the heart muscle that is feeded by the obstructed vessel leads to oxygen deprivation and, subsequently, acute MI characterized by necrosis of cardiac-resident cells such as parenchymal cardiomyocytes, endothelial cells, and fibroblasts^{2, 3}. In order to restore blood flow, most cases of MI are treated by reperfusion therapy, i.e. by percutaneous coronary intervention or pharmacological thrombus lysis⁴. However, MI inflicts a wound to the heart and the perishing cells release signals that activate the host's immune system to initiate postinfarction cardiac healing involving inflammatory and anti-inflammatory reactions⁵. The quality of cardiac wound healing and therefore postinfarction clinical outcome is pivotally influenced by the host's immune system that facilitates cell debris clearance in the infarct zone and replacement of the irreversibly injured myocardium by a solid scar. Immunity has originally evolved as a defence system comprising different organs, cell types and molecules that protect the body from disease. Aside of its role in pathogen elimination and healing, the system is able to prevent malignancies, but is also involved in the rejection of allografts⁶. Generally, the immune system is subdivided into two major branches, i.e. innate and adaptive immunity⁶.

3.1 Innate immunity

Mechanical barriers like epithelial cells or soluble factors such as the complement system constitute a first line of defence against invading pathogens. Myeloid cells comprising monocytes, macrophages, dendritic cells, NK cells as well as neutrophilic, basophilic and eosinophilic granulocytes represent the cellular components of the innate immune system⁷. Bearing germline-encoded receptors (pathogen recognition receptors, PRRs), the cells are capable of sensing pathogen-derived molecular patterns (PAMPs) that, after engagement, provoke active germ elimination by the

means of pathogen phagocytosis or the secretion of toxic granules⁸. A cardinal task of innate immune cells is to trigger inflammation by the release of pro-inflammatory mediators⁶. Furthermore, macrophages and dendritic cells are able to present antigens on major histocompatibility complexes (MHC) which constitutes a prerequisite for T cell activation (“priming”) in terms of an adaptive immune response⁶. Aside of pathogen elimination, innate immune cells play a dominant role in wound healing processes such as during scar tissue construction in the infarcted myocardium. Danger-associated molecular patterns (DAMPs) released from injured tissues are capable of engaging PRRs⁹. Activated innate immune cells contribute substantially to healing by cell debris clearance, and by the secretion of growth factors and cytokines involved in orchestrating the reparative response¹⁰.

3.2 Adaptive immunity

In addition to innate immunity, an adaptive immune system has evolved in higher vertebrates comprising cellular and humoral effectors⁷. T and B lymphocytes represent the cellular components arising from lymphoid progenitor cells in the bone marrow, and antibodies secreted from B cell-derived plasma cells mediate humoral immune reactions. In contrast to innate immunity, an adaptive immune response mounts slow, imprints an immunological memory and is highly specific due to the principle of clonal selection. T and B cells bear an individual antigen receptor (T cell receptor, TCR and B cell receptor, BCR) generated by random somatic recombination of receptor encoding gene segments. Cells that encounter their cognate antigen during an immune response become activated and expand in a clonal fashion ensuring an efficient and highly specific immune reaction⁷.

3.2.1 Development of CD4⁺ and CD8⁺ αβ T lymphocytes

T cells originate from hematopoietic stem cells (HSCs) residing in specialized bone marrow niches. HSC-derived lymphoid progenitors leave the bone marrow, populate the cortex of the thymus and expand by cellular division to generate a large pool of immature thymocytes¹¹. In the double-negative (DN) CD4⁻CD8⁻ developmental stage, thymocytes start rearranging TCR gene segments at the DNA level characterized by somatic recombination of V- and J-segments, or, V-, D- and J-segments encoding the TCR alpha (α) or beta (β) chain, respectively. Successful recombination of the

TCR beta chain results in expression and formation of a pre-TCR composed of the “rearranged” beta chain and a surrogate TCR alpha chain. In the subsequent double-positive (DP) CD4⁺CD8⁺ stage, successful somatic recombination is completed by formation of a mature, heterodimeric $\alpha\beta$ TCR¹¹. Individual recombination in each T cell generates a highly diverse TCR repertoire comprising both non-functional or potentially autoreactive receptors. A two-stage selection process ensures that only functional T cells without specificity for self-antigens exit the thymus. Migrating from the cortex to the thymic medulla, thymocytes interact with macrophages, dendritic cells, cortical thymic epithelial cells (cTECs) and medullary thymic epithelial cells (mTECs) presenting self-peptides loaded on MHC molecules¹¹. T cells bearing a low affinity TCR for the peptide-MHC complexes receive survival signals resulting in positive selection. T cells which are not capable of interacting with peptide-MHC complexes die by apoptosis due to a lack of TCR engagement. However, a fraction of cells that bear a TCR of intermediate self-reactivity develops into so-called naturally occurring Foxp3⁺ regulatory CD4⁺ T cells¹².

Positive selection accounts for MHC-restricted antigen recognition and therefore T cell lineage commitment¹¹. Thymocytes recognizing peptide-MHC I complexes develop into CD8⁺ cytotoxic T cells, whereas positive selection in the context of MHC class II results in commitment to the CD4⁺ helper T cell lineage. The subsequent process of negative selection assures deletion of potentially harmful auto-reactive cells from the selected repertoire¹³. Medullary thymic epithelial cells are capable of presenting tissue-restricted antigens expressed in specialized peripheral tissues such as insulin-derived peptides from the pancreas (Fig. 1). T cells that bear a TCR reactive for the presented self-antigens die by apoptosis^{13, 14}. However, as central tolerance is not perfect, peripheral tolerance mechanisms have evolved, e.g. peripheral immuno-suppression by regulatory cells¹⁴.

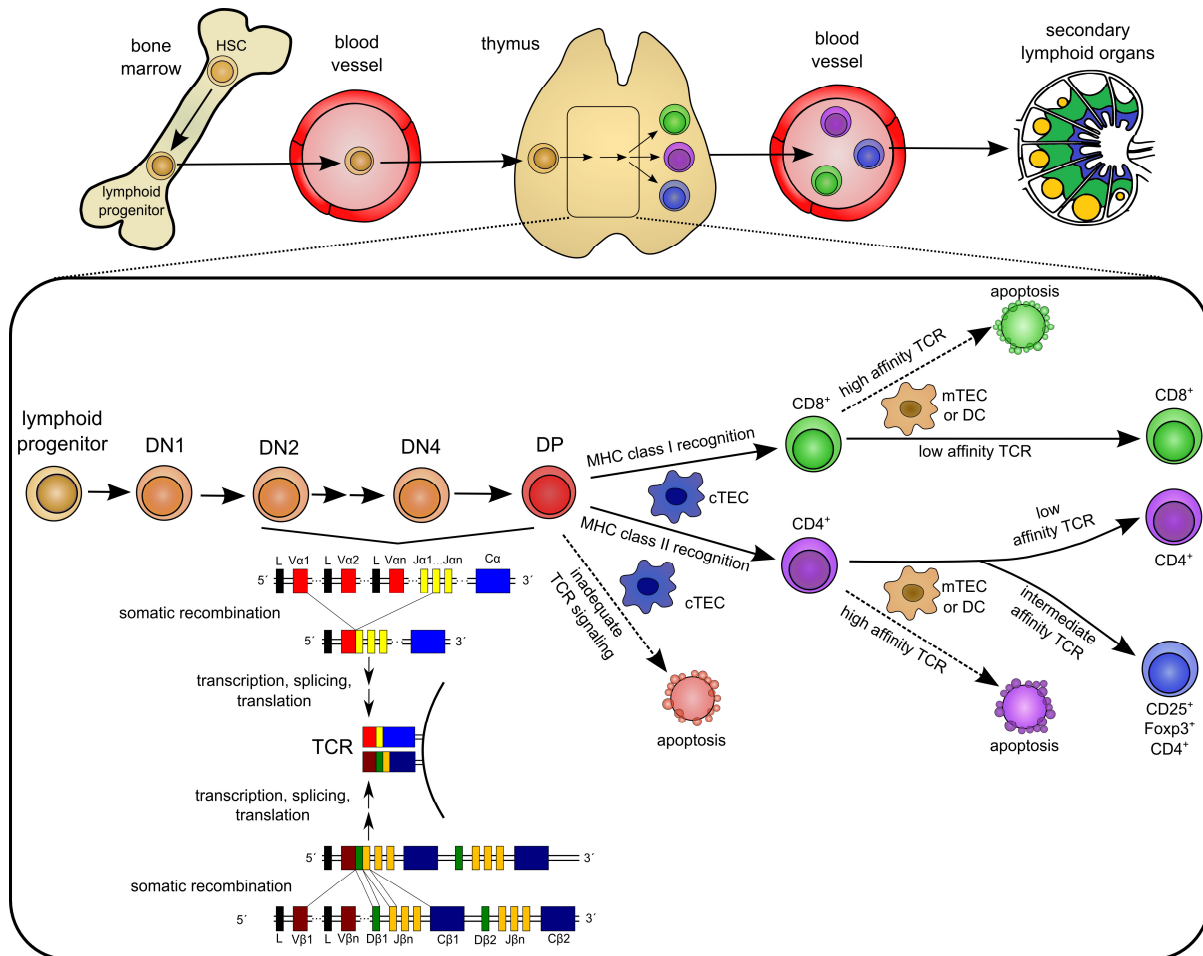


Fig. 1: Development of $\alpha\beta$ T cells. Lymphoid progenitors originating from the hematopoietic stem cells (HSC) seed the thymus and undergo somatic recombination of TCR gene segments at the double-negative (DN) stage. Successful rearrangement of V-J and V-D-J segments results in expression of a functional TCR. Thymocytes bearing a functional TCR recognize self-peptides in the context of major histocompatibility complex (MHC) class I or class II on cortical thymic epithelial cells (cTECs) and become positively selected towards $CD8^+$ or $CD4^+$ T cells. Thymocytes bearing non-functional TCRs undergo apoptosis (“death by neglect”). During subsequent negative selection, T cells interact with medullary thymic epithelial cells (mTECs) or dendritic cells (DCs). Thymocytes bearing highly reactive TCRs undergo apoptosis whereas TCRs of low affinity induce weak signaling promoting further positive selection. A small subset of $CD4^+$ cells experience intermediate signals and develop into $CD25^+Foxp3^+$ regulatory T cells. Mature T cells exit the thymus and circulate freely in the lymphoid system. The content of the figure is based on (11, 12, 13, 14).

3.2.2 Antigen-presenting cells and T cell activation

T cell activation takes place in secondary lymphoid organs such as the lymph node⁷. The cells enter the organ via high endothelial venules or the afferent lymphatics and interact with professional antigen-presenting cells (APCs) that display antigens on their surface^{15, 16}. Professional APCs comprise dendritic cells (DCs), monocytes, macrophages and B cells⁷. After phagocytosis or pinocytosis-mediated antigen internalization, APCs degrade the antigen in acidic lysosomes and present the antigen-derived peptides on both MHC class I (“cross-presentation”) and MHC class

II molecules^{17, 18}. Intracellular antigens such as peptides derived from host proteins or intracellular pathogens are presented on MHC class I^{17, 19}. The entity of all MHC antigens is termed H-2 antigen in mice, and human leukocyte antigen in men. An individual's MHC repertoire is polygenic comprising multiple genes that are co-dominantly expressed from both chromosomes²⁰. MHC alleles in a population are highly polymorphic, i.e. diversely varying from individual to individual within a certain species^{6, 20}.

T cell priming requires TCR ligation by the cognate peptide-MHC complex and CD28 co-stimulation by B7 molecules that are upregulated on the surface of activated APCs^{21, 22}. The activation of APCs results from an engagement of pathogen recognition receptors such as Toll-like receptors by pathogen- or danger associated molecular patterns. After T cell priming, conventional non-regulatory T cells secrete significant amounts of interleukin-2 (IL-2) that represents a central T cell growth and differentiation factor²³. Activated T cells upregulate their IL-2 receptor alpha chain (CD25) to further increase their receptor affinity for the ligand²⁴. Eventually, differentiated effector T cells leave the lymph node via efferent lymphatics and home to inflammatory sites where they exert specific effector functions⁷ (Fig. 2).

Due to their potency to express high levels of MHC and co-stimulatory B7 molecules on their surface, DCs represent likely the most important APCs. Generally, three DC subgroups can be distinguished, i.e. monocyte-derived DCs (mDCs), conventional DCs (cDC) and plasmacytoid DCs (pDC)²⁵. Both cDC and pDC reside in lymphoid and non-lymphoid peripheral tissues and originate from a common DC precursor in the bone marrow^{26, 27}. In contrast, mDCs differentiate from blood monocytes that significantly potentiate their immunogenic capacity in presence of lipopolysaccharide, or gram-negative bacteria²⁸. Lymphoid-resident DCs reside in secondary lymphoid organs and capture antigens from the lymph²⁶, whereas tissue-resident DCs migrate actively to the draining lymph nodes to present the sampled antigens²⁶. However, the other professional APCs are also able to activate T cells. In analogy to DCs, lymphoid-resident macrophages are distinguished from tissue-resident macrophages with migratory capacity^{29, 30 26}. Monocytes and B cells circulate freely in the blood and the lymphatic system. To interact with T cells, monocytes and B cells enter secondary lymphoid organs via high endothelial venules, or afferent lymphatic vessels^{31, 32}.

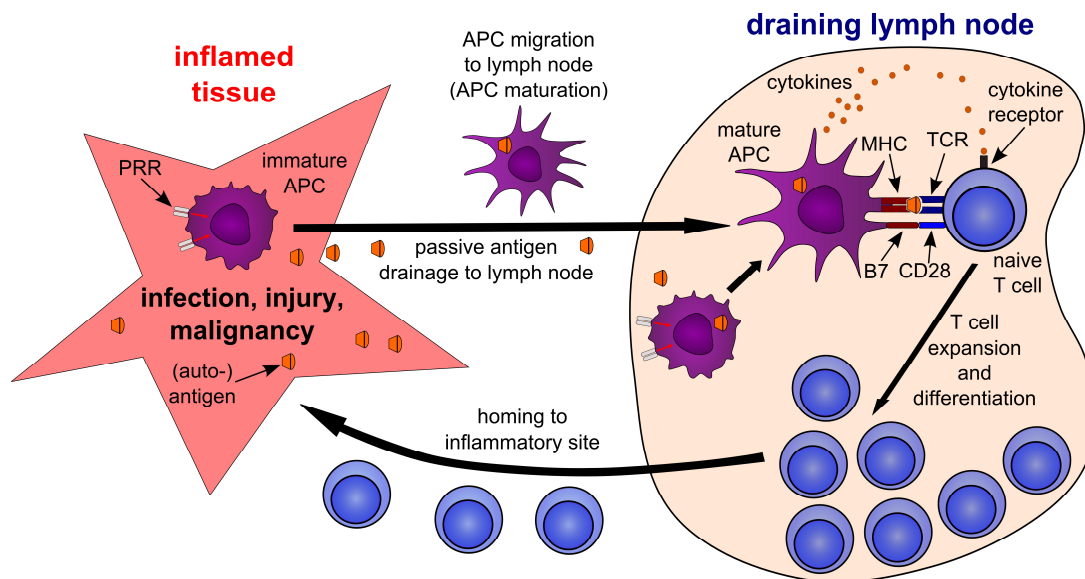


Fig. 2: T cell activation in secondary lymphoid organs. Tissue-resident and lymphoid-resident APCs continuously sample and present foreign as well as self-antigens on MHC molecules. Engagement of PRRs by DAMPs or PAMPs in terms of inflammation results in APC activation characterized by an upregulation of costimulatory and accessory molecules such as B7. Peptide-MHC recognition via cognate TCRs on naïve T cells in presence of costimulation provokes T cell activation and proliferation. Activated conventional CD4⁺ and CD8⁺ T cells secrete IL-2 that further promotes T cell proliferation and differentiation in an autocrine and paracrine fashion. Depending on the prevailing cytokine milieu and the APC activation state, CD4⁺ T cells differentiate into distinct T cell subsets such as Th1 cells. Differentiated cells leave the lymph nodes and home to the inflammatory site where the cells exert specific effector functions.

The APC activation state dictates T cell effector cell differentiation during priming. Depending on the quality of PRR ligands, APCs upregulate distinct mediators that direct the outcome and function of CD4⁺ T cell differentiation (see 3.2.3). Intracellular bacteria and viruses, for instance, induce the secretion interleukin (IL)-12 and an upregulation of Notch receptor ligands, i.e. *Delta-like (DLL) 1* and *DLL 4*^{33, 34}. IL-12 receptor engagement and Notch ligation by DLL ligands promote the differentiation towards the T helper type 1 (Th1) CD4⁺ T cell subset^{33, 35}. In contrast, extracellular parasites such as *Schistosoma mansoni* or *Vibrio cholera* induce an upregulation of Jagged 1 and Jagged 2 on the DC surface^{33, 36}. Notch engagement by the Jagged ligands, in turn, can induce Th2 subset differentiation^{34, 37}. More recently, the ligation by *C-type lectin receptors* by carbohydrates derived from the cell wall of fungi or certain bacteria has been demonstrated to initiate DC maturation associated with the production of Th17-polarizing cytokines³⁸.

In addition to their relevance for the initiation of an immune reaction, the DC maturation state is decisive in terms of peripheral tolerance induction. In contrast to

mature DCs, immature DCs express low levels of MHC and neither co-stimulatory molecules, nor inflammatory cytokines³⁹. Antigen recognition on immature DCs in absence of co-stimulation results in T cell anergy and constitutes an important mechanism to impart tolerance on the peripheral T cell repertoire towards the presented antigens^{39, 40, 41}. Furthermore, a third DC maturation state has been described. These semi-mature DCs are tolerogenic and express high levels of both MHCII and co-stimulatory molecules, but lack the secretion of inflammatory cytokines³⁹. In presence of TGF β or retinoic acid, T cell priming by semi-mature DCs can provoke the peripheral induction of Foxp3⁺ regulatory CD4⁺ T cells⁴².

3.2.3 T cell subsets

3.2.3.1 Conventional T cells

In secondary lymphoid organs, CD4⁺ and CD8⁺ T cells become activated in response to TCR engagement by cognate peptide-MHC complexes in presence of CD28-mediated co-stimulatory signals^{7, 43}. Professional antigen-presenting cells such as dendritic cells present the peptides on MHC class I as well as class II molecules on their surface and provide the indispensable co-stimulatory signals in form of B7 molecules that engage CD28 on the T cell surface. Naive CD8⁺ T cells recognize peptides in the context of MHC class I molecules and differentiate into CD8⁺ cytotoxic T cells that are capable of secreting perforins, granzymes and cytotoxic cytokines to induce apoptosis in infected or malignant target cells⁴⁴. In contrast, CD4⁺ T cells recognize peptides loaded on MHC class II. After priming, effector cell differentiation obeys the prevailing cytokine milieu⁴⁵ (Fig. 3). Both IL-12 and IFN γ induce T helper type 1 (Th1) cells that mediate immune reactions against intracellular pathogens by releasing pro-inflammatory cytokines such as IFN γ or TNF α . IL-4 and IL-13, in contrast, favor Th2 subset polarization that is involved in humoral immune responses as Th2 cells stimulate B cell proliferation as well as B cell receptor class switching. Furthermore, Th2 cells mediate immune reactions against extracellular pathogens including helminths. However, Th2 cells play also a critical role in pathologic immune disorders such as allergic reactions or in settings of chronic inflammation. Pro-inflammatory Th17 cells develop in presence of TGF β and IL-6 and contribute to immune reactions against certain types of microbes such as extracellular bacteria or

fungi, especially at epithelial or mucosal barriers. However, Th17 are deregulated in some autoimmune disorders causing inflammation and tissue destruction, e.g. in terms of multiple sclerosis or psoriasis⁴⁶. Follicular helper T cells (T_{FH} cells) are created in secondary lymphoid organs in presence of IL-6 and IL-21⁴⁷. T_{FH} cells secrete IL-21 and upregulate CD40L to interact with CD40 on cognate follicular B cells that present peptide-MHC complexes to the T cells. This interaction, in turn, supports the formation of a germinal center and promotes follicular B cell maturation that is characterized by isotype class switching and somatic hypermutation⁴⁷. Moreover, the support of T_{FH} cells in the germinal center reaction facilitates the generation of antibody-secreting, long-lived plasma cells and memory B cells^{47, 48, 49}. However, aside of $CD4^+$ T cell differentiation states that mediate immunity, suppressive or regulatory $CD4^+$ T cells are also generated in the periphery following antigen recognition. Especially the presence of IL-10 or $TGF\beta$ in combination with IL-2 favors the induction of regulatory $CD4^+$ T cells (see paragraph 3.2.3.2.3). Additionally to the aforementioned classic T cell subsets, more recent studies indicate a role of so-called Th9-differentiated cells in immune reactions against parasitic helminth infections⁵⁰.

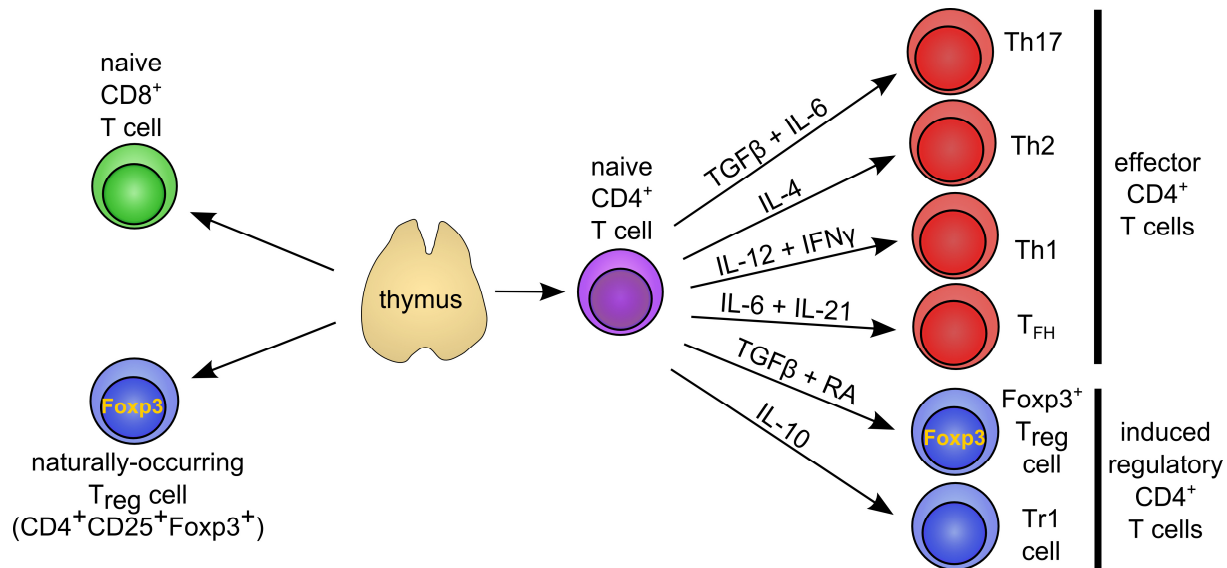


Fig. 3: T cell subsets. T cell progenitors develop in the thymus into both naïve $CD8^+$ and $CD4^+$ T cells as well as $CD25^+Foxp3^+$ naturally-occurring regulatory $CD4^+$ T cells. After egress into the periphery, $CD4^+$ T cell differentiation after antigen recognition depends substantially on the prevailing cytokine milieu. $CD4^+$ T cells can differentiate into effector T cells such as T helper type 1 (Th1) cells, Th2 cells, Th17 cells, and follicular helper T (T_{FH}) cells, or develop into regulatory cells such as peripherally induced $Foxp3^+$ T_{reg} cells and type 1 regulatory (Tr1) cells. IL: interleukin; $TGF\beta$: transforming growth factor beta; RA: retinoic acid. The figure content is based on (51, 52).

3.2.3.2 Regulatory CD4⁺ T cells

Regulatory T cells (T_{reg} cells) are specialized cells that actively suppress immune reactions and their existence had been postulated decades ago^{53, 54}. In 1995, Sakaguchi and colleagues identified a fraction of suppressive CD4⁺ T cells that constitutively express the IL-2 receptor α chain (CD25)⁵⁵. The emergence of autoimmune syndromes in neonatally thymectomized mice indicated that these cells originated from the thymus⁵⁶. Later, the transcription factor *forkhead box protein 3* (Foxp3) was identified as an indispensable determinant for the function of these regulatory T cells⁵⁷. T_{reg} cell depletion by anti-CD25 monoclonal antibodies or in genetically modified rodents such as Foxp3^{DTR} mice leads to the development of fatal and systemic autoimmune disorders. This observation underscores the cardinal relevance of T_{reg} cells for the protection from exuberant or misguided immune reactions as well as for the prevention of autoimmunity. The development of autoimmune disease in T_{reg} cell-depleted adult mice further indicates that T_{reg} cells are not only important for the prevention of autoimmunity in neonates, but throughout the entire lifetime.

3.2.3.2.1 Development of thymus-derived Foxp3⁺ T_{reg} cells

Foxp3⁺ T_{reg} cells constitute 10 to 15% among peripheral CD4⁺ T cells in mice and can be detected already in the fetal thymus^{56, 58}. The majority of T_{reg} cells is probably generated from cells that already underwent positive selection towards the CD4⁺ lineage⁵⁹. In addition to TCR ligation, T_{reg} cell development indispensably requires CD28-mediated co-stimulation and, moreover, engagement of other receptors that belong to the CD28 or *tumor necrosis factor receptor superfamily*, e.g. *cytotoxic T-lymphocyte antigen 4*, *programmed death 1*, *inducible T-cell co-stimulator*, or *CD40 ligand*^{60, 61, 62}. Similar to conventional CD4⁺ T cells, T_{reg} cells express a heterodimeric $\alpha\beta$ TCR of equivalent diversity, but, however, remarkably different antigen specificity⁶³. TCR repertoire analyses indicate that TCR specificities in the T_{reg} cell compartment are, in most instances, absent in the non-T_{reg} cell compartment, implying that antigen specificity influences T_{reg} cell lineage commitment^{63, 64}. Once controversial, the preponderance of current data supports the hypothesis that self-reactivity is the primary determinant for thymic T_{reg} cell differentiation⁶⁵. T_{reg} cell development in TCR transgenic mice requires cognate antigen expression in the thymus via a second transgene^{66, 67}. Additionally, T_{reg} cells seem to resist negative

selection which constitutes the central mechanism for the deletion of self-reactive conventional T cells that recognize auto-antigens⁶⁵. This is consistent with data derived from transgenic mice that express GFP in response to TCR stimulation. In these mice, GFP was found to be significantly higher in thymic CD4⁺ T cells that express Foxp3 as compared to Foxp3-negative cells, corroborating the hypothesis that increased TCR signaling correlates with T_{reg} cell lineage commitment⁶⁸. The observation that T_{reg} cells compete intracellonally for ligand binding suggests that TCR ligands that select T_{reg} cells are presumably rare and tissue-specific rather than ubiquitously expressed antigens⁶⁵. Consistently, a recently characterized TCR capable of inducing T_{reg} cell differentiation seems to be specific for a skin antigen⁶⁹. After development and egress from the thymus, T_{reg} cell survival and their suppressive function in the periphery strictly relies on the presence of IL-2 signals^{70, 71}.

3.2.3.2.2 Forkhead box protein 3 (Foxp3)

The functional relevance of Foxp3 *in vivo* becomes apparent in so-called “scurfy” mice. A frameshift mutation in these animals leads to a loss of the Foxp3 forkhead domain, resulting in a dysfunctional Foxp3 protein. Scurfy mice develop a severe and lethal autoimmune syndrome associated with skin inflammation and destruction of the dermo-epidermal junctions that became eponymous for the “scurfy” phenotype⁷². In humans, the functional role of Foxp3 is underscored in patients that suffer from IPEX (*immunodysregulation, polyendokrinopathy and enteropathy, X-linked syndrome*). In IPEX patients, a variety of mutations in the Foxp3 locus is responsible for a dysfunctional T_{reg} cell compartment that leads to the development of a fatal multi-organ autoimmune disease^{73, 74}.

Foxp3 belongs to the forkhead protein family that is involved in a plethora of biological functions⁷⁵. As a member of the forkhead protein subgroup “P”, Foxp3 has a forkhead domain as well as both a zinc finger and a leucine zipper motif⁷⁶. The forkhead domain mediates both DNA binding and Foxp3 homo-dimerization. The leucine zipper domain mediates homo-dimerization and hetero-multimerization, but is also involved in mediating DNA binding^{77, 78, 79}. Between mouse, rat and human, Foxp3 homology is about 86%. Mice express one Foxp3 isoform, whereas two different Foxp3 isoforms derived from alternative mRNA splicing variants are present in men^{80, 81}. Foxp3 is not expressed in murine conventional CD4⁺ T cells in contrast

to humans where the protein can become transiently expressed in activated conventional CD4⁺ T cells that do not exert a regulatory function^{82, 83}.

The transcription factor Foxp3 regulates about 700 target genes and shows direct DNA binding in 10-20%. In most instances, Foxp3 functions as a transcriptional repressor, but enhancement of gene expression can also be observed, for instance, by increasing *cytotoxic T-Lymphocyte antigen 4 (CTLA-4)* expression^{84, 85, 86}. Mechanistically, Foxp3 is able to recruit histone deacetylases such as histone deacetylase (HDAC) 7, or HDAC9, but also histone acetyl transferases such as *Tat-interactive protein 60 kDa (TIP60)*^{87, 88, 89}. The recruitment of these enzymes leads to acetylation of Foxp3 itself and, moreover, to modifications of the Foxp3 target loci. The epigenetic changes of the Foxp3 targets render the chromatin structure permissive or repressive, resulting in mRNA expression, or suppression of message synthesis⁹⁰⁻⁹². Another important mechanism for Foxp3-mediated suppression of gene expression is by hetero-multimerization with other transcription factors such as the *Nuclear factor of activated T-cells (NFAT)*, the *nuclear factor kappa-light-chain-enhancer of activated B cells (NF-κB)* proteins or the *acute myeloid leukemia1/ runt-related transcription factor1 (Aml1/ Runx1)*^{91, 92}. Suppression of IL-2 synthesis is thereby paradigmatic for this mechanism of gene silencing. In conventional T cells, AP-1 and NFAT cooperatively drive the expression of IL-2. In T_{reg} cells, however, Foxp3 competes with AP-1 for NFAT binding. As a consequence, the formation of a repressive Foxp3/ NFAT complex prevents AP-1/ NFAT binding to the IL-2 locus⁹³. Runx1- and NFκB-mediated gene transcription is suppressed in a similar fashion^{92, 94}.

3.2.3.2.3 Induced regulatory CD4⁺ T cells

In addition to thymus-derived naturally occurring T_{reg} cells, regulatory cells can arise peripherally and develop from conventional Foxp3⁻CD4⁺ T cells^{95, 96}. Peripherally induced regulatory T cells are considered to play an important role in tolerance induction towards foreign antigens such as dietary antigens or antigens derived from commensal gut bacteria⁹⁷. Depending on the cytokine milieu, conventional CD4⁺ T cells differentiate into Foxp3-negative type 1 regulatory T cells (Tr1) that develop in presence of IL-10 or IL-27^{95, 96}. Furthermore, Foxp3 can become peripherally induced in presence of IL-2 in combination with TGFβ or retinoic acid^{96, 98, 99}. Aside of the prevailing cytokine milieu, the most important determinants for peripheral Foxp3 induction are both TCR affinity and avidity as low avidity TCR engagement by potent

ligands accompanied by suboptimal co-stimulation favors Foxp3 induction^{100, 101, 102}. Furthermore, inhibitory signals seem to stabilize Foxp3 induction since *cytotoxic T-lymphocyte antigen 4* KO mice exhibit an impaired peripheral Foxp3 induction¹⁰³.

3.2.3.2.4 Immuno-regulation by T_{reg} cells

T_{reg} cells are an integral pillar of peripheral tolerance. By actively suppressing immune cells, T_{reg} cells are involved in the termination of immune reactions and prevent allergy as well as auto-immune diseases¹⁰⁴. Mediators such as IL-10, TGFβ, IL-35 or galectin-3 have been shown to exert immuno-regulatory functions by acting on many different cell types^{102, 104} (Fig. 4). The cytokines are involved in peripheral T_{reg} cell induction denominated as “*infectious tolerance*”^{104, 105}. T_{reg} cell-derived cytokines have been demonstrated to restrain dendritic cell (DC) maturation characterized by an attenuated B7 and MHC upregulation^{102, 105}.

Another T_{reg} cell-mediated mechanism for immuno-suppression of conventional T cells is by interfering with the metabolism of the target populations. Thymus-derived T_{reg} cells constitutively express the IL-2 receptor α-chain that trimerizes with the receptor β- and γ-chain forming a high-affinity IL-2 receptor¹⁰⁵. IL-2 constitutes a major growth and differentiation factor for all lymphocyte subsets and is primarily secreted by conventional T cells. IL-2 deprivation by T_{reg} cells raises the threshold for an immune response and may lead to apoptosis induction in weakly activated conventional T cells (“*metabolic disruption*”)^{102, 105}.

The second messenger cyclic adenosine monophosphate (cAMP) constitutes an important mediator involved in peripheral tolerance induction. T_{reg} cells show high intracellular cAMP levels and are capable of “injecting” cAMP into cAMP-depleted conventional T cells resulting in the repression of cell proliferation and IL-2 synthesis¹⁰⁵. Thymus-derived T_{reg} cells bear the ecto-enzymes CD39 and CD73 on their surface metabolizing extracellular ATP and ADP to adenosine¹⁰⁵. Engagement of the purinergic receptor A2A on conventional T cells by adenosine, in turn, provokes an accumulation of intracellular cAMP suppressing T cell effector functions^{102, 105}.

In addition to their suppressive capacity, T_{reg} cells may directly kill responder T cells by granzyme- and perforin-dependent mechanisms^{102, 104}, or by releasing apoptosis-inducing interferon gamma. Moreover, T_{reg} cells can induce cell death in target cells by engaging cell death-inducing receptors by ligands such as Galectin-1 or the *TNF*-

related apoptosis-induced ligand (TRAIL) that are both highly expressed in T_{reg} cells^{102, 105}.

One of the most important peripheral tolerance mechanisms represents the modulation of APC functions. Full DC maturation is characterized by high expression of co-stimulatory molecules which is indispensable for effective T cell priming³⁹. Immature or semi-mature DCs, in contrast, exhibit a low expression of co-stimulatory molecules and induce T cell anergy, or Foxp3⁺ regulatory cells. T_{reg} cells have been demonstrated to physically interact with DCs restraining their capacity to prime conventional T cells. T_{reg} cells express the CD4 homolog *lymphocyte activation gene 3* (LAG3) that engages MHCII molecules on the DC surface to prevent their maturation^{102, 105}. The protein receptor CTLA-4 is constitutively expressed on the T_{reg} cell surface and competes with CD28 on conventional T cells for the binding of B7^{102, 105}. CTLA-4/ B7 interactions can further lead to the trogocytosis of B7 molecules resulting in a diminished DC capacity to activate T cells¹⁰⁶. Moreover, B7 ligation by CTLA-4 induces an upregulation of indoleamine-2,3-dioxygenase (IDO) in DCs which catalyzes the conversion of tryptophan to kynurenine¹⁰². Tryptophan deprivation renders conventional T cells apoptotic, and kynurenine exerts cytotoxic effects on T cells adjacent to the IDO-expressing DCs^{104, 105}.

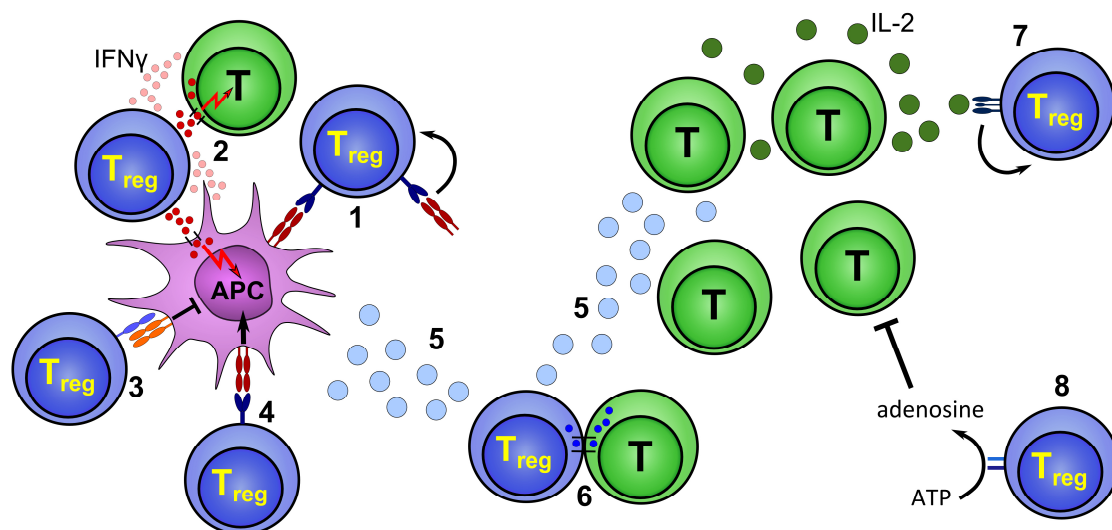


Fig. 4: Immuno-suppression by T_{reg} cells. T_{reg} cells harness 3 different kinds of mechanisms to suppress non-regulatory T cells (T). First, T_{reg} cells are potent modulators of antigen-presenting cells (APC). This includes removal of costimulatory molecules from their surface (1), transmission of inhibitory signals by receptor ligation (3), and induction of indoleamine-2,3-dioxygenase (4). Second, T_{reg} cells induce apoptosis in target cells in a granzyme- and perforin-dependent or independent manner, e.g. by interferon gamma (IFN γ) release (2). Third, T_{reg} cells interfere with the metabolism of target cells by releasing immuno-modulatory cytokines (5), by injecting inhibitory molecules such as cAMP into target cells (6), or by generating extracellular adenosine (8). IL-2 deprivation by T_{reg} cells impedes the expansion of conventional T cells (7). The figure content is based on (102, 104, 107).

3.3 Postinfarction healing and remodeling

The MI-inflicted wound shares many characteristics with injury resulting from trauma. In general, healing post-MI is divided into several phases that are orchestrated by the immune system. Early after MI, release of inflammatory mediators provoke an influx of neutrophils and monocytes into the infarct zone that clear the wound from cell and extracellular matrix (ECM) debris to pave the way for the healing phase^{108, 109, 110}. During early infarct healing, leukocytes and neo-angiogenic capillary sprouts constitute a *de novo* formed granulation tissue. In parallel, reparative pathways become activated promoting the formation of a collagenous scar that ultimately replaces the irreversibly injured parenchyma¹⁰⁹.

Remodeling after MI is a dynamic process that accompanies healing over several days to weeks¹¹¹. Ventricular remodeling is characterized by changes in both ventricular topography and structure comprising differential alterations in the infarct core and the peri-infarct zone. After large MI, an early infarct expansion and disproportionate thinning of the left-ventricular (LV) wall provokes an LV dilatation. Subsequently, deteriorated cardiac function is compensated by progressive hypertrophy in the non-infarct zone that develops over weeks to maintain both blood pressure and cardiac output¹¹¹.

In parallel to the ventricular remodeling, the extracellular matrix undergoes substantial changes that crucially influence global ventricular shape¹¹². An initial ECM disruption in the infarct zone promotes an early infarct expansion that is followed by the deposition of parenchyma-replacing collagen and *de novo* ECM construction^{112, 113}. In this phase of healing, the ECM turnover rate crucially influences the mechanical stability of the emerging scar. Impaired and belated ECM construction or an exuberant ECM degradation by collagenolytic enzymes provokes the occurrence of infarct ruptures. Collagen-synthesizing fibroblasts gradually differentiate into myofibroblasts that acquire contractile functions mediating scar contraction^{112, 113}. During late-stage healing, scar tissue maturation is accomplished by cross-linking of ECM components. After large MI, however, collagen degradation in the peri-infarct zone further promotes a progressive ventricular dilatation that develops over weeks. Ultimately, interstitial fibrosis emerges in the peri-infarct zone preserving cardiac tensile strength at the expense of ventricular function¹¹².

In summary, pronounced LV dilatation and overall cardiac remodeling results in fatally deteriorated cardiac function, a disease denominated as congestive heart failure characterized by the insufficiency to maintain cardiac output (Fig. 5).

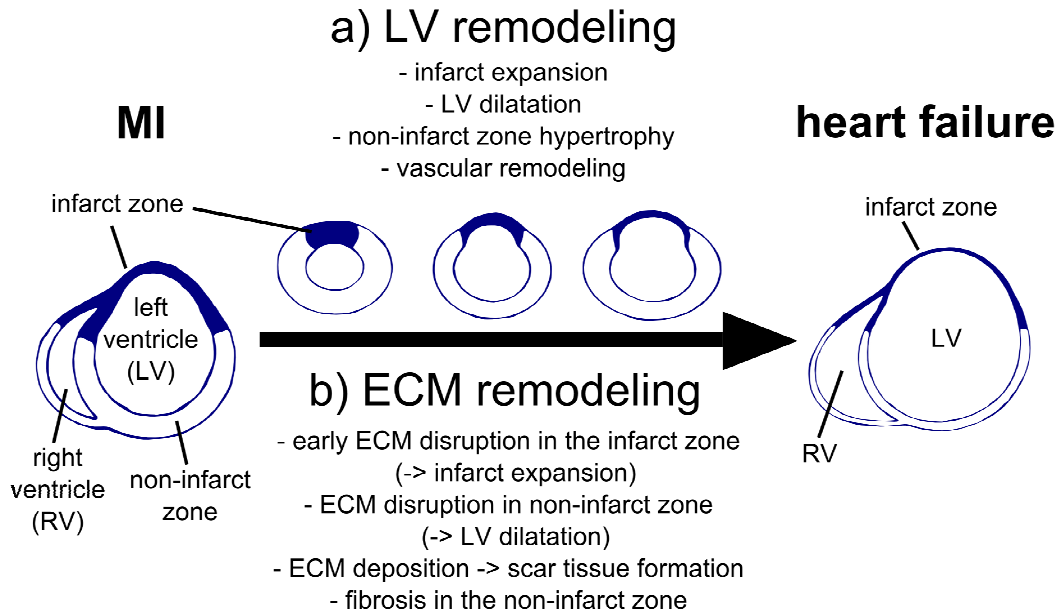


Fig. 5: Remodeling of the left ventricle (LV) and the extracellular collagen matrix (ECM) after myocardial infarction (MI). LV and ECM remodeling are characterized by substantial morphological changes extending over several days to weeks. Ultimately, exuberant cardiac remodeling leads the development of heart failure describing a state of cardiac pump insufficiency. The figure content is based on (112, 113).

3.3.1 The relevance of innate immunity in wound healing after MI

The quality of wound healing and the severity of postinfarction remodeling are inevitably linked and pivotally modulated by the immune system. The involved leukocyte fractions comprise various classes of myeloid and lymphoid cells that mediate both inflammatory and anti-inflammatory reactions. After MI, the leukocyte profile in the myocardium changes dramatically and tissue-resident macrophages and dendritic cells^{114, 115} are overwhelmed by infiltrating leukocytes deployed from tissues outside of the heart¹¹⁶.

3.3.1.1 Neutrophils

Shortly after MI, endothelial cells upregulate adhesion molecules like selectins and integrins which, along with secreted cytokines, trigger neutrophil infiltration into the

infarct zone, resulting in an early neutrophil peak on day 1 after MI in mice^{117, 118}. In terms of wound healing after skin injury, neutrophils protect from infections by phagocytosis of bacteria and release of cytotoxic mediators like reactive oxygen species. In terms of MI, neutrophils contribute to cell debris clearance in the infarct zone which constitutes a prerequisite for proper wound healing. Furthermore, neutrophils secrete chemokines provoking monocyte recruitment to the site of inflammation^{118, 119}. However, neutrophil-derived inflammatory mediators, proteolytic enzymes, or reactive oxygen species further harm the cardiomyocytes that have survived the ischemic episode¹¹⁸ (Fig. 6). Consistently, experimental neutrophil ablation or interference with neutrophil recruitment into the infarct zone reduces the infarct size^{120, 121}. Therefore, in terms of cardiac healing, neutrophils are regarded deleterious as their functions constitute immunological misfire that targets at cardiomyocytes. However, neutrophil numbers wane quickly and, in mice, the majority of neutrophils is vanished from the infarct zone three days post-MI¹¹⁷.

3.3.1.2 Mononuclear cells

Monocytes and macrophages are key players for wound healing after MI¹²². The classic but rather simplistic model proposes that monocytes circulate in the blood and trans-differentiate into macrophages upon entry of peripheral tissues¹²³. However, the spatial restriction of monocytes and macrophages to defined tissues as well as their linear developmental relationship has been revised. Monocytes can develop extramedullarily in the spleen, especially during inflammatory conditions such as during MI^{124, 125, 126}. Furthermore, tissue-resident macrophages are not necessarily derived from blood monocytes but can rather seed peripheral tissues from the yolk sac during ontogeny before the onset of hematopoiesis¹²⁷. Interestingly, these tissue-resident macrophages have the capacity to self-renew by proliferation *in situ*¹²⁸. During steady state conditions, the heart harbors very few macrophages. After MI, however, macrophage numbers in the infarct zone increase dramatically and both monocyte influx and proliferation of pre-existing macrophages may contribute to the numerical increase in the infarct zone¹¹⁶.

The monocyte compartment comprises different monocyte subsets that fulfil a broad spectrum of complementary tasks¹⁰⁸. Similarly, macrophages show a considerable plasticity and the capacity to exert a plethora of biological functions.

3.3.1.2.1 Monocytes

In the steady state, monocytes are generated from hematopoietic stem cells in the bone marrow and enter the blood via CCR2¹²⁹. In mice, monocyte subsets are separated on the basis of Ly-6C expression, a GPI-anchored surface protein of unknown biological function. 60% of blood monocytes belong to the inflammatory Ly-6C^{high} CCR2^{high} CX3CR1^{low} CD62L⁺ subset that accumulates preferentially at inflammatory sites¹³⁰. Ly-6C^{high} monocytes build up a splenic reservoir in the subcapsular red pulp that is rapidly deployed to inflammatory sites such as the healing myocardium¹³¹. During inflammatory conditions, the frequency of this monocyte subset escalates owing to medullary and splenic monocytopoiesis¹²⁶. After homing into peripheral tissues, the cells undergo apoptosis or trans-differentiate into macrophages¹²².

The Ly-6C^{low} CCR2^{low} CX3CR1^{high} CD62L⁻ monocyte subset patrols the vasculature and accumulates only at low numbers^{27, 132}. So far, the developmental relationship between the murine monocyte subsets is not totally clear, but, however, evidence suggests that Ly-6C^{low} monocytes arise from the Ly-6C^{high} subset by conversion in both blood and bone marrow^{133, 134, 135}. In men, monocyte subsets can be separated on the basis of CD14 and CD16 expression, but the functional homology between murine and human subsets is still a matter of debate¹²².

The Ly-6C^{high} monocytes infiltrate the infarct zone during the first days after MI via the chemokine receptor monocyte chemoattractant protein-1 (MCP-1) and show a numerical peak approximately 2-3 days post-MI (Fig. 6). In terms of MI, the two monocyte subsets perform complementary tasks in postinfarction healing. Ly-6C^{high} monocytes secrete inflammatory mediators such as TNF α or ECM-degrading proteases. The cells contribute to debris phagocytosis (*efferocytosis*) and gain the initial inflammatory reaction to stimulate reparative pathways^{108, 117}. A large proportion of infiltrating monocytes dies within hours *in situ*, but both medullary and splenic monocytopoiesis replenish the continuously high demand of monocytes within the infarct region¹²⁶.

Successively, monocytes wane from the infarct zone due to apoptosis or differentiation into Ly-6C^{low} macrophages^{126, 136}.

In contrast to Ly-6C^{high} monocytes remains to role of Ly-6C^{low} monocytes uncertain. A former model proposed that monocyte subsets become sequentially recruited to the healing myocardium fulfilling complementary tasks¹¹⁷. Ly-6C^{low} cells were considered

to infiltrate the heart in a second wave of monocyte influx to facilitate neo-angiogenesis or *de novo* ECM construction^{108, 117}. However, a revised model proposes that Ly-6C^{low} cells in the second phase of healing constitute rather terminally differentiated macrophages¹³⁶ (Fig. 6). In contrast, Ly-6C^{low} genuine monocytes accumulate at very low numbers in the infarct zone. Nevertheless, these cells might be crucially involved in postinfarction healing, e.g. by patrolling the vasculature, or by marking injured endothelial cells for disposal^{132, 137}.

3.3.1.2.2 Macrophages

Generally, macrophages are grouped into two distinct subsets, i.e. classically activated M1 cells and alternatively activated M2 cells¹³⁸.

The classification stems from experiments *in vitro* showing that bone marrow-derived macrophages possess completely different transcriptomes in response to distinct cytokines. In presence of lipopolysaccharide or IFN γ , macrophages differentiate into M1 cells that have pro-inflammatory characteristics¹³⁹. M1 macrophages are capable of secreting factors such as TNF α , induced NO synthase (iNOS), IL-1 β or IL-6. In contrast, IL-4, IL-13, IL-10 or TGF β polarize macrophages towards M2 that express inflammation-resolving factors and mediators fostering healing, e.g. TGF β , transglutaminase factor XIII, IL-10, osteopontin or arginase I^{139, 140, 141, 142, 143, 144}. However, *in vivo*, macrophage polarization rather constitutes a continuum between the classic M1 and M2 definitions. In terms of inflammation resolution, M1 macrophages are successively replaced by M2 cells^{145, 146, 147}.

In the context of MI, the emergence of M1 and M2 mediators in the infarct zone follows a biphasic pattern¹⁴⁸ (Fig. 6). However, a refined model suggests that Ly-6C^{high} monocytes rather than M1 cells prevail during early infarct healing driving initial inflammation¹³⁶. Subsequently, these Ly-6C^{high} monocytes differentiate into Ly-6C^{low} M2-like macrophages that secrete mediators involved in inflammation resolution as well as neo-vessel formation and scarring. These monocyte-derived cardiac macrophages, in turn, self-renew robustly *in situ* by local proliferation¹⁴⁹.

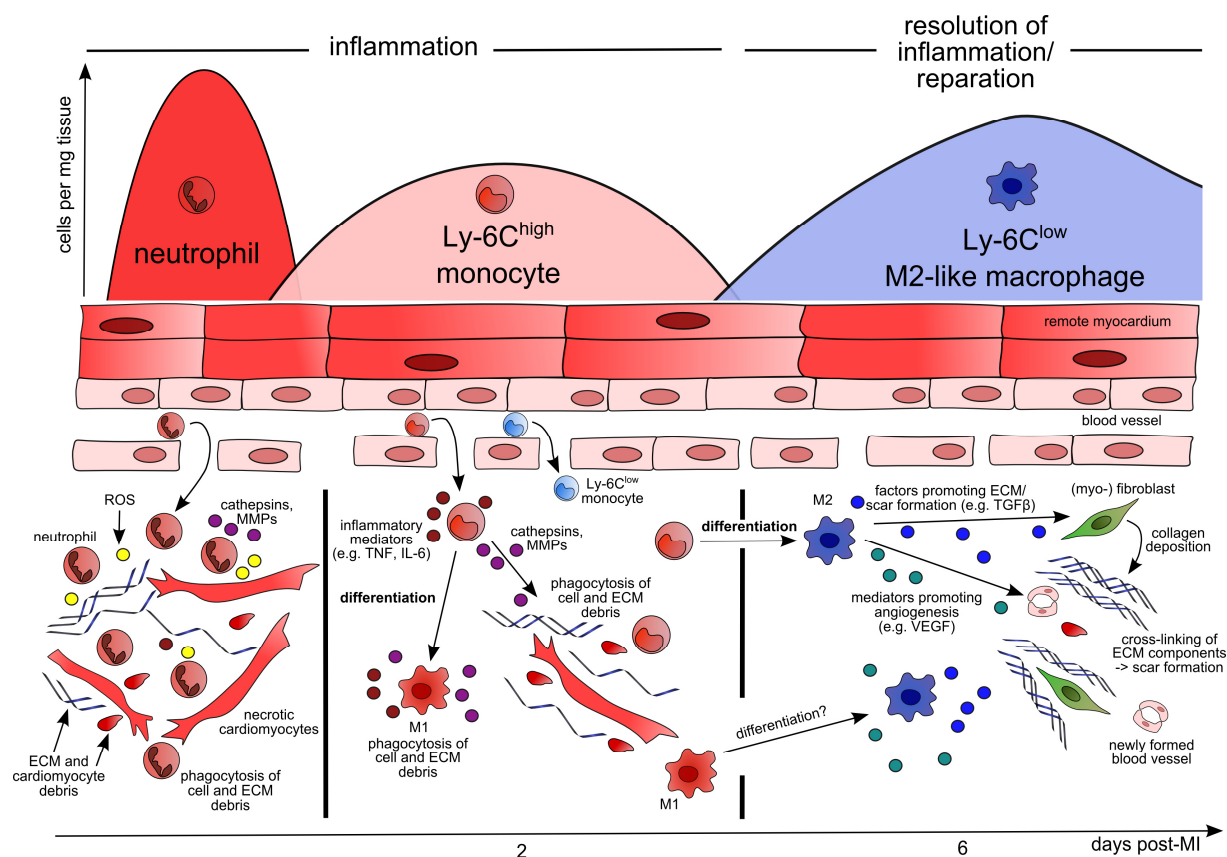


Fig. 6: The role of innate immunity in wound healing after MI. Neutrophils infiltrate the infarct zone numerous immediately after MI and amplify the initial local inflammation by secretion of mediators such as reactive oxygen species (ROS). Recruited neutrophils secrete collagenolytic enzymes (cathepsins and matrix metalloproteinases, MMPs) that promote extracellular collagen matrix (ECM) degradation. Neutrophil numbers wane quickly by apoptosis and phagocyte-mediated clearance *in situ*. In the murine system, neutrophils become successively replaced by Ly-6C^{high} monocytes that accumulate at high numbers in the infarct zone approx. 2 days after MI. These cells further gain the inflammation by secreting factors such as TNF α and collagenases. The majority of this monocyte subset dies locally by apoptosis, but a proportion differentiates into M1 macrophages that exert pro-inflammatory functions. During late-stage healing, Ly-6C^{high} monocytes downregulate Ly-6C expression and differentiate into Ly-6C^{low} M2-like macrophages. These cells have potent anti-inflammatory and healing-fostering characteristics as they secrete mediators such as vascular endothelial growth factor (VEGF) and transforming growth factor beta (TGF β) that, among other mediators, drives collagen deposition by scar-constructing myofibroblasts. The role of Ly-6C^{low} monocytes for postinfarction healing is unclear so far. The figure content is based on (117, 136).

3.3.2 Activation of adaptive immunity after MI

The role of innate immunity in cardiovascular pathologies has been studied in great detail. In contrast, the relevance of adaptive immunity in the context of atherosclerosis, hypertension, and myocardial infarction has been widely disregarded. However, experimental studies and clinical trials suggest that T cells become also activated after MI. Splenocytes from infarcted rats, for instance, contain a subset of CD8⁺ T cells that show cytotoxic activity against cardiomyocytes *in vitro*, contrary to splenocytes from non-infarcted rats¹⁵⁰. Cheng and colleagues found

elevated proportions of IFN γ -producing CD4⁺ T cells in the blood of infarct patients, but no frequency shifts with respect to the expression of IL-4 indicating a Th1/ Th2 imbalance after MI¹⁵¹. Furthermore, Moraru et al. were able to show that a proportion of patients with a recent history of MI showed a proliferative response of peripheral blood mononuclear cells to cardiac myosin in contrast to control subjects that did not exhibit a cellular reaction¹⁵². Consistent with these hints that T cells become activated in terms of MI, Abbate and colleagues detected activated T cells in the peri-infarct zone as well as in the remote myocardium of necroscopy specimen from patients that succumbed to acute MI, whereas control hearts did not show an accumulation of T cells¹⁵³. However, although a line of reports implicates that T cells are activated in the wake of MI, T cell effector functions or their role in postinfarction healing and remodeling have not been systemically addressed.

A major challenge to decipher T cell priming in human patients arises from the fact that the development of atherosclerosis usually precedes the occurrence of MI. Atherosclerotic plaque rupture represents the most frequent etiology for MI and several plaque components have been demonstrated to serve as T cell antigens. Th1- and Th17-polarized CD4⁺ cells are frequently present in atherosclerotic lesions indicating that CD4⁺ T cells become activated in terms of atherosclerosis^{154, 155}. Furthermore, unstable plaques harbor CD28-negative CD4⁺ T cells that have downregulated CD28 due to repetitive stimulation^{155, 156}, implying a state of chronic inflammation and T cell activation in the atheroma already *before* the occurrence of MI. As atherosclerosis-related inflammation, thus, may interfere with immune reactions provoked by cardiac injury, MI-specific T cell activation cannot be studied in man. The (mouse) model of *permanent* coronary artery ligation, in contrast, provides a defined system to study the T cell response in terms of MI independent of atherosclerosis-related T cell activation.

Aside of interfering effects of atherosclerosis on T cell priming and function in postinfarction wound healing, recent reports have indicated that CD4⁺ T cells influence post-ischemia reperfusion injury that impacts on healing and remodeling secondary to T cell effects on infarct size^{157, 158}. T cell-deficient mice show smaller infarcts following an ischemic episode of 45 minutes left coronary artery occlusion as compared to T cell-sufficient controls. As the infarct size represents a major determinant for the degree of postinfarction remodeling, the influence of T cells on healing and, consequently, cardiac remodeling cannot be studied in reperfused

hearts. Although the precise mechanism behind this detrimental T cell effect is not well understood, it seems that especially CD4⁺ T cells contribute to reperfusion injury. However, by using a (mouse) model of *permanent* coronary artery ligation, reperfusion injury can be obviated allowing a non-ambiguous examination of T cell effects on postinfarction healing.

3.4 Aim of the study

The role of the innate immune system for wound healing and remodeling after MI has been investigated in great detail. In contrast, the contribution of adaptive immunity to healing has been widely disregarded. The present study addressed therefore the following aspects:

(1.) Experimental studies and clinical trials implicate that CD4⁺ T cells become activated after MI^{151, 153}. However, so far, the activation of CD4⁺ T cells in terms of MI and their relevance in cardiac wound healing has not been systematically addressed. The principal aim of this study was to investigate whether CD4⁺ T cells become activated after MI, and whether T cells influence postinfarction healing and remodeling.

(2.) Healing after MI involves inflammatory and anti-inflammatory reactions. Despite the importance of inflammation for early infarct healing, a prolonged or accentuated inflammatory response is regarded deleterious. Foxp3⁺CD4⁺ T_{reg} cells are self-reactive and have potent anti-inflammatory characteristics. The study investigated particularly whether Foxp3⁺ T_{reg} cells become activated in the wake of MI and whether these cells modulate cardiac wound healing.

(3.) T_{reg} cells are involved in the suppression of exuberant immune reactions and detrimental auto-immunity. The study investigated whether a therapeutic T_{reg} cell activation can be harnessed to improve cardiac wound healing and clinical outcome after MI.

4 Methods and Materials

4.1 Materials

4.1.1 Fine chemicals and reagents

The following fine chemicals and reagents were used. Unless otherwise specified, all substances were acquired from Amersham Biosciences, AppliChem GmbH, Calbiochem, Carl Roth GmbH, Gibco BRL/ Life Technologies, Merck, Roche Diagnostics, cp-pharma and Sigma-Aldrich.

Acetone	Luminol
Acetic acid	Magnesium chloride
Alexa488-phalloidin	Magnesium sulfate
Aluminium sulfate	Methanol
Ammonium persulfate	L-glutamine
β -mercaptoethanol	Liquid nitrogen
Bovine serum albumin	Paraformaldehyde
Calcium chloride	Rotihistol
Citric acid	Sirius red (Direct red 80)
DAPI (4',6-diamidino-2-phenylindole)	Sodium azide
Diphtheria toxin	Sodium chloride
Disodiumhydrogenphosphate	Sodiumdihydrogenphosphate
DMSO	Sodium pyruvate
Dry mild, fat-free	Paraffin Medite Tissuewax
EDTA	Picric acid
Eosin	Ponceau S
Ethanol	Potassium chloride
FCS (fetal calf serum)	Sodium azide
Glycin	Tetramethylethylenediamine (Temed)
Glycerol	Tris (Tris(hydroxymethyl)aminomethane)
Hematoxylin	Trypan blue
Heparin	Tween 20
Isopropyl alcohol	4-Hydroxycoumarin
Isoflurane	

4.1.2 Antibodies

Fluorophore- and biotin-labeled FACS antibodies directed against mouse antigens

Antibody	Supplier
anti-CD11b-PE (M1/70)	eBioscience
anti-CD45-efluor 450 (clone 30-F11)	ebioscience
anti-F4/80-FITC (clone BM8)	eBioscience
anti-Foxp3-PE-Cy5.5 (FJK-16s)	eBioscience
anti-Ly-6C-PerCP-Cy5.5 (clone HK1.4)	eBioscience
anti-CD4-Alexa647 (clone RM4-5)	BioLegend
anti-CD8a-Pe-Cy7 (clone 53-6.7)	eBioscience
anti-Helios-Pacific Blue (clone 22F6)	BioLegend
anti-CD19-Biotin (clone 6D5)	BioLegend
anti-Ly-6G-Alexa647 (clone 1A8)	BioLegend
anti-Ki67-PE (clone B56)	eBioscience
anti-CD3 ϵ -Pe-Cy7 (clone 145-2C11)	BioLegend
anti-TNF α -BV421 (clone MP6-XT22)	BioLegend
anti-IFN γ -PE (clone XMG1.2)	BioLegend
anti-CD19-biotin (clone 6D5)	BioLegend
anti-CD25-PE (clone PC61)	BioLegend

Primary antibodies used for Western blot, immunohistochemical and immunofluorescence stainings directed against mouse antigens:

anti-alpha smooth muscle actin (clone 1A4)	Dako
anti-collagen type I (polyclonal)	Cedarlane
anti-collagen type III (polyclonal)	Cedarlane
anti-Foxp3 (clone FJK-16s)	eBioscience

Secondary antibodies for Western blot and immunofluorescence stainings:

goat-anti-rat IgG-HRP (polyclonal)	Santa Cruz
goat-anti-rat IgG-Alexa 555 (polyclonal)	Molecular Probes

4.1.3 Buffers and solutions

All buffers and solutions were prepared in desalted water.

PBS	NaCl (pH 7.4)	137 mM
	Na ₂ HPO ₄	10 mM
	KCl	2.6 mM
	KH ₂ PO ₄	1.8 mM
FACS buffer	NaCl (pH 7.4)	137 mM
	Na ₂ HPO ₄	10 mM
	KCl	2.6 mM
	KH ₂ PO ₄	1.8 mM
	BSA	0.1% (w/v)
	NaN ₃	0.1% (w/v)
Laemmli buffer	Tris-HCl (pH 6.8)	125 mM
	SDS	4% (w/v)
	Glycerol	20% (v/v)
	2-mercaptoethanol	10% (v/v)
	Bromophenol blue	0.004% (w/v)
BSS/ (BSA)	KCl	5.33 mM
	KH ₂ PO ₄	0.44 mM
	NaCl	138 mM
	NaHCO ₃	4 mM
	Na ₂ HPO ₄	0.3 mM
	(BSA)	(5%)

Erythrocyte lysis buffer	NH ₄ Cl	150 mM
	NaHCO ₃	10 mM
	EDTA	0.15 mM
SDS-PAGE running buffer	Tris-HCl (pH 8.5)	25 mM
	Glycine	192 mM
	SDS	0.1% (w/v)
Transfer buffer	Tris-HCl (pH 8.3)	25 mM
	Glycine	192 mM
	Methanol	20 % (v/v)
TBST	Tris-HCl (pH 7.6)	50 mM
	NaCl	150 mM
	Tween 20	0.05% (v/v)
Blocking buffer	TBST	
	Fat-free dry milk	5%
Detection reagent Solution A	Tris-HCl (0.1M, pH 8.6)	200 ml
	Luminol	50 mg
Detection reagent Solution B	DMSO	10 ml
	4-Hydroxycoumarin	11 mg
Stripping buffer	Tris-HCl (pH 6.8)	65 mM
	SDS	2% (w/v)
	2-mercaptoethanol	100 mM
Neutral-buffered formaline	Formaldehyde	3.7%
	Na ₂ HPO ₄	46 mM
	NaH ₂ PO ₄	29 mM

Mayer's Hematoxylin	Acetic acid	2%
	Glycerol	30%
	Hematoxylin	1%
	Aluminium sulfate	5%
Picro-sirius red	Picric acid	1.5%
	Sirius red	0.1%

4.1.4 Ready for use kits and solutions

Kit	Supplier
ARK™ peroxidase kit	Dako
CD3ε MicroBeat kit	Miltenyi
Cytometric Bead Array	BD
Entellan	Merck
Foxp3 Transcription Factor Staining Buffer Set	eBioscience
Quantikine ELISA Mouse/ RAT Osteopontin	R&D
Quantikine ELISA Mouse IL-13	R&D
Quantikine ELISA Mouse TGF-beta 1	R&D
RNeasy Micro Kit	Qiagen
RNeasy Mini Kit	Qiagen
Trinucleotide mRNA amplification Pico Kit	AmpTec
DNase 1, Amplification Grade, AMP-D1	Sigma
iScript cDNA Synthesis Kit	Bio-Rad
Ladewig staining solution kit	Morphisto
Protein Extraction Reagent Type 4	Sigma
RNAlater Solution	Ambion
TaqMan Master Mix	Life Technologies
Vectashield mounting medium	Vector Laboratories
3,3'-diaminobenzidine solution	Abcam

4.1.5 TaqMan probes

All probes for Real-time RT-PCR analyses were purchased from Life Technologies.

Gene	Probe number
Arginase I	Mm00475988_m1
TGF β 1	Mm01178820_m1
Alpha smooth muscle actin	Mm00725412_s1
TIMP-1	Mm00441818_m1
TIMP-2	Mm00441825_m1
MMP-2	Mm00439498_m1
MMP-9	Mm00442991_m1
Osteopontin	Mm00436767_m1
FXIIIa	Mm00472334_m1
GAPDH	Mm99999915_g1
Collagen alpha 1 (type 1)	Mm00801666_g1
Collagen alpha 1 (type 3)	Mm01254476_m1
iNOS	Mm00440488_m1
Interleukin-10	Mm00439615_g1
Interleukin-13	Mm00434204_m1
Interleukin-1 β	Mm0043228_m1
Interleukin-6	Mm00446190_m1
TNF α	Mm99999068_m1
IFN γ	Mm01168134_m1
von Willebrand factor	Mm00455669_m1
Vimentin	Mm01333430_m1

4.1.6 Antibodies, ligands, and fine chemicals for cell culture

Chemical	Supplier
Human TGF β 1	BioLegend
Mouse Interleukin-10	BioLegend
Mouse Interleukin-13	Biolegend

Human Interleukin-2 (Proleukin)	Novartis
Anti-mouse-TGF β (clone 1D11)	R&D
CD28-SA	Exbio
Dynabeads Pan Mouse IgG	Life Technologies
Monensin 1000x	BioLegend
Penicillin/ Streptomycin	Gibco
Phorbol 12-myristate 13-acetate (PMA)	Sigma
Streptomycin	Invitrogen
Ionomycin	Sigma

4.1.7 Enzymes

Collagenase Type 2	Worthington
DNase I	Sigma

4.1.8 Animals

All mice were between 8-10 weeks old at the day of surgery. Transgenic and knock-out mice had a C57BL/6 background and wildtype littermates were used as reference controls. The study conformed to the regulations for animal experiments and was approved by the local government.

Mouse strain	Supplier
Wildtype C57BL/6J	Harlan or Jackson Laboratory
MHCII KO	Jackson Laboratory
OT-II	Jackson Laboratory
DEREG	Jackson Laborator

4.1.9 Consumables

Consumable	Supplier
Catheter Vasofix Safety	Braun
Cell separation columns	Miltenyi
Cell strainer (70 and 100 μ m mesh)	BD Biosciences

Centrifuge tubes	Greiner
Cover slips 24 x 50mm	Menzel
Cryo tube (1.8 ml)	Nunc
Entellane	Merck
FACS tubes	BD
Filter paper	Whatman
Microseal film for PCR plates	Bio-Rad
Microtome blades S35 Typ	Feather
Needles (25 gauge and 19 gauge)	Braun
Nitrocellulose transfer membrane	Whatman
Object slide, SuperFrost Ultra plus	R. Langenbrinck
PageRuler Prestained Protein Ladder	Fermentas
PCR tubes (0.2 ml)	Eppendorf
Pipette tips (10 µl, 200 µl, 1000 µl)	Starlab
Polypropylene suture (0.7 metric)	Vömel
Reaction tubes (1.5 ml and 2 ml)	Eppendorf
Scalpel	Hartenstein
Serological pipettes	Greiner
Sterile Filter (0.45 µm)	Machery-Nagel
Tissue culture dishes (35 mm)	Greiner
Tissue Ruptor Disposable Probes	Qiagen
Tissue-Tek O.C.T. compound	Sakura
96-well plates (U-bottom, V-bottom)	Greiner/ Nunc/ Ratiolab
96-well PCR plates	Bio-Rad

4.1.10 Instruments

Analytical balance	Kern
Biofuge Fresco	Heraeus
Block heater	Biosan
Centrifuge 5810 R	Eppendorf
Cell sorter FACS Aria III	BD Biosciences
ELISA-Reader, MRX tc	Dynex
Flow cytometer LSR II	BD Biosciences

Fluorescence microscope Axio imager Z1m	Zeiss
iCycler	Biorad
Incubator, Hera cell 150	Thermo Scientific
Isoflurane Vaporizer	Harvard Apparatus
Laminar flow hood	Heraeus
Light-optical microscope Axioskop 2 plus	Leica Microsystems
Magnetic stirrer	Labinco
Microtome Hn40	Reichert-Jung
Paraffin embedding station	Bavimed
Pipettes	Eppendorf
Power supply PowerPac 2000	Bio-Rad
pH meter	WTW
Qubit Fluorometer	Life Technologies
Thermocycler	Eppendorf
Tissue Ruptor	Qiagen
Ultrasound instrument (Aplio System)	Toshiba
Vortex mixer	Labinco
Western blot chamber	Bio-Rad
Western blot scanner C-DiGit	LI-COR
2100 Bioanalyzer	Agilent

4.1.11 Electronic data processing

Data acquisition, analysis and presentation were performed using the following software on diverse Windows-operated personal computers provided by Fujitsu-Siemens:

Adobe Photoshop CS3	Microsoft Word 2007
BD FACSDiva 5.0	Systat Software SigmaScan
ImageJ	Thomson EndNote 9.0
GraphPad Prism 4.03	TomTec Image Arena
Microsoft Excel 2007	Tree Star FlowJo 8.8.6

4.2 Methods

4.2.1 *In vivo* experiments

4.2.1.1 Surgeries

Mice were anesthetized in a chamber containing a 2% isoflurane atmosphere, placed in a supine position, intubated and ventilated with 100% oxygen supplemented with 0.8% isoflurane to sustain anaesthesia. The paws were taped to the operation table the chest opened using a midline sternotomy to expose the heart. A nylon suture was passed under the left anterior descending coronary artery using a tapered needle to place the ligature. After artery occlusion, the chest was closed. For sham operations, thoracotomy was conducted without subsequent coronary artery ligation. For pre-emptive analgesia, buprenorphine was routinely administered after surgery. Operations were conducted by Charlotte Dienesch and Barbara Bayer.

4.2.1.2 T_{reg} cell depletion in DEREg mice

T_{reg} cells were depleted by using “depletion of regulatory T cell (DEREG)” mice that specifically express the human diphtheria toxin receptor (DTR) in Foxp3-positive cells¹⁵⁹. All experiments were conducted utilizing a distinct strain of DEREg mice that had been generated by using a Foxp3 targeting vector¹⁵⁹. T_{reg} cells were depleted before MI induction by intraperitoneal administration of 500 ng diphtheria toxin (DTX) on day 2 and day 1 before surgery. To prevent a rebound of T_{reg} cells, 250 ng DTX were injected on day 2 and day 4 after MI induction.

4.2.1.3 Antibody-mediated depletion of Foxp3⁺CD4⁺ T_{reg} cells

Depletion was achieved by administration of a rat anti-mouse CD25 monoclonal antibody labeling thymus-derived T_{reg} cells that constitutively express high levels of CD25 on their cell surface. 1 mg anti-CD25 antibody (clone PC61) were injected intraperitoneally 8 day prior to MI induction to effectuate T_{reg} cell depletion by phagocytes^{160, 161}.

4.2.1.4 T_{reg} cell activation *in vivo*

T_{reg} cell expansion was conducted by a single intraperitoneal injection of a superagonistic anti-CD28 monoclonal antibody (CD28-SA) that cross-links CD28 molecules on the T cell surface provoking a vigorous activation signal^{162, 163}. As T_{reg} cells are highly responsive to CD28-SA stimulation, the CD28-SA was administered at low dose of 300 µg per mouse to elicit a net expansion of T_{reg} cells over conventional T cells.

4.2.1.5 IL-2/ anti-IL-2 monoclonal antibody (mAB) complex treatment

Recombinant murine IL-2 (PeproTech) was mixed with anti-IL-2 monoclonal antibody (clone JES6-1, eBioscience) in 0.9% sterile NaCl solution and incubated for 30 min at room temperature. IL-2 and anti-IL-2 mAB were mixed at a molar ratio of ~2:1¹⁶⁴. Each mouse was treated on three consecutive days receiving a dose of 6 µg IL-2/ anti-IL-2 mAB complexes per injection (1 µg IL-2 and 5 µg anti-IL-2) corresponding to approximately 5000 IU IL-2 per day and mouse^{164, 165}.

4.2.1.6 Echocardiography

Mice were anesthetized in a chamber containing a 2% isoflurane atmosphere. After immobilizing the mice in a supine position, the snout was placed in a nose cone connected to the anesthesia system. Steady-state sedation level was maintained using 0.4% to 0.6% isoflurane mixed with 0.5 L/min 100% oxygen. Cardiac ultrasound analysis was performed on a Toshiba Aplio system. After shaving the chest, ultrasound gel was applied and the probe lowered parasternally onto the thorax for short-axis echocardiographic measurements at both the level of the mid-papillary muscles and the apex. Anesthesia was adjusted to obtain a target heart rate higher than 500 beats per minute.

Two-dimensional imaging of the left ventricle was conducted and both luminal end-diastolic and end-systolic area (EDA, ESA) were assessed. To obtain fine measurements of luminal diameters and the wall thickness, transversal M-mode echocardiography was performed providing a 1-dimensional view of the left-ventricular (LV) luminal diameter and both the anterior and posterior wall thickness. All measurements were conducted both at the papillary and the apical level. Images

were analyzed using Image Arena (TomTec). To assess left-ventricular contractile function, LV fractional shortening (FS) was determined using the following formula¹⁶⁶:

$$FS (\%) = 100 \times [(EDD - ESD) / EDD]$$

FS: fractional shortening

EDD: end-diastolic diameter (left-ventricular lumen)

ESD: end-systolic diameter (left-ventricular lumen)

Echocardiography measurements were performed by Sandra Umbenhauer and Barbara Bayer.

4.2.2 Organ preparation

Infarcted mice were anesthetized and injected with heparin (40 IU per mouse) to prevent blood clotting. After thoracotomy, blood vessels were depleted from blood by perfusing the vascular system with ice cold PBS. After perforation of the right ventricle, a cannula was inserted into the left ventricle and the PBS slowly injected. The mouse was perfused with approximately 10 ml PBS until the tissues became “pale”. After heart excision, the right ventricle was removed and the left-ventricular infarcted apex dissevered. Depending on the analysis, the tissue was processed differently. For protein analysis, a part of the apex was transferred into a tube for cryo-conservation, frozen in liquid nitrogen and stored at -80°C. For mRNA expression analyses, a part of the infarcted tissue was incubated overnight at 4°C in RNAlater (ambion). After incubation, the tissue was transferred into a tube for cryo-conservation and stored at -80°C. For flow cytometry analyses, the tissue was minced and digested with collagenase type 2 (1000 IU/ml) and DNase I (60 IU/ml) for 35 min at 37°C. The remaining tissue pieces were grinded against a cell strainer of 100 µm pore size to obtain a single cell suspension.

Transversal left-ventricular cross-sections adjacent to the cardiac apex were used for histochemical and immunofluorescence stainings. For histochemistry, tissue was incubated in 4% formaldehyde solution for fixation. For immunofluorescence stainings, the tissue was embedded in Tissue-Tek providing a specimen matrix and stored at -80°C.

Spleen and lymph nodes were collected in BSS/ BSA. Single cell suspensions were generated by grinding the organ against a cell strainer of 40 µm pore size. To deplete

erythrocytes from splenic suspensions, cells were treated with erythrocyte lysis buffer for 2 min and washed with BSS/ BSA.

For final blood analyses, samples were collected by puncture of the heart after thoracotomy before perfusion of the vascular system. For evaluation of antibody treatments, mice were narcotized with isofluorane and blood collected by inserting a heparin-filled cannula into the venous plexus behind the eye. Erythrocytes were eliminated by incubation in erythrocyte lysis buffer for 10 min and subsequently washed with BSS/ BSA.

4.2.3 Cell culture

Generally, primary cells were incubated in an atmosphere containing 5% CO₂ at 37°C. Cells were cultivated in supplemented RPMI medium from Gibco.

RPMI medium, supplemented with	10% FCS
	2 mM L-glutamine
	1 mM sodium pyruvate
	100 U/ ml penicillin/ streptomycin
	50 µM 2-mercaptoethanol

Cells were pelletized by centrifugation at 500 g at room temperature. Cell numbers were assessed using a Neubauer hemocytometer by mixing 10 µl cell of suspension with 10 µl Trypan blue to distinguish dead from vital cells.

4.2.4 Immunological methods

4.2.4.1 Flow cytometry

Flow cytometry is a laser-based technology for cell counting, cell sorting and evaluation of protein expression on a per-cell basis. During measurements, a cell suspension streams through a detection apparatus performing a multi-parameter analysis. Different lasers are directed on the suspension stream exciting fluorescent dyes that label the cell components of interest. The combination of scattered and

fluorescent light, in turn, provides information about the analyzed cell type and expression levels of targeted proteins.

Up to 10^6 cells were suspended in 50 μ l FACS buffer containing anti-CD16/ CD32 monoclonal antibody (clone 2.4G2, 1:400) to block unspecific Fc-receptor binding. After blocking at 4°C for 15 min, fluorophore-conjugated antibodies were added to the cell suspension and incubated for 15 min at 4°C. The Foxp3 / transcription factor staining buffer set (eBioscience) was used for intracellular staining. Cells were fixed by 30 min incubation in fixation buffer at room temperature. After washing in permeabilization buffer, cells were incubated for 30 min at room temperature in presence of fluorophore-labeled antibodies directed against intracellular targets diluted 1:50 in permeabilization buffer. In order to stain cytokines intracellularly, cells were incubated for 6 hours in presence of ionomycin (1 μ g/ ml, Sigma), phorbol-12-myristate-13-acetate (PMA, 50 ng/ ml, Sigma) and monensin (1:1000, BioLegend) before staining. Finally, cells were washed, resuspended in FACS buffer and analyzed on an LSR II flow cytometer (BD Biosciences). FlowJo (TreeStar Inc) was used for data analysis. Plots are shown as log₁₀ fluorescence intensities.

4.2.4.2 Fluorescence-activated cell sorting (FACS)

FACS is a special type of flow cytometry and constitutes a method to sort a heterogeneous cell suspension based on cell-specific light scattering and fluorescence characteristics. The cell suspension stream is arranged in a way to guarantee a large interspace between individual cells relative to their diameter. A vibrating mechanism causes the flow to break into droplets containing single cells. Before droplet formation, fluorescence and scattered light from the cells are measured. Droplets containing cells of interest are charged and, thereafter, sorted by an electrostatic deflection system.

4.2.4.3 Enzyme-linked Immunosorbent Assay (ELISA)

In order to evaluate bio-molecule concentrations in cell culture supernatants, an enzyme-linked immunosorbent assay (ELISA) of the “sandwich” type was used. For all experiments, ELISA kits from R&D were used according to the manufacturer’s protocol. In sandwich ELISAs, capture antibodies are non-covalently coated to polystyrene plates via the hydrophobic Fc-region of the immunoglobulin molecule.

After blocking, diluted cell culture supernatants were added to the wells and incubated for 2 hours. For analysis of TGF β 1 concentrations, samples were pre-treated with 1N HCl to reveal antibody binding sites before the supernatants were added to the wells. After extensive plate washing, biotinylated detection antibodies were added to the wells and incubated for another 2 hours. After 5 additional washing steps, horseradish peroxidase (HRP)-conjugated streptavidin was added. For detection of antigen-antibody complexes, the HRP substrate tetramethylbenzidine was supplemented resulting in chromogen conversion into a blue chromophore. The reaction was stopped after 30 min of incubation by addition of sulphuric acid converting the color to yellow. Extinction was measured at 450 nm using a 96-well plate ELISA reader (Dynex MRX Revelation TC 96).

4.2.4.4 Magnetic cell separation (MACS)

To enrich monocytic cells from lymphoid organs, lymphocytes were depleted from single cell suspensions derived from spleens as well as inguinal, axillary, brachial, cervical and lumbar lymph nodes. To this end, the CD3 ϵ MicroBeat kit from Miltenyi was used in a modified protocol. 10^8 cells per ml BSS/ BSA were blocked for 15 min on ice using 2.4G2 blocking antibody (1:400) and incubated in presence of both biotinylated anti-mouse CD3 ϵ (dilution 1:10) and biotinylated anti-mouse CD19 (dilution 1:300). After 15 min incubation on ice, cells were washed and, subsequently, 1.2×10^8 cells per ml BSS/ BSA magnetically labeled using anti-biotin microbeads (dilution 1:5). After 10 min incubation on ice, cells were washed in BSS/ BSA and loaded onto an LS-MACS column placed in the magnetic field of a MACS separator. After rinsing the column with 9 ml BSS/ BSA, negatively-selected cells represented the lymphocyte-depleted monocyte/ macrophage enriched fraction.

4.2.5 Molecular biology

4.2.5.1 RNA isolation

RNA from tissue or primary cells in culture was isolated using the RNeasy Mini kit (Qiagen) or the RNeasy Micro kit (Qiagen), respectively. After tissue or cell homogenization in lysis buffer, samples were spun for 3 min at 8.000 g at room

temperature to pelletize hydrophobic constituents. The aqueous phase containing the hydrophilic RNA was mixed with one volume 70% ethanol in water and transferred onto the RNA-binding silica-membrane spin columns. After centrifugation at 8.000 g for 15 sec, RNA was purified on-column using the provided washing buffer. RNA was eluted in 40 µl nucleic acid-free water and stored at -80°C.

4.2.5.2 RNA quantification

4.2.5.2.1 Fluorometric RNA quantification

RNA concentrations were determined using the Qubit fluorometer (Life Technologies). Generally, the method exploits fluorescent dyes that show a weak fluorescence before binding to their specific target, i.e. nucleic acids or proteins. Dyes in complex with their target increase their fluorescence intensity by several orders of magnitude linearly reflecting the amount of bulk RNA or protein within the sample.

4.2.5.2.2 Bioanalyzer measurement

The Bioanalyzer (Agilent) is a microfluidics-based platform to evaluate quality, amount and size of RNA. The RNA is electrophoretically separated by size in a gel matrix. Dye molecules intercalate into RNA strands and are subsequently detected by laser-induced fluorescence proportional to the amount of RNA. Data is translated into gel-like images or electropherograms.

4.2.5.3 DNA digestion

To eliminate DNA contaminations in RNA solutions, DNA was digested using the AMP-D1 kit (Sigma). Up to 1 µg total RNA was mixed with 1 µl reaction buffer and 1 µl DNase I solution. The volume was adjusted to 10 µl using nucleic acid-free water and the sample was incubated for 10 min at room temperature. After addition of 1 µl stop solution, the sample was incubated at 70°C for 10 min.

4.2.5.4 Reverse transcription of RNA

Copy DNA (cDNA) is synthesized by reverse transcription from an RNA matrix. For cDNA generation, the iScript cDNA synthesis kit (Bio-Rad) was used. 1 µg RNA was

mixed with 4 μ l nuclease free-water, 4 μ l reaction buffer and 1 μ l reverse transcriptase. The volume was adjusted to 20 μ l and cDNA synthesis conducted in a thermo cycler using the following program:

5 min	25°C
30 min	42°C
5 min	85°C
5 min	4°C

The cDNA was stored at - 20°C for further experiments.

4.2.5.5 Real-time (RT) polymerase chain reaction (PCR)

Real-time RT-PCR is a technique to quantify the amount of DNA within a sample. The reaction is conducted in a thermal cycler with capacity to illuminate the sample and simultaneously detect the fluorescence from an excited fluorophore. The PCR process generally consists of a series of temperature changes. In a first step (50°C), uracil-N-glycosylase treatment prevents re-amplification of potential carry-over PCR products by removing any uracil incorporated into single- or doublestranded amplicons. After cDNA denaturation at 95°C, temperature decreases to 60°C for primer annealing and DNA strand elongation.

For Real-time RT-PCR analyses, target-specific TaqMan probes (Life Technologies) containing forward and reverse primers were utilized. The commercially available TaqMan Master Mix (Life Technologies) provides the Taq polymerase and deoxynucleoside triphosphates. Reagents were used according to the manufacturer's protocol:

Master Mix	12.5 μ l
Probe	1.25 μ l
H ₂ O	6.25 μ l
cDNA	5 μ l containing 5-20 ng cDNA

The following program was used for PCR reaction:

50°C	2 min	
95°C	10 min	
95°C	15 sec	} 40x
60°C	1 min	

DNA quantification was performed during strand polymerization using fluorescent reporter probes that bind specifically to the target gene. The probes are coupled to a fluorescent dye at the 5' probe end and a quencher at the 3' probe end suppressing reporter fluorescence. During strand elongation, the DNA polymerase-intrinsic 5' to 3' exonuclease activity catalyzes probe breakdown resulting in a spatial dissociation of the quencher from the reporter. The released reporter, in turn, can become excited to fluoresce. Increasing amplicon amounts, thus, lead to a proportional increase of fluorescence intensity. A threshold for the detection of reporter fluorescence is set slightly above the background signal and the number of cycles at which the fluorescence exceeds the threshold is denoted as threshold cycle (C_t). Relative quantification of gene expression was performed by using the ΔC_t -method, i.e. a normalization of the target gene C_t value to the C_t value of the housekeeping gene glyceraldehyde 3-phosphate dehydrogenase (GAPDH). Relative expression changes are presented as $2^{-\Delta C_t}$.

4.2.5.6 RNA *in vitro* transcription

RNA *in vitro* transcription constitutes a method to amplify small amounts of RNA. Generally, the RNA is reversely transcribed into copy DNA (cDNA) that serves as matrix for the subsequent RNA transcription. For gene expression analysis in sorted or cultivated monocytes, the isolated RNA was amplified by two rounds *in vitro* transcription using the TRinucleotide mRNA amplification Pico Kit (amptec) according to the manufacturer's protocol. Briefly, isolated RNA was reversely transcribed into cDNA. After DNA purification on the provided silica matrix-based spin columns, RNA was synthesized overnight by *in vitro* transcription of the cDNA. After RNA purification using silica gel matrix spin columns, a second round of cDNA transcription and RNA synthesis was performed to further increase RNA yield.

4.2.6 Protein biochemistry

4.2.6.1 Protein extraction and assessment of protein concentration

Scar tissue was homogenized in Protein Extraction Reagent Type 4 (Sigma). After centrifugation at 8000 g and 4°C for 10 min, the supernatant was used for subsequent analyses. Protein was quantified using the Qubit fluorometer (see above). Samples were stored at -80°C.

4.2.6.2 Electrophoretic protein separation (SDS-PAGE)

Proteins were separated in a polyacrylamide gel electrophoresis (PAGE) on the basis of their molecular weight. Gels were produced according to the following formulae:

Stacking gel (5%):	ddH ₂ O	4.1 ml
	30% acrylamide	1 ml
	1M Tris (pH 6.8)	0.75 ml
	10% Sodium dodecyl sulfate (SDS)	0.06 ml
	10% ammonium persulfate	0.06 ml
	TEMED	0.006 ml
Resolving gel (15%):	ddH ₂ O	4.6 ml
	30% acrylamide	6 ml
	1.5M Tris (pH 8.8)	3.8 ml
	10% SDS	0.15 ml
	10% ammonium persulfate	0.15 ml
	TEMED	0.006 ml

Gels were manufactured in a Mini-gel chamber from Bio-Rad. At first, the resolving gel was polymerized between the two glass plates and covered with isopropyl alcohol. The stacking gel was loaded onto the resolving gel and inserted with a comb to spare the sample pockets. The chamber was filled with running buffer and samples were loaded into the pockets. Voltage was set to constant 100V. Separation was stopped when the resolution was adequate in the region of interest.

4.2.6.3 Sample preparation for SDS-PAGE

20 µg of total protein were boiled for 5 min at 95°C in Laemmli buffer containing β-mercapthoethanol (β-ME). The high temperature, β-ME and SDS assured protein denaturation and breakdown of the disulfide bridges. After protein unfolding, the anionic SDS molecules bind to the polypeptides and outweigh their intrinsic charge. The mechanism safeguards protein separation according to their molecular mass, and not due to interfering effects of protein-intrinsic charge. As the gel constitutes a micro-sieve, small proteins wander at higher velocity along the electric field as compared to higher molecular proteins. As a consequence, proteins are separated according to their molecular mass.

4.2.6.4 Western blot and protein detection

SDS-PAGE-separated proteins were transferred from the gel onto a nitrocellulose membrane by so-called “semi-dry” blotting. Filter papers, membrane and gel were equilibrated in transfer buffer and stacked within a transfer chamber that was energized at constant 20V. The transfer was stopped after 120 min and transfer efficiency evaluated by unspecific protein staining using Ponceau S.

Target proteins on the membrane were specifically detected by antibodies. To prevent unspecific antibody binding, the membrane was blocked in 5% non-fat dry milk in TBST (w/v) for 1 hour. The membrane was incubated overnight at 4°C in 5% nonfat dry milk/ TBST containing the primary antibody diluted to a concentration according to the manufacturer’s recommendation. After three 10 min washing steps in TBST, a horseradish peroxidase (HRP)-conjugated secondary antibody directed against the primary antibody was diluted in TBST and incubated with the membrane for 1 hour. After 5 additional 5 min washing steps, the membrane was incubated in a detection reagent containing luminol that emits light during HRP-mediated cleavage. The detection reagent was mixed immediately before usage (1 ml solution A, 100 µl solution B, 0.3 µl H₂O₂). Chemoluminescence was detected using a LI-COR C-DiGit luminescence scanner.

4.2.6.5 Membrane stripping

In order to detach antibodies, the membrane was incubated for 20 min in stripping buffer at 50°C. After washing in TBST, the membrane was blocked again in TBST/ 5% non-fat dry milk and, subsequently, incubated with a primary antibody.

4.2.7 Optical imaging

4.2.7.1 Immuno-/ histochemical stainings on paraffin sections

4.2.7.1.1 Preparation of paraffin sections

After fixation for 24 hours in 4% formaldehyde, the tissue was put into a tissue cassette and dehydrated by successively increasing ethanol concentrations in the tissue environment. Subsequently, ethanol was replaced by xylene and ultimately by paraffin. The following dehydration protocol was used:

- | | |
|-----------------------------|--------------------------------------|
| 1. 70 % ethanol: 1 h | 6. 100 % xylol: 1,5 h |
| 2. 90 % ethanol: 1 h | 7. 50:50 xylol:paraffin: 1 h at 60°C |
| 3. 96 % ethanol: 5 h | 8. 100 % paraffin: 1,5 h at 60°C |
| 4. 50:50 xylol:ethanol: 1 h | 9. 100 % paraffin: 3 h at 60°C |
| 5. 100 % xylol: 1,5 h | |

Eventually, tissue was embedded in liquid paraffin at 68°C for conservation. After paraffin curing at room temperature, tissue blocks were sliced into 5 µm and 7 µm sections using a microtome and transferred onto glass slides. Paraffin sections were deparaffinized and rehydrated by successively decreasing the content of organic solvents according to the following protocol:

- | | |
|---------------------|-------|
| 1. rotihistol | 1 min |
| 2. xylene | 1 min |
| 3. xylene:ethanol | 5 min |
| 4. ethanol 96 % | 5 min |
| 5. ethanol 75 % | 5 min |
| 6. ethanol 50 % | 5 min |
| 7. H ₂ O | 5 min |

4.2.7.1.2 Picrosirius red staining

Picrosirius red (PSR) binds specifically to collagen fibers indicating the infarcted region where cardiomyocytes have been replaced by a collagenous scar. For PSR staining, rehydrated 7 μm paraffin tissue sections were stained in PSR solution for 20 min. Sections were dehydrated, mounted in entellan and stored at room temperature.

4.2.7.1.3 Ladewig staining

The Ladewig trichrome staining provides insight into collagen fiber arrangement a histomorphological evaluation of parenchyma integrity and leukocyte infiltrate. Ladewig staining indicates collagen fibers in blue, nuclei in black and the cytoplasm in red and erythrocytes in orange. Staining was conducted using the Ladewig kit from Morphisto. Rehydrated 5 μm paraffin sections were stained for 3 minutes in the provided Weigert's iron hematoxylin solution and subsequently washed for several times in tap water. Sections were incubated in phosphoric acid (1% w/ v) for 5 min, washed in desalted water and incubated in Ladewig staining solution for 3.30 min. After dehydration, slides were mounted with entellan and stored at room temperature.

4.2.7.1.4 Alpha smooth muscle actin staining

To assess myofibroblast numbers in the healing myocardium, alpha smooth muscle actin (α -SMA) was stained immunohistochemically using the Dako ARK™ peroxidase kit. On dehydrated sections, tissue-endogenous peroxidases were inactivated for 5 min by incubation in peroxidase blocking reagent containing H_2O_2 . The anti- α -SMA monoclonal antibody (clone 1A4, Dako) was biotinylated in antibody diluent for 15 min and the antibody solution afterwards supplemented with the provided blocking reagent. Sections were incubated in presence of the antibody/ blocking reagent for 15 min at a final antibody dilution of 1:50. After washing, sections were covered with the provided HRP-conjugated streptavidin solution for 15 min. For visualization, the chromogen 3,3'-diaminobenzidine (DAB, Abcam) was used according to the manufacturer's protocol indicating α -SMA-positive cells after HRP-mediated DAB conversion into a brown chromophor. After washing, sections were stained with hematoxylin solution for 5 min, washed and mounted with entellan for light microscopy.

4.2.7.2 Immunofluorescence staining of Foxp3

Immunofluorescence microscopy is characterized by visualization of cells or sub-cellular components utilizing fluorophores. Frequently, protein labeling is achieved by fluorophore-conjugated antibodies directed against the target. After excitement with light of specific quality, fluorophores emit light in a defined wave length range. The usage of appropriate fluorophore and filter combinations allows the simultaneous visualization of different targets. The microscope, aperture, photo-multiplier and filters are operated from the computer.

Tissue-Tek-covered samples were sliced into 5 μm sections using a cryo-microtome. Cryosections were fixed in 4% formaldehyde for 10 min and permeabilized in 0.5% dodecyltrimethylammonium with a 5 min PBS washing step in between. Sections were blocked in PBS containing 5% fetal calf serum for 30 min. After blocking, sections were covered with blocking buffer containing rat anti-mouse Foxp3 (clone FJK-16s) diluted 1:100 and incubated for 45 min. After two washing steps in PBS, an Alexa555-conjugated goat antibody directed against rat immunoglobulins diluted 1:200 in PBS was added and sections incubated for 30 min. Additionally, Alexa488-conjugated phalloidin was added (1:200) to stain filamentous actin. Nuclei were stained using DAPI. After washing, sections were mounted using Vectashield mounting medium (Vector laboratories). Samples were stored in the dark at 4°C.

4.2.7.3 Image acquisition

Bright-field images were acquired using an Axioskop 2 plus (Zeiss). For acquisition of immunofluorescence images, a Z1m Imager epifluorescence microscope (Zeiss) equipped with appropriate filter sets was employed.

4.2.8 Infarct size determination

To evaluate infarct size, PSR-stained cross-sections of the left ventricle were photographed at 25-fold magnification. Endocard and epicard length of the infarct zone were assessed using ImageJ software. The infarct size was calculated after assessment of both the entire left-ventricular endocard and epicard perimeter.

4.2.9 Evaluation of collagen content in the scar

Collagen content was assessed by using circularly polarized light microscopy¹⁶⁷. Collagen fibers have anisotropic properties and show birefringence under polarized light that is further enhanced by PSR. From each sample, one image was acquired using polarized light and a second image under bright-field illumination. The latter image was resolved into its cyan, yellow, magenta and black components using SigmaScan Pro. In the black-component image, collagen fibers appear dark gray/black while non-collagen elements appear light gray/ white. In contrast, the image acquired by polarized light illumination shows collagen fibers as bright structures and non-collagen elements as dark structures. Digital subtraction of the “non-collagen” area in the black-component image from the polarized light image eliminates the area of interstitial and parenchymal space. The remaining image of “pure” collagen was kept for further analysis. The color of PSR-stained collagen fibers viewed with polarized light depends on fiber thickness. As fiber thickness increases, the color changes from green to yellow/ orange and red. In order to determine the collagenous area, the image depicting pure collagen was resolved into its hue (color), saturation and value. From the hue component, a histogram of hue frequency was obtained. Hue range smaller 129 was considered as collagen. The number of collagen pixels in the hue range was normalized to the total number of pixels in the image indicating the relative collagen area in the scar.

4.2.10 Statistics

Data are presented as mean value and SEM per group. For two group comparison, a Wilcoxon signed rank-sum test or, if suitable, an unpaired t test was conducted. For multiple comparisons, a one-way ANOVA was performed. Survival is shown as Kaplan-Meier curve analyzed by a log-rank test. Variance in a group was evaluated using the χ^2 test. Group values were considered significantly different at $P < 0.05$. Data analysis was performed using GraphPad Prism 4.03.

5 Results

5.1 Both conventional and Foxp3⁺ regulatory CD4⁺ T lymphocytes become activated in response to MI

To test whether CD4⁺ T cells become activated after MI, the expression of T cell activation markers was evaluated in infarcted and sham-operated mice. As T cell priming takes place in lymph nodes that drain the inflamed organ, heart-draining lymph nodes in the mediastinum were analyzed for CD4⁺ T cell proliferation. On day 7 post-MI, the frequency of CD4⁺ T cells that expressed the proliferation marker Ki67 was significantly increased as compared to sham-operated mice, indicating CD4⁺ T cell activation in lymph nodes after MI (Fig. 7A, B).

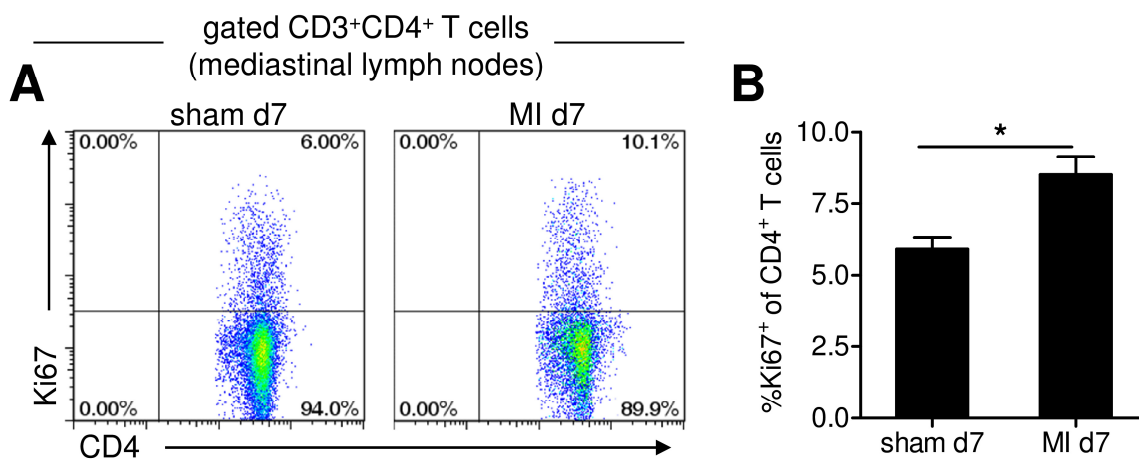


Fig. 7: CD4⁺ T cell proliferation after MI. Representative FACS plots (A) and the related analysis (B) showing the frequency CD4⁺ T cells expressing the proliferation marker Ki67 in heart-draining lymph nodes 7 days post-MI (n=4-5 per group, **P*<0.05).

To evaluate whether conventional or regulatory CD4⁺ T cells become activated after MI, both subsets were analyzed for the expression of the activation marker CD25. Compared to sham-operated mice, infarcted animals showed elevated frequencies of CD25-positive cells among conventional Foxp3-negative CD4⁺ T cells 3 days after MI (Fig. 8A, B), and absolute numbers of Foxp3⁻CD4⁺ T cells increased over time (Fig. 8C). However, 56 days post-MI, the conventional CD4⁺ T cell compartment had contracted again to baseline levels (Fig. 8C).

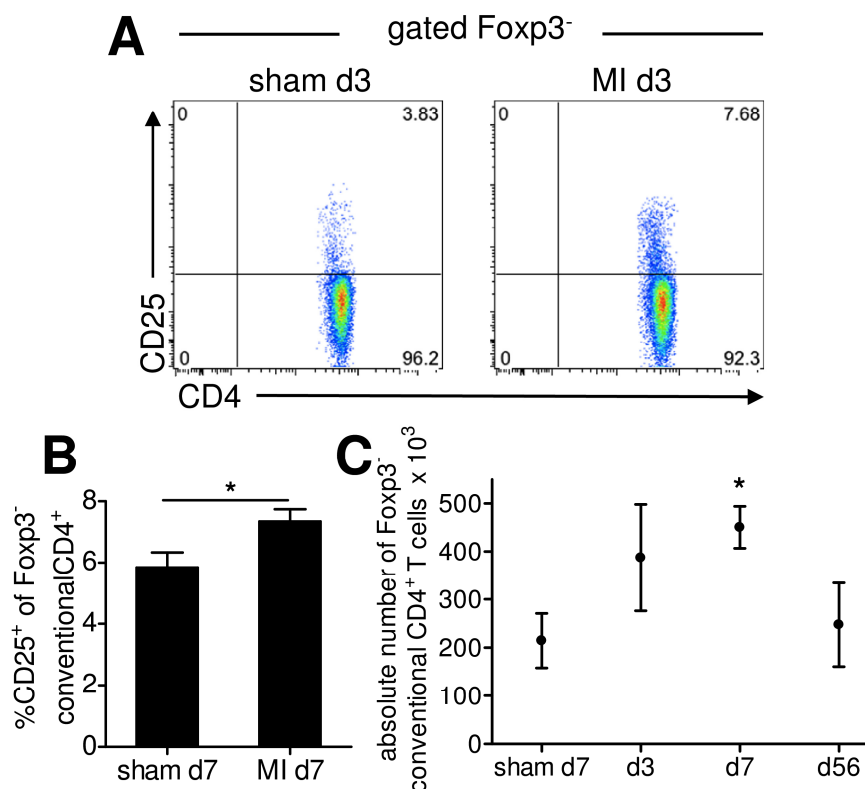


Fig. 8: Activation and expansion of Foxp3-negative conventional T cells. A: Representative FACS plots showing CD25 expression on Foxp3-negative conventional cells. B: Frequencies of CD25-positive cells among conventional CD4⁺ T cells (n=11-16 per group, * $P < 0.05$). C: Absolute numbers of Foxp3-negative CD4⁺ T cells in heart-draining lymph nodes (n=5-7 per group, $P < 0.05$).

Similar to the activation of Foxp3-negative CD4⁺ cells, Foxp3⁺ T_{reg} cells upregulated CD25 expression on a per-cell basis after MI as compared to sham-operated mice (Fig. 9A). The frequency of Foxp3⁺ cells among CD4⁺ T cells increased over time indicating that T_{reg} cell proliferation overcame the expansion of conventional CD4⁺ T cells (Fig. 9B). Elevated frequencies of Foxp3⁺ cells persisted even after completion of healing and were still evident 56 days post-MI. In accordance with the observation that T_{reg} cells become activated after MI, absolute T_{reg} cell numbers escalated in heart-draining lymph nodes over time (Fig. 9C).

Conclusively, both Foxp3-negative conventional and Foxp3⁺CD4⁺ regulatory T cells became activated after MI and expanded in heart-draining lymph nodes.

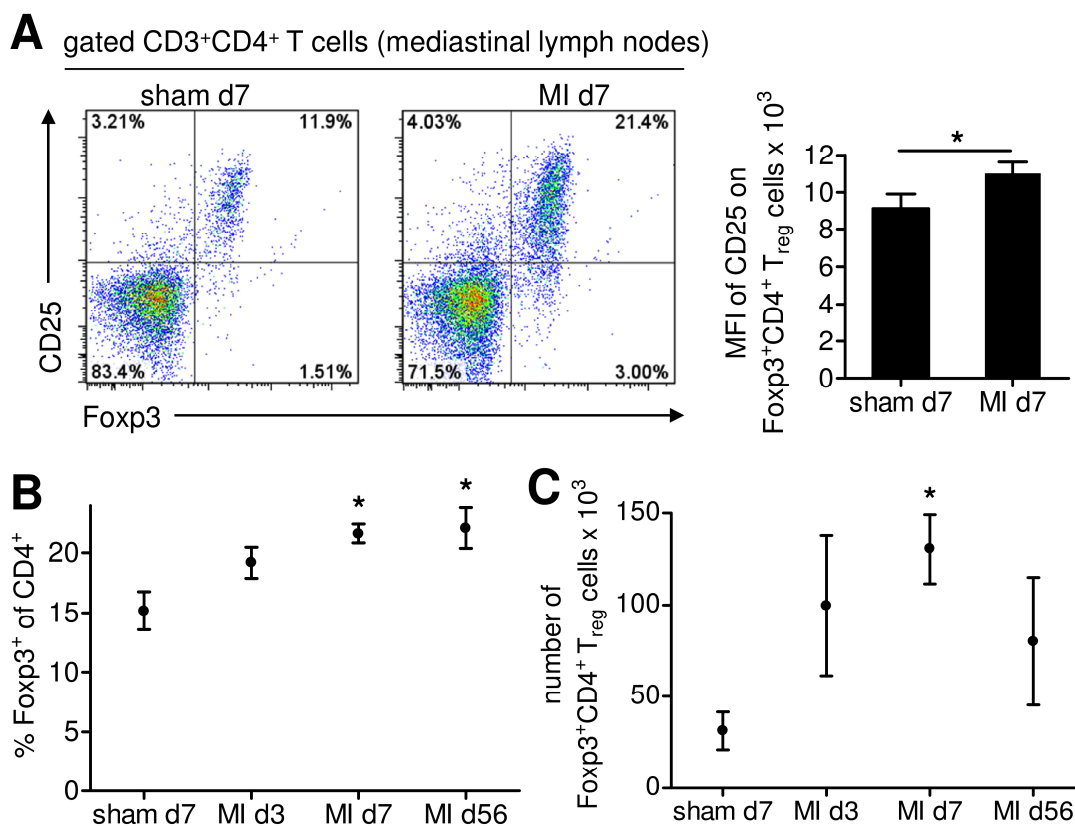


Fig. 9: Activation and expansion of T_{reg} cells in heart-draining lymph nodes. A: Representative FACS plots and analysis of CD25 expression on T_{reg} cells (right, n=3-4, *P<0.05). B: Frequency of Foxp3⁺ cells among CD4⁺ T cells (n=4-7 per group, *P<0.05 vs. sham d7). C: Absolute T_{reg} cell numbers (n=4-6 per group, *P<0.05). (Weirather et al., Circulation Research, 2014¹⁶⁸)

5.2 CD4⁺ T Lymphocytes infiltrate the myocardium after MI

Having observed that CD4⁺ T cells become activated after MI, T cell infiltration into the healing myocardium was evaluated. Compared to sham-operated animals, the proportion of Foxp3⁺ cells among CD4⁺ T cells, but also absolute T_{reg} cell numbers in the infarct zone increased over time (Fig. 10A, B), whereas numbers of conventional CD4⁺ T cells escalated only by trend (Fig. 10C). As the FACS data indicated that T_{reg} cell accumulated in the healing myocardium, their spatial distribution was evaluated using immunofluorescence microscopy. In line with the FACS analysis, Foxp3-positive cells could be found in the infarct zone (Fig. 10D). Moreover, Foxp3⁺ cells were detected in both the infarct border and the non-injured remote myocardium, i.e. still functional parenchyma that was not subjected to ischemia (Fig. 10D).

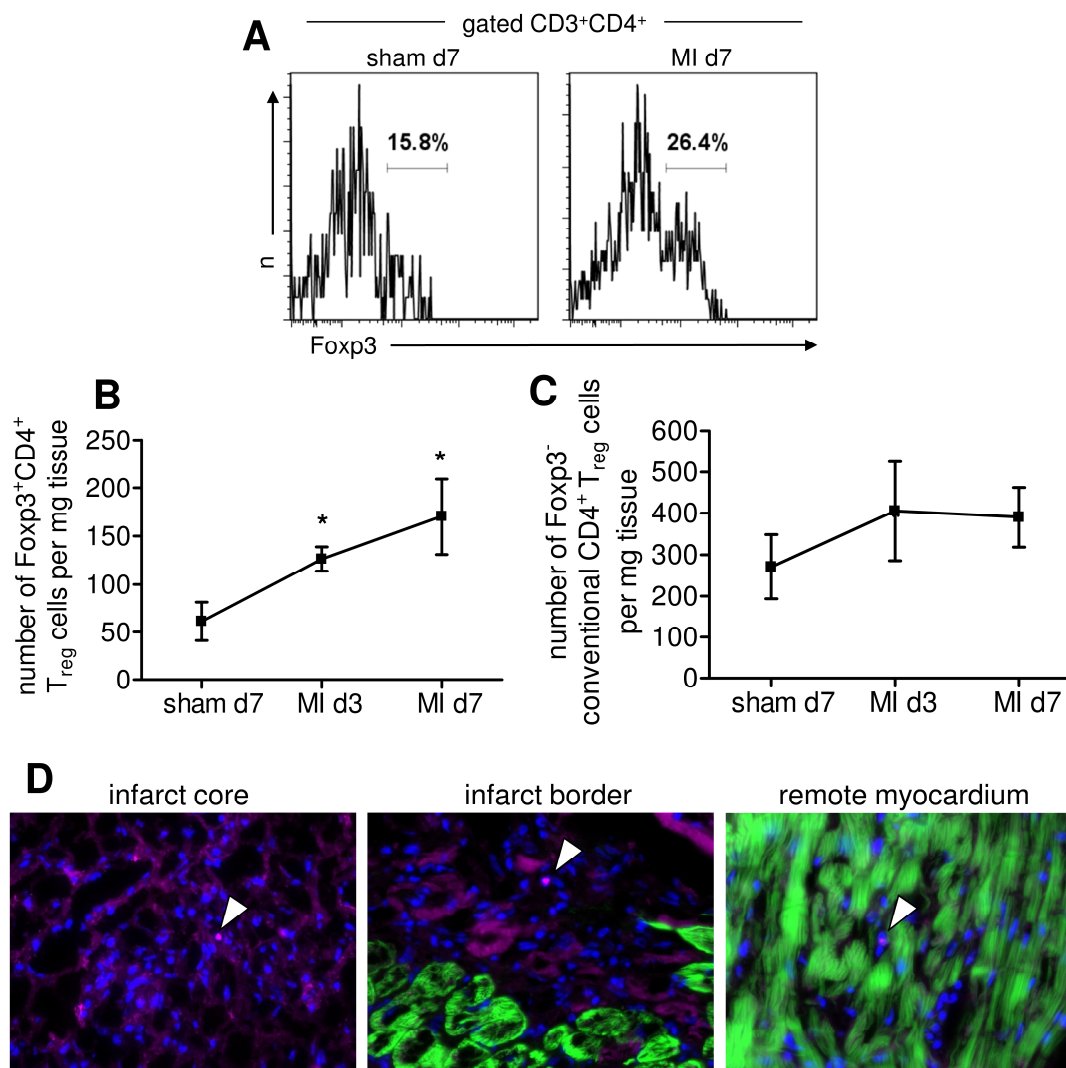


Fig. 10: CD4⁺ T cells in hearts of sham-operated or the healing myocardium of infarcted mice. A: Frequency of Foxp3⁺ cells among CD4⁺ T cells. B: Absolute T_{reg} cell numbers in the heart (n=3-8 per group, **P*<0.05). C: Absolute numbers of conventional CD4⁺ T cells in the heart (n=6-9 per group, **P*<0.05). D: Immunofluorescence microscopy of Foxp3-positive cells in the infarct core, the infarct border and the remote myocardium adjacent to the infarct zone. Foxp3-positive cells are depicted in purple (arrow heads). Phalloidin-positive surviving cardiomyocytes are shown in green. Nuclei were stained using DAPI (blue). Images were acquired at 400-fold magnification. (Weirather et al., *Circulation Research*, 2014¹⁶⁸)

5.3 Survival and wound healing are impaired in MHC class II-deficient mice

In order to reveal the functional role of CD4⁺ T cells for wound healing post-MI, permanent coronary artery ligation was induced in MHC class II-deficient mice that lack MHCII-restricted $\alpha\beta$ CD4⁺ T cells. In comparison to WT mice, MHCII KO mice showed a significantly impaired survival due to a higher incidence of left-ventricular ruptures (WT: 79% vs. MHCII KO 52%, Fig. 11A). However, infarct size, left-

ventricular remodeling or fractional shortening were not significantly different between genotypes (Fig. 11B, C, D).

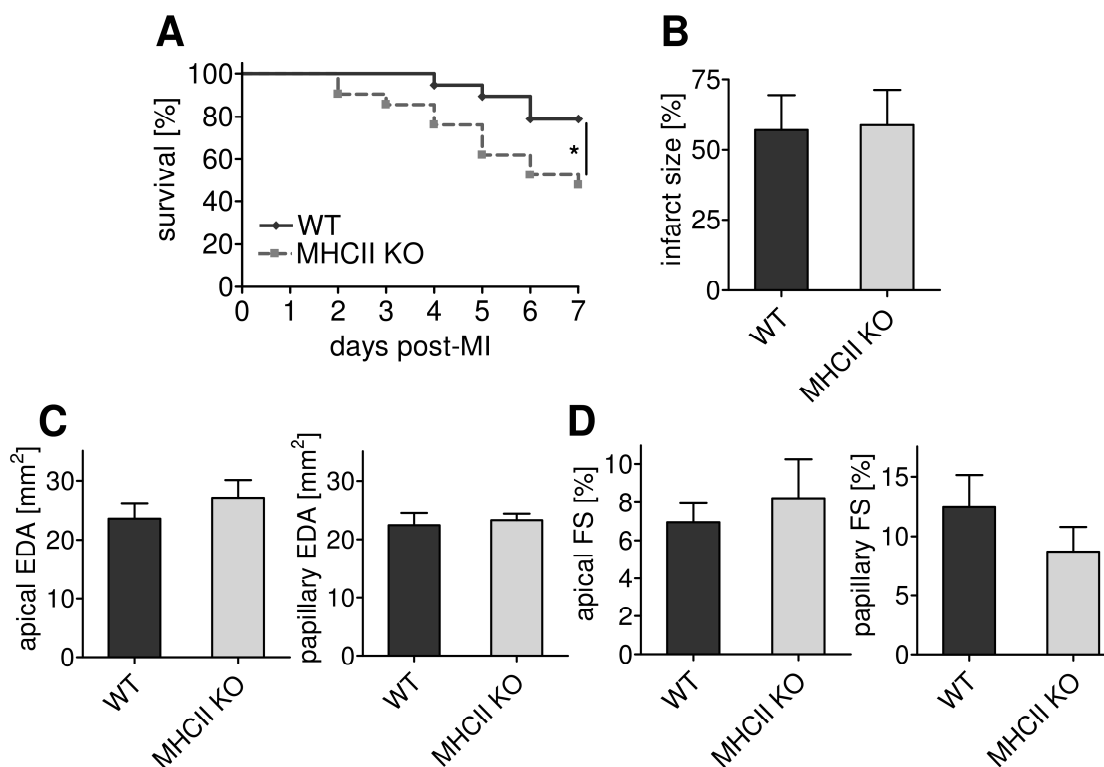


Fig. 11: Clinical outcome of wildtype (WT) and MHCII KO mice after MI. A: Cumulative survival of infarcted mice (n=19-21 per group, * $P < 0.05$). B: Infarct size 7 days after MI. C, D: Echocardiographic evaluation of end-diastolic area (EDA) and fractional shortening (FS) in infarcted mice 7 days after MI. (Hofmann, Beyersdorf, Weirather et al., *Circulation*, 2012¹⁶⁹)

The prevalence of infarct ruptures in MHCII KO mice spurred an evaluation of the scar tissue integrity. Compared to WT mice, MHCII KO littermates showed a reduced collagen density and disarrayed collagen fiber deposition in the infarct zone on day 7 post-MI as evaluated by Ladewig staining (Fig. 12A). Collagen density in the infarct zone was assessed by polarized light microscopy of Picrosirius Red (PSR)-stained LV cross-sections. As compared to WT littermates, less collagen per unit area was found in MHCII KO mice, indicating that scarring was disturbed these animals (Fig. 12B, C).

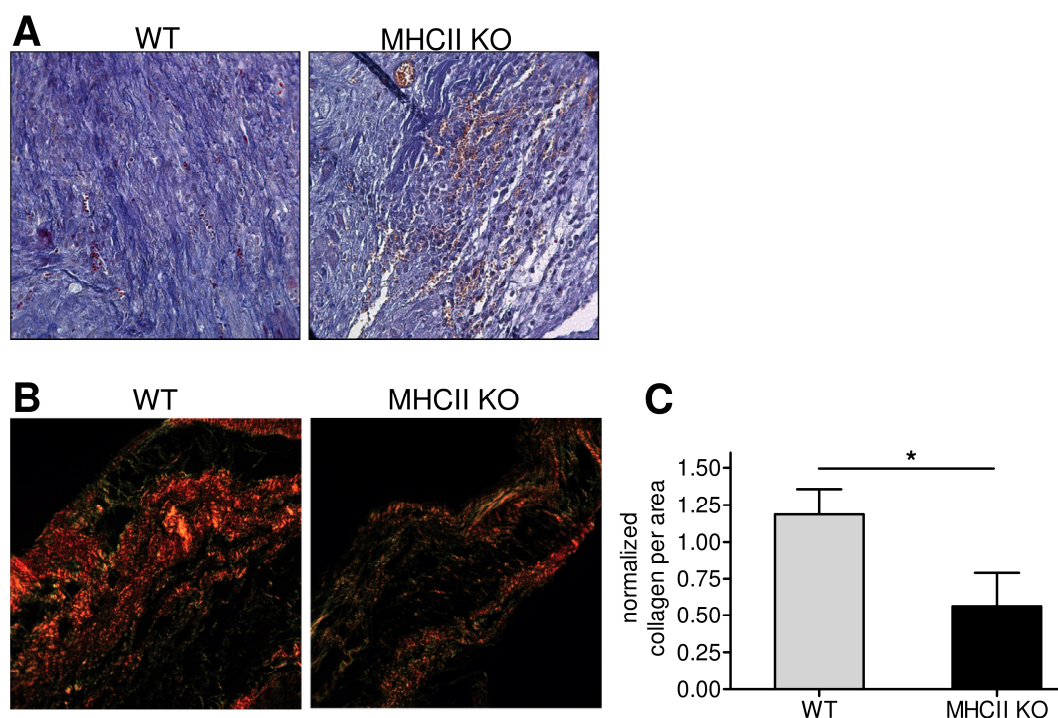


Fig. 12: Scar tissue formation in infarcted wildtype and MHCII KO mice. A: Representative images showing the infarct core 7 days post-MI after Ladewig staining. Collagen fibers are stained blue, nuclei black, erythrocytes orange and cytoplasm red. Images are shown at 400-fold magnification. B: Representative images showing PSR-stained collagen (red) by polarized light microscopy. Images were acquired at 200-fold magnification. C: Normalized proportion of the collagen amount in the infarct zone of wildtype (WT) and MHCII KO mice (n=3-4 per group, * $P < 0.05$). (Hofmann, Beyersdorf, Weirather et al., *Circulation*, 2014¹⁶⁹)

In summary, compared to WT animals, MHCII KO mice were characterized by an increased mortality due to a disturbed scar tissue formation that resulted in a higher prevalence of left-ventricular ruptures.

5.4 Survival and wound healing are impaired in OT-II mice

To address whether the mere absence or functional deficits of $CD4^+$ T cells were responsible for the fatal clinical outcome of MHCII KO mice, MI was induced in OT-II mice. In these animals, most $CD4^+$ T cells bear a transgenic TCR specific for an ovalbumin-derived peptide presented in the context of MHC class II. As the TCR repertoire in the $CD4^+$ T cell compartment is highly limited in OT-II mice, the vast majority of $CD4^+$ T cells cannot recognize self-peptides such as auto-antigens released during myocardial injury. Compared to WT animals, OT-II mice showed, similar to MHCII KO mice, a significantly impaired survival due to a prevalence of left-ventricular ruptures. By day 56, survival was 77% in WT and 49% in OT-II mice (Fig.

13A). Regarding infarct size, left-ventricular remodeling or fractional shortening, no differences were found between genotypes (Fig. 13B, C, D). As OT-II mice deceased primarily due to left-ventricular ruptures in the first 7 days post-MI, scar tissue formation was assessed. Similar to MHCII-deficient animals, Ladewig staining revealed a decreased collagen density and disarrayed collagen fiber alignment in the infarct zone of OT-II mice as compared to WT animals (Fig. 13E).

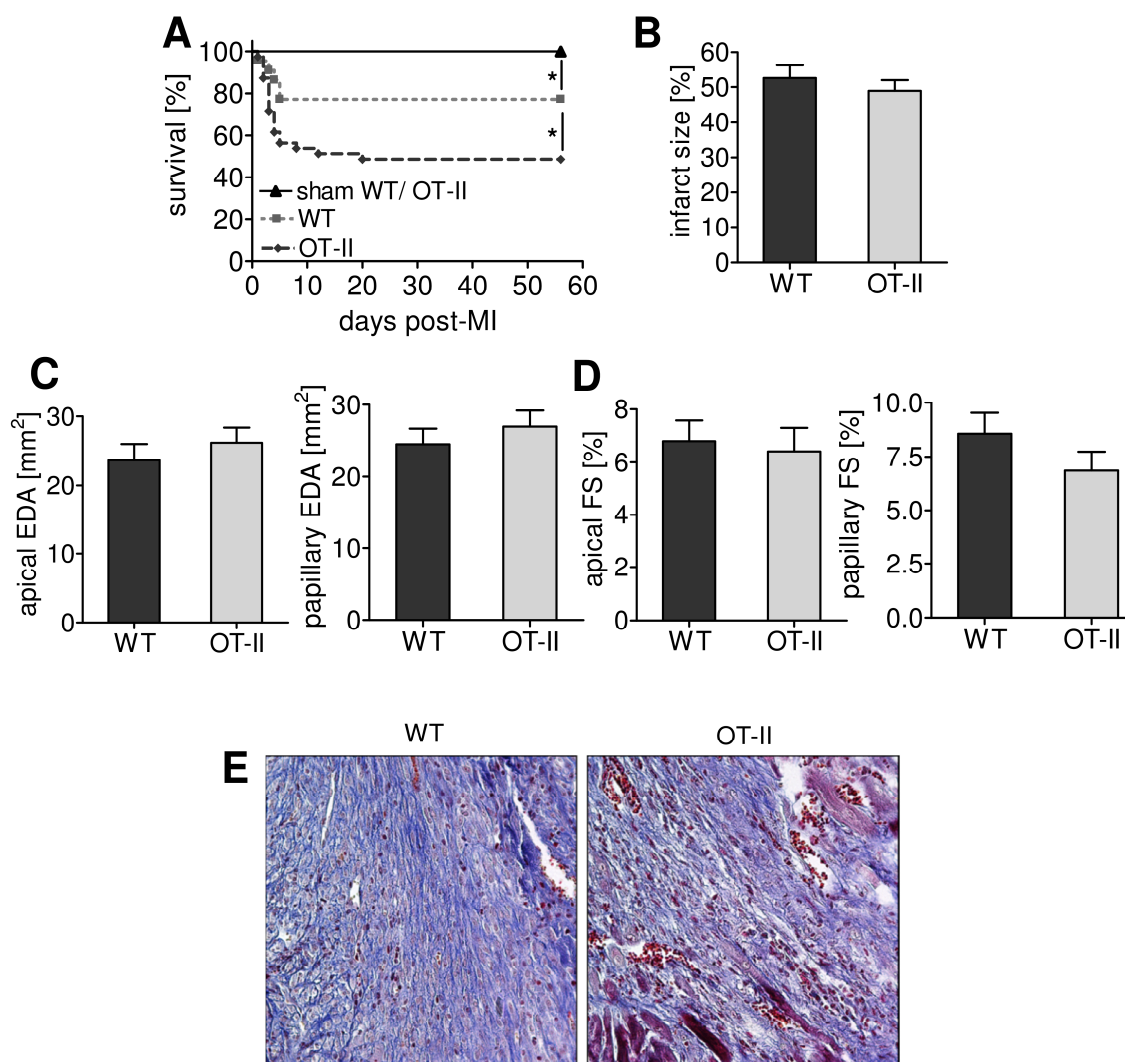


Fig. 13: Clinical outcome of wildtype (WT) and OT-II mice. A: Cumulative survival after MI or sham surgery (n=39-44, * $P < 0.05$). B: Infarct size 7 days after MI. C, D: End-diastolic area (EDA) and fractional shortening (FS) 7 days after MI. E: Representative images showing the infarct core 7 days post-MI after Ladewig staining. Collagen fibers are stained blue, nuclei black and cytoplasm red. Images are shown at 400-fold magnification. (Hofmann, Beyersdorf, Weirather et al., *Circulation*, 2012¹⁶⁹)

In summary, the clinical postinfarction phenotype of OT-II mice closely resembled the phenotype of MHCII KO mice characterized by impaired survival and disturbed scar

tissue formation that ultimately led to a higher incidence of left-ventricular ruptures. The data indicates that antigen recognition by CD4⁺ T cells constitutes an indispensable prerequisite for proper and organized infarct healing.

5.5 Activation of conventional and regulatory CD4⁺ T cells in response to MI depends on antigen recognition

Having observed that antigen recognition by CD4⁺ T cells is crucial for wound healing post-MI, activation and expansion of both conventional and regulatory T cells was studied in heart-draining lymph nodes. On day 3 after MI induction, WT animals showed, compared to sham-operated WT mice, increased frequencies of CD25-positive cells among Foxp3-negative conventional CD4⁺ T cells indicating T cell activation in these mice (Fig. 14A, B). In contrast, CD4⁺ conventional T cells in infarcted OT-II mice did not show upregulated CD25 levels as compared to sham-operated OT-II animals (Fig. 14A, B). Similarly, Foxp3⁺ T_{reg} cell frequencies were elevated in infarcted WT mice in comparison to sham-operated WT controls, but not in infarcted OT-II mice as compared to OT-II sham controls (Fig. 14A, C). Consistently, on day 7 post-MI, both absolute numbers of conventional and regulatory T cells were increased in heart-draining lymph nodes of wildtype mice, but not in TCR transgenic OT-II mice (Fig. 14D).

Collectively, the activation of both conventional and regulatory CD4⁺ T cells after MI is strictly antigen-dependent and requires antigen recognition via the TCR.

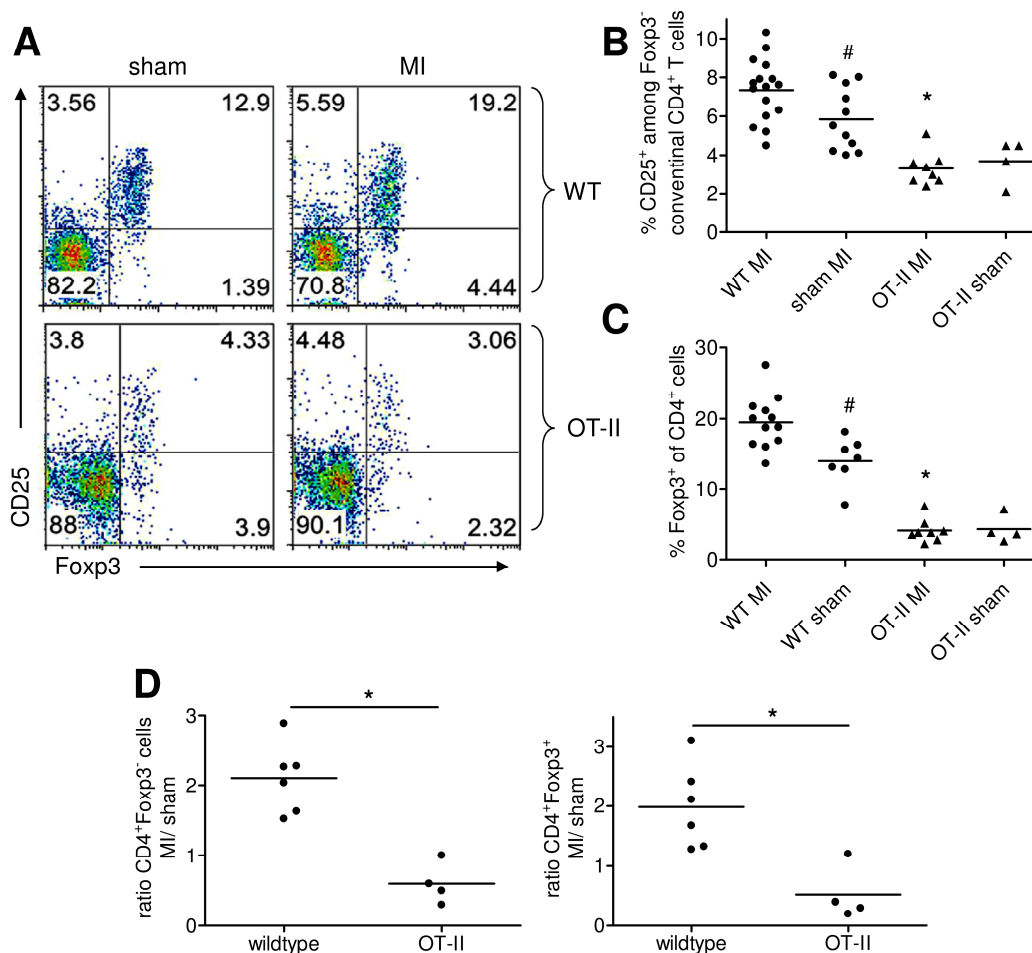


Fig. 14: Activation and expansion of conventional CD4⁺ T cells and Foxp3⁺CD4⁺ T cells in heart-draining lymph nodes of wildtype (WT) and OT-II mice 7 days after MI. A: Representative FACS plots showing CD25 expression on conventional Foxp3⁻CD4⁺ cells and Foxp3⁺CD4⁺ cells. B: Evaluation of CD25 upregulation on Foxp3⁻CD4⁺ T cells (# $P < 0.05$ vs. WT MI, * $P < 0.05$ vs. sham MI). C: Analysis of Foxp3⁺ frequencies among CD4⁺ cells (# $P < 0.05$ vs. WT MI, * $P < 0.05$ vs. sham MI). D: Ratio of CD4⁺ T cell numbers to CD4⁺ T cell numbers in sham-operated mice. Left: Fold-change of Foxp3-negative conventional CD4⁺ T cells. Right: Fold-change of Foxp3⁺CD4⁺ T_{reg} cells (* $P < 0.05$). (Hofmann, Beyersdorf, Weirather et al., Circulation, 2012¹⁶⁹)

5.6 Specific diphtheria toxin-induced T_{reg} cell ablation in DEREG mice leads to increased infarct size and deteriorated cardiac function.

The observation that CD4⁺ T cell crucially influence healing and clinical outcome after MI raised the question for the mechanistic link between CD4⁺ T cell activation and scar tissue construction as well as cardiac inflammation. Hypothesizing that anti-inflammatory T_{reg} cells, but not conventional T cells facilitate wound healing after MI spurred additional experiments focusing on the functional relevance of T_{reg} cells in postinfarction healing and remodeling.

To test whether T_{reg} cells influence healing and clinical outcome after MI, the T_{reg} cell compartment was specifically ablated by diphtheria toxin (DTX) administration to DEREG mice in which $Foxp3^+$ cells transgenically express the human DTX receptor. T_{reg} cells were depleted 2 days prior to MI induction. To prevent a T_{reg} cell rebound from the bone marrow, DTX was additionally injected on day 2 and day 4 after surgery. In comparison to DTX-treated wildtype littermates, DEREG mice exhibited an efficient depletion of $Foxp3^+$ cells from the peripheral blood and the heart-draining lymph nodes at the time point of MI induction (Fig. 15). Moreover, accumulation of T_{reg} cells in the healing myocardium was prevented in DEREG mice (Fig. 15).

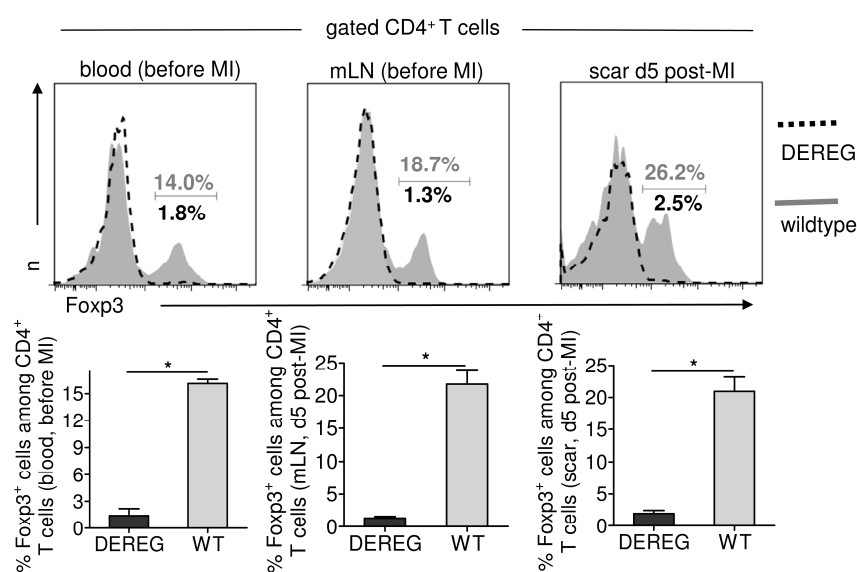


Fig. 15: Evaluation of T_{reg} cell depletion in DEREG mice. Representative FACS plots and quantitative analyses showing the frequency of $Foxp3^+$ cells among $CD4^+$ T cells in blood, mediastinal lymph nodes and the healing myocardium of diphtheria toxin-treated wildtype and DEREG mice. (Weirather et al., *Circulation Research*, 2014¹⁶⁸)

T_{reg} cell depletion had no impact on the cumulative survival (Fig. 16A). However, DTX-treated DEREG mice showed significantly larger infarcts as compared to DTX-treated wildtype littermates (Fig. 16B). Furthermore, lung weight to body weight ratios were increased in T_{reg} cell-deficient mice indicating pulmonary edema due to impaired cardiac output (Fig. 16C). To evaluate whether T_{reg} cell ablation would influence remodeling and cardiac function, non-invasive echocardiography was performed at baseline, on day 3 and on day 7 post-MI. At baseline, no differences in echocardiographic parameters were found between the groups (data now shown).

However, compared to T_{reg} cell-sufficient mice, T_{reg} cell-depleted animals exhibited a tendency towards an increased left-ventricular dilatation on day 7 post-MI (Fig. 16D). Moreover, apical fractional shortening was significantly impaired on day 3 and, by trend, on day 7 post-MI, indicating deteriorated LV contractile function in T_{reg} cell-deficient mice (Fig. 16E).

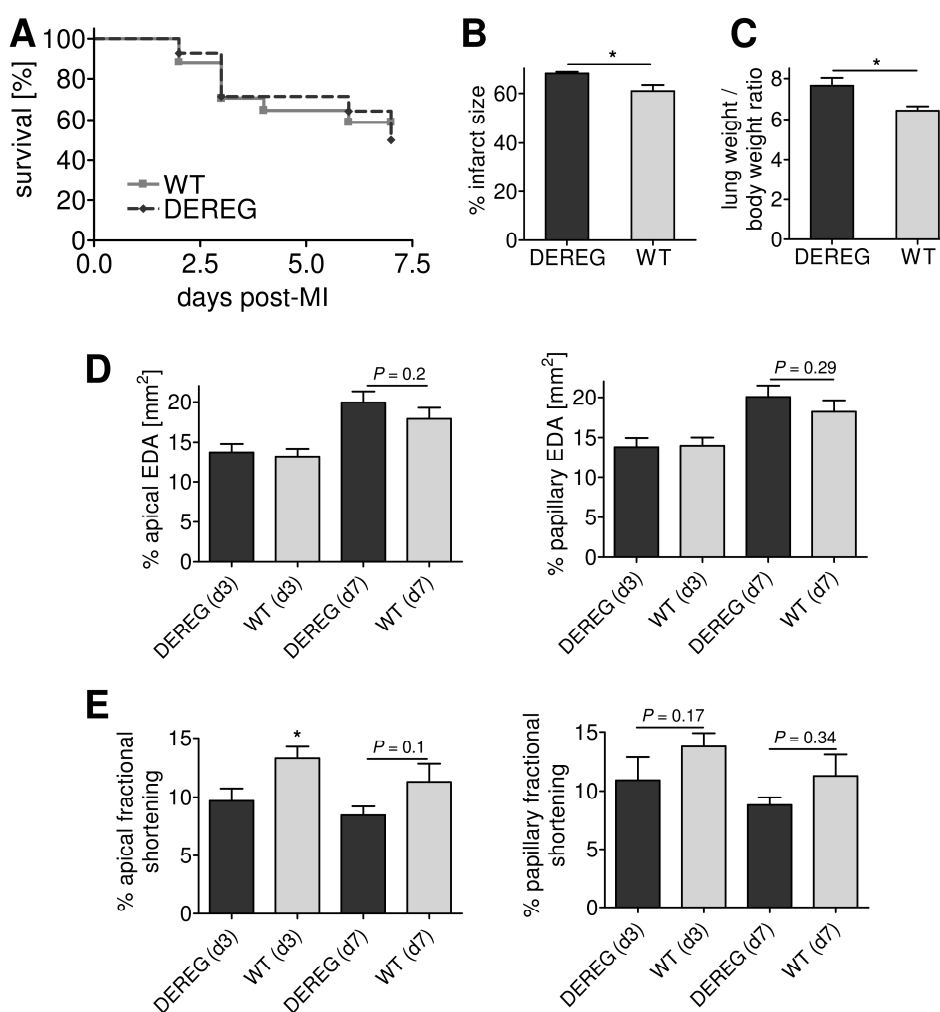


Fig. 16: Clinical outcome of T_{reg} cell-sufficient wildtype (WT) and T_{reg} cell-ablated DEREg mice after MI. A, B: Survival (n=14-17) and infarct size 7 days post-MI (n=8-11, * $P < 0.05$). C: Apical end-diastolic area (EDA) on day 7 after MI (n=8-11 per group, * $P < 0.05$). D: Percentage of apical fractional shortening (FS) on day 3 and day 7 (n=8-11 per group, * $P < 0.05$). E: Lung weight to body weight ratios (n=8-11 per group, * $P < 0.05$). (Weirather et al., Circulation Research, 2014¹⁶⁸)

To evaluate if disturbed scar tissue formation was responsible for the observed cardiac deterioration in DEREg mice, the expression of pro-collagens as well as collagenolytic enzymes was assessed. Compared to DTX-treated WT mice, T_{reg} cell-depleted DEREg mice did not show differences regarding pro-collagen alpha 1 (III)

and pro-collagen alpha 1(I) expression that predominantly contribute to the early postinfarction scar tissue construction (Fig. 17A). Matrix metalloproteinases (MMPs) catalyse the collagen turnover in the healing myocardium. As MMP-2 and MMP-9 have been demonstrated to critically influence LV remodeling, the expression of both enzymes was assessed. At the mRNA level, however, no differences regarding MMP-2 and MMP-9 mRNA synthesis were found between the groups (Fig. 17B). *In vivo*, MMPs are tightly regulated by tissue inhibitors of matrix metalloproteinases (TIMPs). As net MMP activity depends on the MMP : TIMP ratio, mRNA expression of MMP-2-regulating TIMP-2 and MMP-9-restraining TIMP-1 were additionally evaluated. Five days after MI, no differences regarding TIMP-1 and TIMP-2 expression were identified between groups (Fig. 17C).

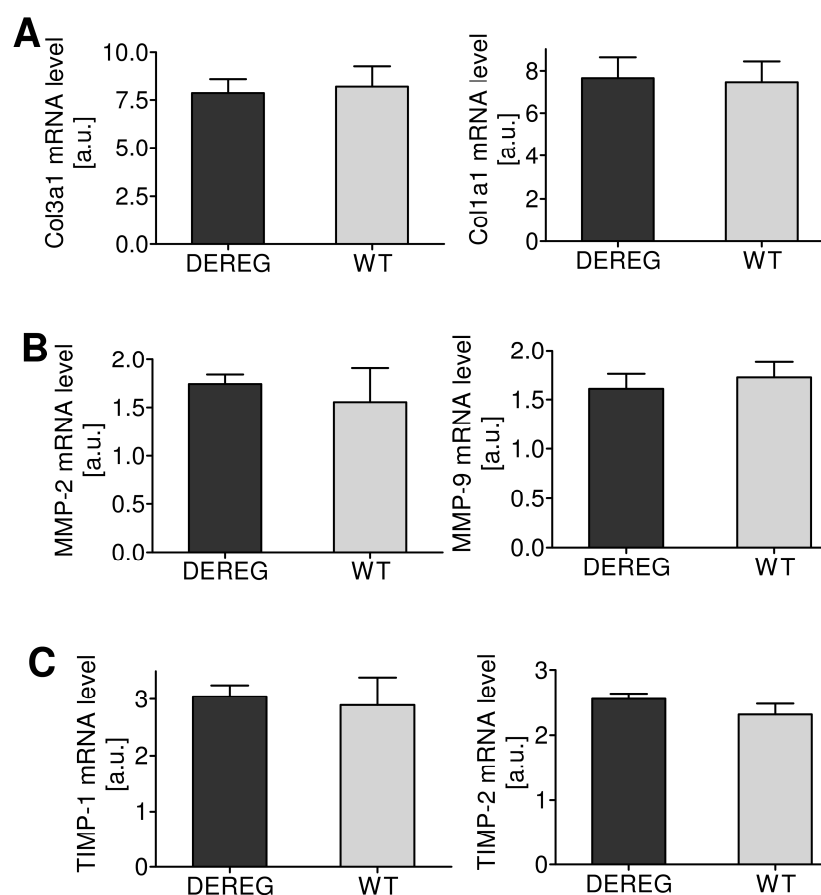


Fig. 17: Real-time RT-PCR analysis of scar-constructing collagens, collagenolytic enzymes and related inhibitors in DEREK and WT mice 5 days after MI. A: mRNA expression of pro-collagens alpha 1 (III) (Col3a1) and alpha 1 (I) (Col1a1) (n=4 per group). B: Real-time RT-PCR analysis of matrix metalloproteinase 2 (MMP-2) and MMP-9 (n=4 per group). C: tissue inhibitor of matrix metalloproteinase 1 (TIMP-1) and TIMP-2 (n=4 per group). (Weirather et al., Circulation Research, 2014¹⁶⁸)

Collectively, T_{reg} cell ablation prior to MI leads to an increased infarct size and deteriorated cardiac function.

5.7 T_{reg} cell ablation in DEREg mice leads to an accumulation of both inflammatory myeloid and T cells in the infarct zone

To elucidate the mechanism why T_{reg} cell-deficient mice exhibit a deteriorated cardiac function, the influx and polarization of both myeloid cells and T cells were evaluated. In comparison to DTX-treated WT mice, absolute numbers of $CD11b^+Ly-6G^+$ neutrophils were increased in the healing infarct of T_{reg} cell-depleted DEREg mice (Fig. 18A). Furthermore, the composition of the monocyte compartment was shifted towards the inflammatory $Ly-6C^{high}$ subset (Fig. 18B).

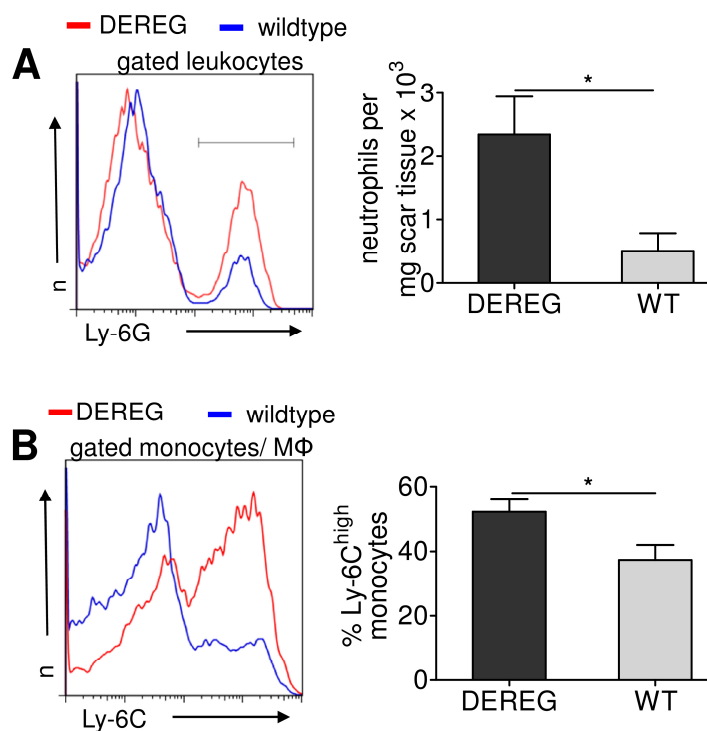


Fig. 18: Neutrophil numbers and monocyte subset composition in the infarct zone of T_{reg} cell-sufficient and T_{reg} cell-depleted mice 7 days after MI. A: Representative FACS histogram showing the proportion of $Ly-6G^+$ neutrophils among leukocytes and absolute neutrophil numbers per mg scar tissue ($n=3-6$ per group, $*P<0.05$). B: Representative FACS plot (left) and analysis (right) depicting the frequency of $Ly-6C^{high}$ monocytes among $CD11b^+Ly-6G^-$ monocytes/macrophages ($n=3-5$ per group, $*P<0.05$). (Weirather et al., Circulation Research, 2014¹⁶⁸)

As macrophages pivotally modulate postinfarction healing, monocyte/ macrophage polarization in the infarct zone was evaluated. To address this question, CD45⁺CD11b⁺Ly-6G⁻ monocytic cells were sorted from the healing myocardium 5 days post-MI. After RNA amplification, cDNA was synthesized and expression levels of classic M1 and M2 mediators evaluated (Fig. 19).

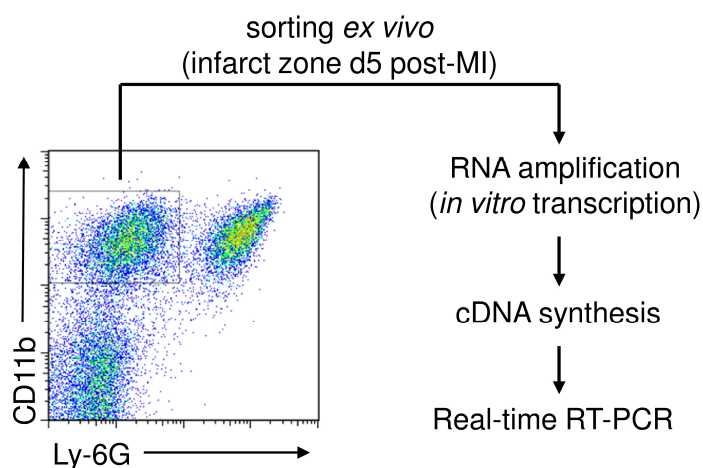


Fig. 19: Workflow to evaluate monocyte/macrophage polarization in the healing myocardium. CD11b⁺Ly-6G⁺ monocytic cells were sorted from the infarct 5 days post-MI. After RNA amplification and cDNA synthesis, expression of prototypical M1 or M2 markers/ mediators was assessed by Real-time RT-PCR.

Monocytes sorted from the infarct of T_{reg} cell-ablated mice showed an increased expression of M1-associated iNOS, but no difference with respect to TNF α mRNA synthesis (Fig. 20A). To evaluate whether the observed M1 bias in sorted monocytic cells correlated with an attenuated M2 polarization, the expression of typical M2-associated mediators involved in healing was assessed. Compared to DTX-treated WT littermates, DEREG mice exhibited an elevated mRNA synthesis of inflammation-resolving IL-10 and TGF β 1 (Fig. 20B). Furthermore, T_{reg} cell depletion was associated with downregulated mRNA synthesis of wound-stabilizing osteopontin (OPN) and, by trend, transglutaminase factor XIII (FXIII) in the sorted monocyte/macrophage population (Fig. 20C).

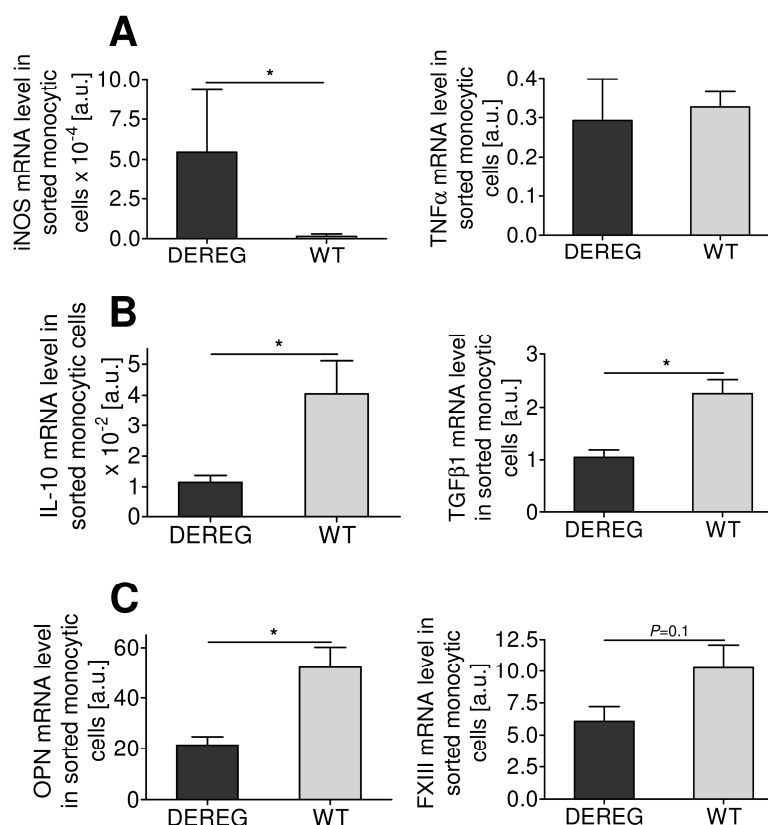


Fig. 20: Real-time RT-PCR analysis of M1- and M2-associated mediators in monocytes/ macrophages sorted from the scar of DTX-treated DEREg and wildtype (WT) mice 5 days after MI. A: mRNA expression of M1-associated induced NO synthase (iNOS) and TNF α (n=5 per group, * P <0.05). B, C: mRNA levels of M2-associated interleukin-10 (IL-10), TGF β 1 (transforming growth factor beta), osteopontin (OPN) and factor XIII (FXIII) (n=5 per group, * P <0.05). (Weirather et al. Circulation Research, 2014¹⁶⁸)

As T cells are capable of secreting soluble mediators that modulate macrophage polarization, T cell infiltration into the healing infarct was assessed. T_{reg} cell-depleted mice showed heightened numbers of both CD4⁺ and CD8⁺ T cells in the infarct zone as compared to wildtype mice 5 days after MI. (Fig. 21A, B). As IFN γ and TNF α represent classic T cell-derived cytokines with capacity to induce M1 cells, the synthesis of both cytokines in the bulk scar tissue was assessed on day 5 post-MI. In accordance with the M1 macrophage polarization in T_{reg} cell-ablated mice, both IFN γ and TNF α mRNA expression were significantly increased in these hearts as compared to WT littermates (Fig. 21C).

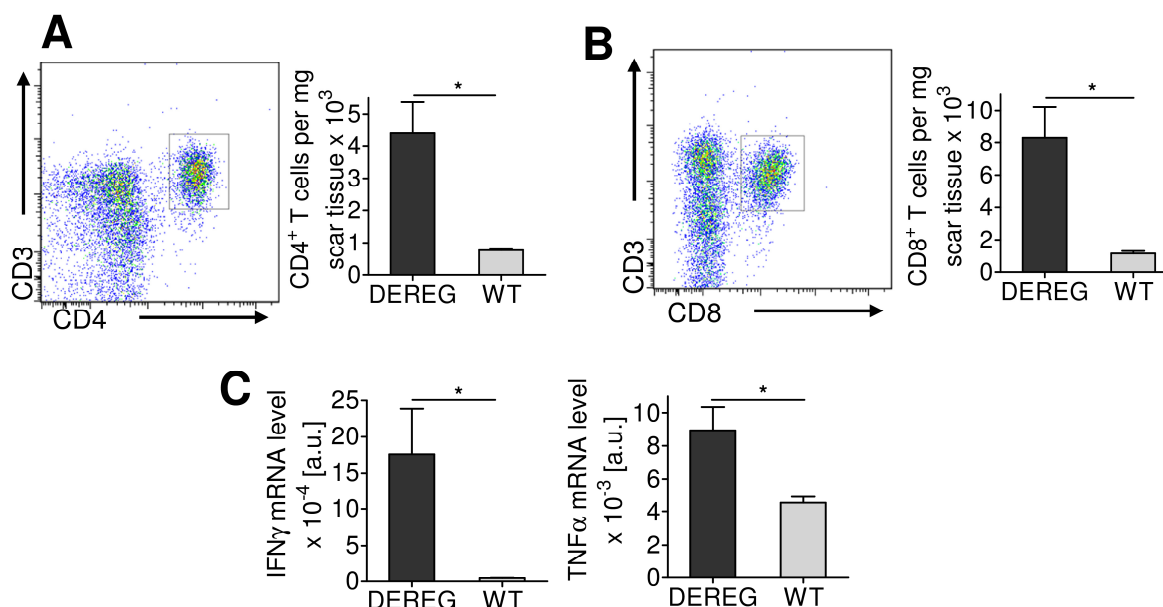


Fig. 21: T cell influx and expression of classic M1-inducing T cell mediators in T_{reg} cell-ablated and T_{reg} cell-sufficient mice. A, B: Representative FACS plots and absolute T cell numbers of both CD4⁺ (A) and CD8⁺ (B) T cells in the healing myocardium 5 days post-MI (n=3 per group, *P<0.05). C: mRNA expression of IFN γ and TNF α in the bulk scar 5 days after MI (n=5 per group, *P<0.05). (Weirather et al., Circulation Research, 2014¹⁶⁸)

To evaluate whether T cells are indeed capable of producing IFN γ and TNF α in infarcted mice, lymphocytes from heart-draining lymph nodes were analyzed for TNF α and IFN γ production by intracellular cytokine staining. In comparison to WT littermates, both CD4⁺ and CD8⁺ T cells showed elevated frequencies of IFN γ -expressing cells in DTX-treated DEREG mice (Fig. 22A, B). Furthermore, the proportion of TNF α -positive cells was elevated in CD8⁺ T cells in lymph nodes from these mice in contrast to CD4⁺ T cells that did not show increased frequencies of TNF-expressing cells after T_{reg} cell ablation (Fig. 22C). However, TNF α mean fluorescence intensity (MFI) of TNF α -positive CD4⁺ cells was higher in T_{reg} cell-depleted animals indicating augmented synthesis on a per cell basis (Fig. 22D).

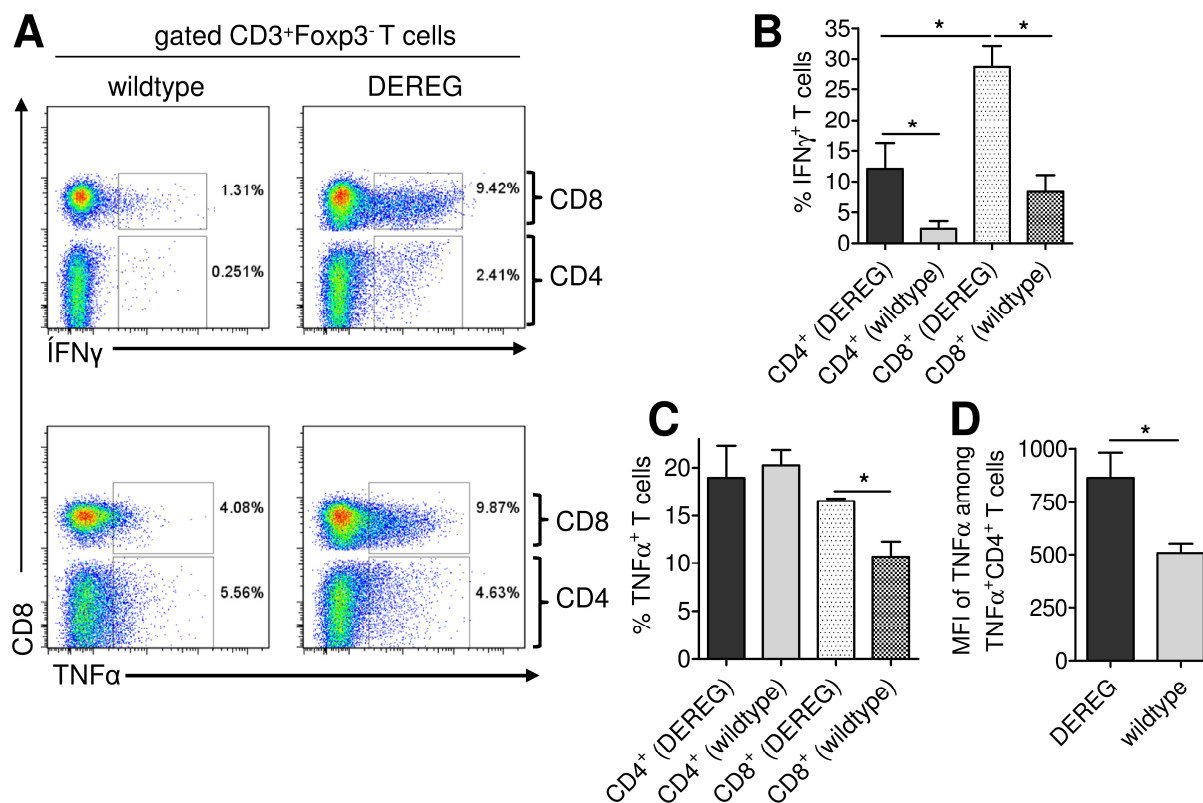


Fig. 22: Cytokine production in both CD4⁺ and CD8⁺ T cells in heart-draining lymph nodes of DTX-treated DEREg and wildtype mice 5 days post-MI. A: Representative FACS plots showing IFN γ - and TNF α -positive T cells (n=3 per group, **P*<0.05). B: Frequency of IFN γ -positive T cells. C: Proportion of TNF α -positive T cells (n=3 per group, **P*<0.05). D: Mean fluorescence intensity (MFI) of TNF α staining in TNF α -positive CD4⁺ T cells (n=3 per group, **P*<0.05). (Weirather et al., Circulation Research, 2014¹⁶⁸)

In summary, T_{reg} cell depletion prior to MI induction provokes an increased recruitment of inflammatory myeloid and T cells into the infarct zone, in line with an M1-like macrophage polarization that is presumably driven by T cell-derived IFN γ and TNF α .

5.8 Anti-CD25 antibody-mediated T_{reg} cell depletion prior to MI leads to impaired survival, aggravated remodeling and increased recruitment of inflammatory myeloid cells.

To reconfirm the results of cardiac exacerbation in T_{reg} cell-ablated mice, a second model of T_{reg} cell depletion was employed, i.e. an anti-CD25 antibody (Ig)-mediated ablation. Compared to the control mice that received an isotype control antibody of irrelevant specificity, anti-CD25 antibody administration resulted in a significant reduction of Foxp3⁺ frequencies among CD4⁺ T cells in the blood and mediastinal lymph nodes (Fig. 23).

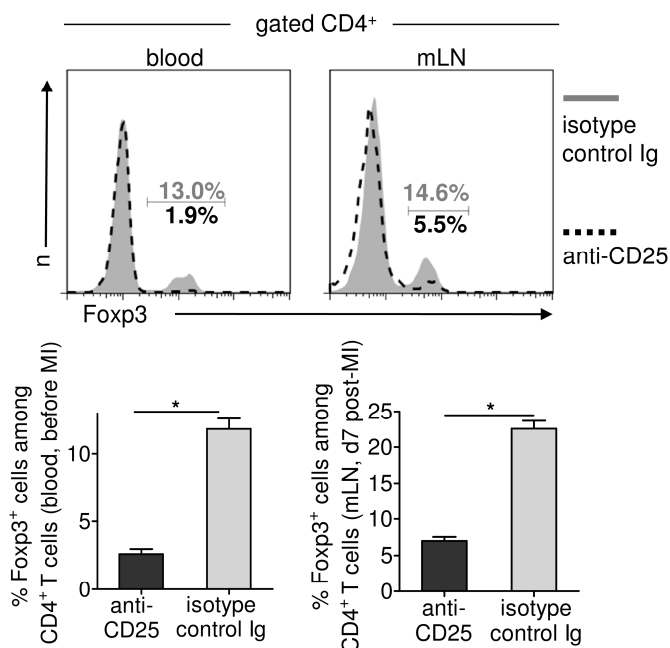


Fig. 23: Evaluation of T_{reg} cell depletion in antibody-treated mice. Representative FACS plots and quantitative analyses showing the frequency of Foxp3⁺ cells among CD4⁺ T cells in blood and mediastinal lymph nodes after anti-CD25 antibody or isotype control antibody (Ig) treatment (n=3 per group; **P*<0.05). (Weirather et al., Circulation Research, 2014¹⁶⁸)

Anti-CD25 antibody treatment resulted in significantly impaired survival as compared to the control group (Fig. 24A). Infarct size was not different between treatment groups evaluated 7 days after MI (Fig. 24B). However, echocardiography revealed an aggravated left-ventricular apical end-diastolic area implying that T_{reg} cell-depleted mice had likely succumbed to heart failure (Fig. 24C). Regarding fractional shortening and the incidence of left-ventricular ruptures, however, no differences were found between the treatment groups (Fig. 24C, D and data not shown).

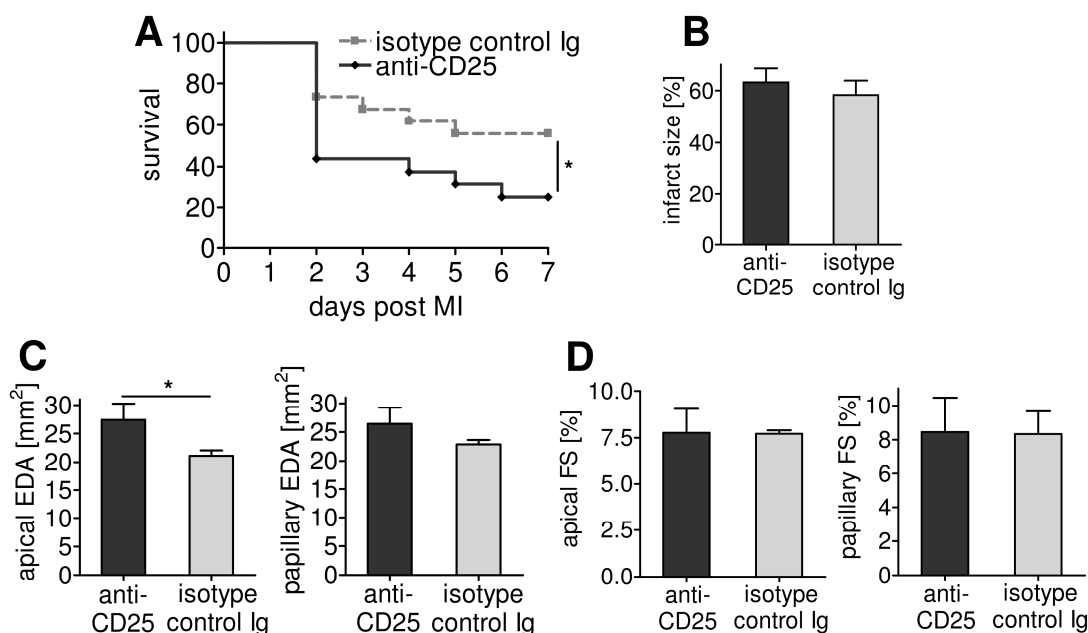


Fig. 24: Clinical outcome of anti-CD25 antibody- and isotype control antibody (Ig)-treated mice. A: Cumulative survival of treated mice (n=16-34 per group at baseline, * $P < 0.05$). B: infarct size evaluated 7 days after MI (n=4-7 per group, * $P < 0.05$). C, D: apical end-diastolic area (EDA) and apical fractional shortening in treated mice 7 days after MI (n=4-7 per group, * $P < 0.05$). (Weirather et al., Circulation Research, 2014¹⁶⁸)

Similarly to DTX-treated DEREG mice, anti-CD25 antibody administration enhanced the influx of inflammatory myeloid cells into the healing infarct zone. Absolute neutrophil numbers as well as the proportion of Ly-6C^{high} monocytes were heightened in hearts of anti-CD25 antibody-treated animals in comparison to control mice (Fig. 25).

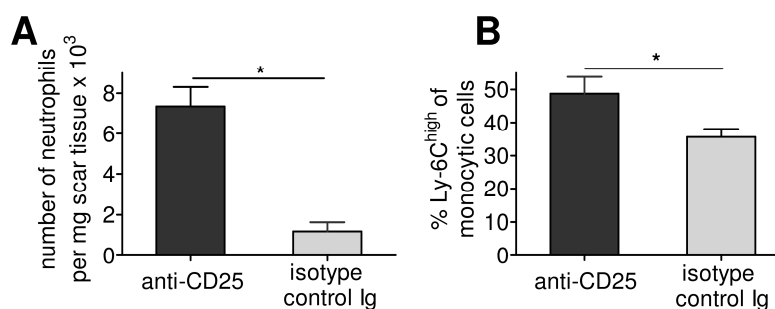


Fig. 25: Composition of myeloid cells in the infarct zone of treated mice 7 days after MI assessed by FACS analysis. A: Absolute number of neutrophils (n=3-7 per group; * $P < 0.05$). B: Proportion of Ly-6C^{high} cells among monocytes (n=3-7 per group; * $P < 0.05$) (Weirather et al, Circulation Research, 2014¹⁶⁸)

In summary, anti-CD25 antibody-mediated T_{reg} cell depletion aggravated postinfarction clinical outcome characterized by impaired survival and deteriorated left-ventricular dilatation.

5.9 CD28-SA administration leads to enhanced T_{reg} cell recruitment into the infarct zone, associated with increased survival and improved scar tissue formation

The observation that T_{reg} cell depletion prior to MI exacerbated clinical outcome raised the hypothesis that an activation and expansion of the T_{reg} cell compartment might improve healing and alleviate adverse cardiac remodeling. T_{reg} cell activation was accomplished by a single injection of a superagonistic anti-CD28 monoclonal antibody (CD28-SA). CD28-SA-mediated T_{reg} cell expansion peaks approximately 2-3 days after administration^{163, 170}. To support the physiological T_{reg} cell expansion that was found to reach its maximum between day 3 and day 7 after MI, the CD28-SA was administered 2 days after surgery. By day 5, the frequency of Foxp3⁺ cells among CD4⁺ T cells in both blood and heart-draining lymph nodes was approximately doubled after CD28-SA injection as compared to control antibody-treated mice (Fig. 26).

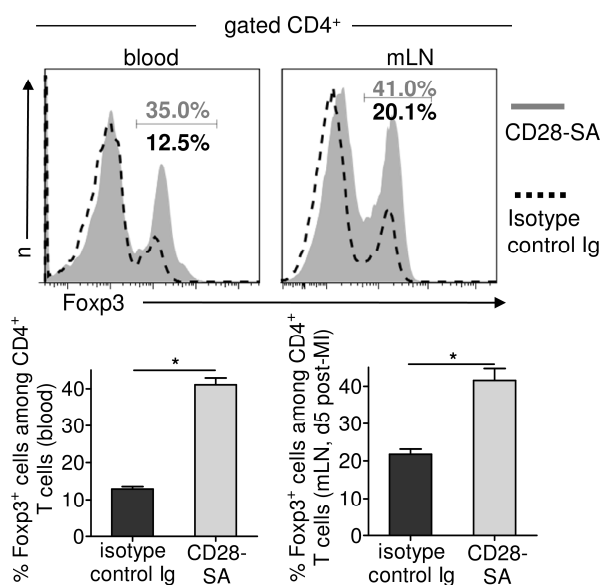


Fig. 26: T_{reg} cell expansion in CD28-SA-treated mice. Representative FACS plots and quantitative analyses showing the frequency of Foxp3⁺ cells among CD4⁺ T cells in blood and mediastinal lymph nodes (mLN) after injection of CD28-SA or an isotype control Ig (n=3 per group; *P<0.05). (Weirather et al., Circulation Research, 2014¹⁶⁸)

Compared to isotype control Ig-treated mice, CD28-SA administration resulted in improved survival and significantly reduced frequencies of left-ventricular ruptures. By day 56, survival was 47.1% in isotype controls and 76.6% in CD28-SA-treated animals (Fig. 27A). Frequencies of left-ventricular ruptures were 23% in control mice

and 5% after CD28-SA treatment (Fig. 27B). Regarding infarct size, left-ventricular dilatation and fractional shortening, however, no significant differences could be found between the treatment groups evaluated by non-invasive echocardiography 7 days after MI (Fig. 27D, E).

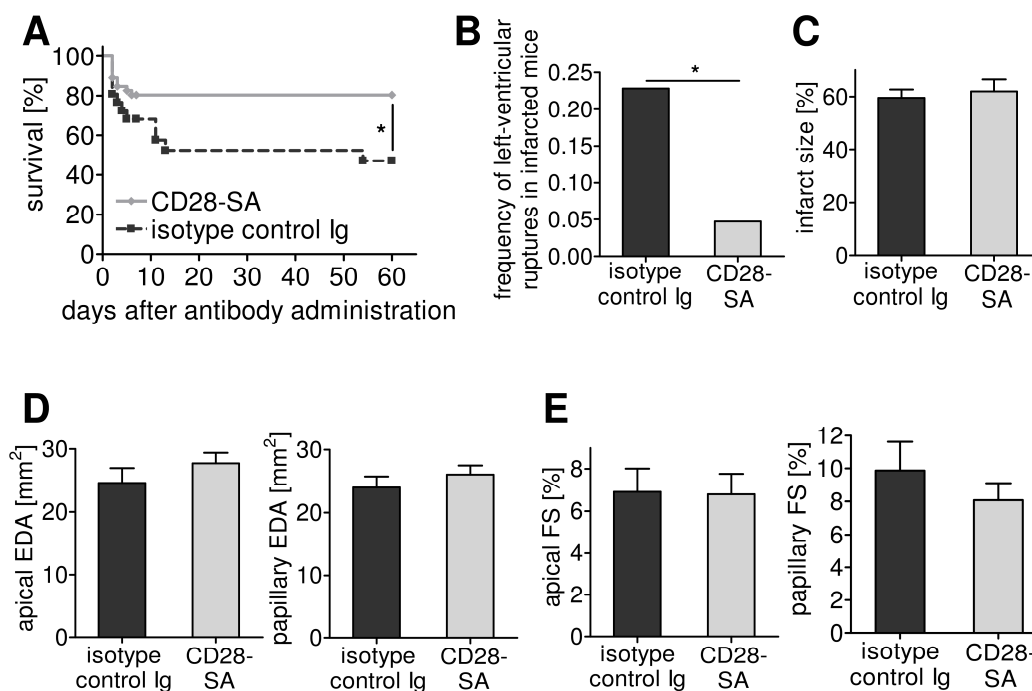


Fig. 27: Clinical outcome of CD28-SA- and isotype control antibody (Ig)-treated mice. A: Cumulative survival after MI (n=42-47 per group at baseline, *P<0.05). B: frequency of left-ventricular ruptures during the first 7 days post-MI (B, n=45-62, *P<0.05). C: Infarct size assessed on day 7 after MI. D: Apical end-diastolic area (EDA) and fractional shortening (FS) 7 days post-MI. (Weirather et al., Circulation Research, 2014¹⁶⁸)

The fact that therapeutic CD28-SA administration resulted in decreased rates of left-ventricular ruptures suggested that scar tissue formation was improved or accelerated in these mice in comparison to controls. Therefore, the quality of scar tissue formation was analyzed in both treatment groups. Collagen I and collagen III constitute integral components of the reparative scar. In comparison to control mice, CD28-SA administration led to increased mRNA expression of pro-collagen alpha-1 (I) and pro-collagen alpha-1 (III) in the emerging scar 5 days after MI (Fig. 28A). The increased expression of collagen I and collagen III in CD28-SA-treated mice was confirmed at the protein level (Fig. 28B). ECM turnover in the infarct zone is, among other enzymes, driven by MMPs. As both MMP-2 and MMP-9 activity in postinfarction healing have been correlated with left-ventricular ruptures, the expression of MMP-2- and MMP-9-restraining TIMPs was assessed. Compared to isotype control antibody-

treated mice, CD28-SA treatment resulted in elevated TIMP-1 as well as TIMP-2 synthesis in the healing infarct 5 days after MI (Fig. 28C).

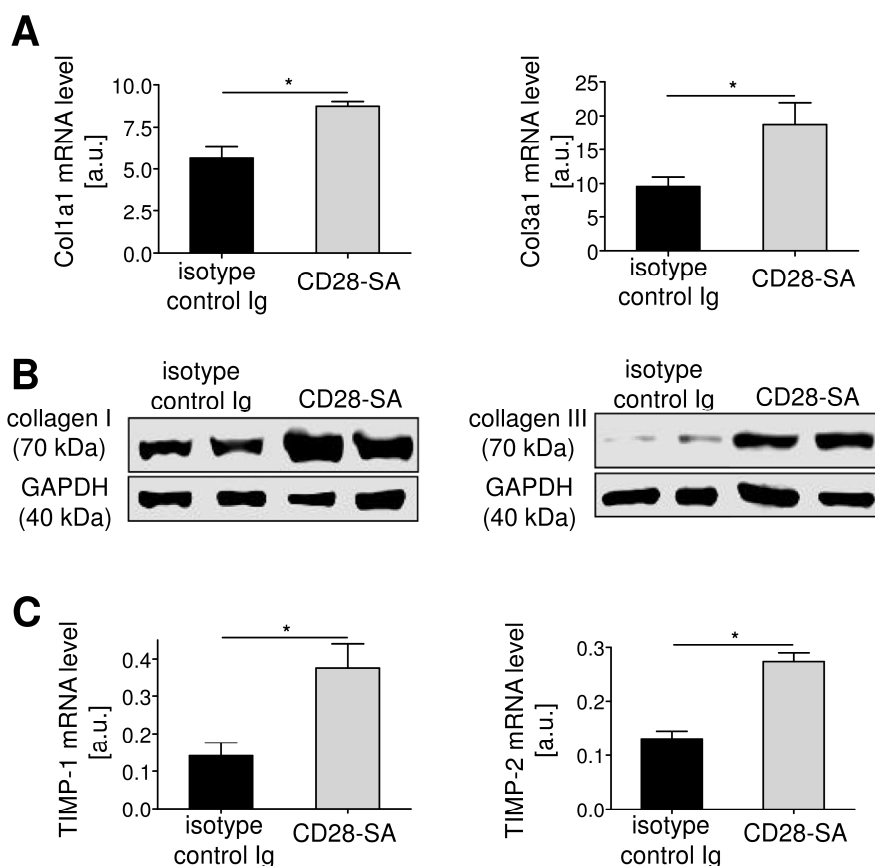


Fig. 28: Scar tissue construction after CD28-SA or isotype control antibody (Ig) administration evaluated on day 5 post-MI. A: mRNA expression of collagen alpha 1 (I) (Col1a1) and collagen alpha 1 (III) (Col3a1) (n=4-7 per group per group, * $P < 0.05$). B: Western blot analysis of both collagen I, collagen III and glyceraldehyde 3-phosphate dehydrogenase (GAPDH). C: Real-time RT-PCR analysis of tissue inhibitor of matrix metalloproteinase 1 (TIMP-1) and TIMP-2 in bulk scar tissue homogenates (n=4-7, * $P < 0.05$). (Weirather et al., Circulation Research, 2014¹⁶⁸)

Collagen deposition in the healing infarct is carried out by mesenchymal alpha smooth muscle actin (α -SMA)-expressing myofibroblasts. As an indirect readout for myofibroblast numbers in the infarct scar, the expression level of both α -SMA and the mesenchymal marker vimentin were evaluated. Compared to control mice, vimentin and α -SMA mRNA expression were significantly upregulated after CD28-SA-treatment on day 5 after MI (Fig. 29A).

As α -SMA can be expressed in endothelial cells, neo-vessel numbers were indirectly assessed by an evaluation of von Willebrandt factor (vWF) expression reflecting the

degree of tissue neovascularization. As compared to isotype control antibody-treated mice, CD28-SA injection did not elicit vWF mRNA upregulation implying that elevated α -SMA mRNA synthesis was not secondary to an accelerated angiogenesis (Fig. 29B). Heightened numbers of α -SMA-expressing cells could be confirmed by immunohistochemistry stainings (Fig. 29C).

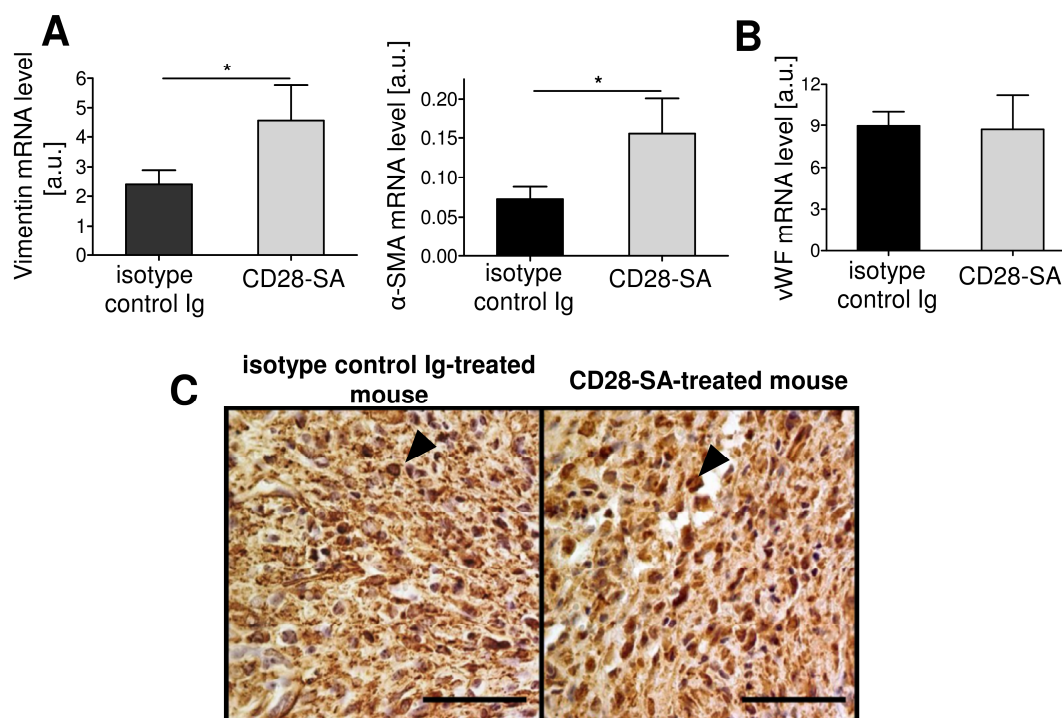


Fig. 29: Evaluation of myofibroblast numbers in the infarct zone of treated mice. A: mRNA synthesis of mesenchymal vimentin and alpha smooth muscle actin (α -SMA) in scar tissue homogenates 5 days after MI (n=4-7 per group; * P <0.05). B: Real-time RT-PCR analysis of von Willebrandt factor (vWF) 5 days after MI (n=4-7 per group; * P <0.05). C: Immunohistochemistry staining of α -SMA 7 days after MI (brown: α -SMA-positive cells exemplarily indicated by arrow head, blue: cell nuclei, bar represents 50 μ m). (Weirather et al., Circulation Research, 2014¹⁶⁸)

In order to unravel whether T_{reg} cells influence cardiac healing directly in the heart, T_{reg} cell influx into the infarct zone was assessed. CD28-SA-treated animals showed similar frequencies of bulk $CD4^+$ T cells among $CD45^+$ leukocytes present on day 5 after MI as compared to control mice (Fig. 30A). However, the proportion of $Foxp3^+$ *bona fide* regulatory T cells among $CD4^+$ T cells was shifted after CD28-SA treatment showing approximately 50% $Foxp3^+$ cells among $CD4^+$ T cells as compared to approximately 25% $Foxp3^+$ cells among heart $CD4^+$ cells of isotype control antibody-treated mice (Fig. 30B, C). Consistently, absolute numbers of $Foxp3^+CD4^+$ regulatory cells were elevated in the healing infarct of CD28-SA-treated animals (Fig. 30D) and heightened T_{reg} cell numbers could be further reconfirmed by

immunofluorescence stainings (Fig. 30E). To assess whether CD28-SA treatment alone imposed heart-seeking capacity on the T_{reg} cell compartment irrespective of cardiac injury, T_{reg} cell influx into the heart of treated mice was assessed after sham surgery. However, CD28-SA administration in absence of MI did not elicit pronounced recruitment of T_{reg} cells into the myocardium, indicating that tissue inflammation during sterile injury in terms of MI constitutes a prerequisite for T_{reg} cell homing into the heart (Fig. 30F).

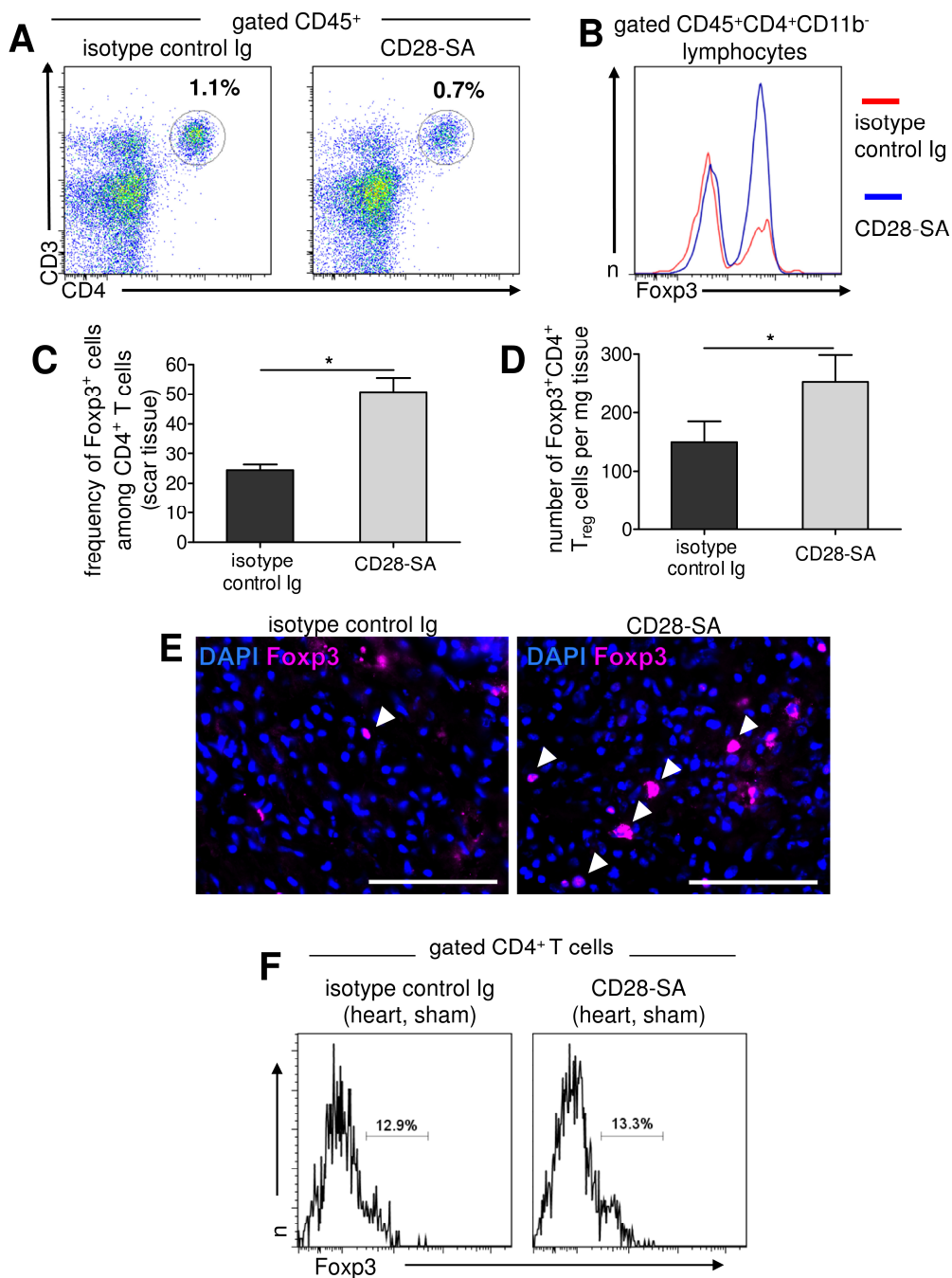


Fig. 30: CD4⁺ T cell infiltrate in the scar tissue of CD28-SA and isotype control antibody (Ig)-treated mice 5 days after MI (A-E) or sham surgery (F). A: Representative FACS plots showing CD4⁺ T cell frequencies among CD45⁺ leukocytes in the scar tissue. Numbers indicate percentage among all CD45⁺ leukocytes. B: Representative histograms depicting Foxp3⁺ cells among CD4⁺ T cells. C: Proportion of Foxp3⁺ cells among CD4⁺ T cells in the scar tissue (n=4-5 per group; *P<0.05). D: Absolute numbers of Foxp3⁺CD4⁺ T_{reg} cells in the scar tissue of treated animals (n=4-5 per group; *P<0.05). E: Immunofluorescence staining of Foxp3⁺ cells in the scar tissue 5 days after MI. Foxp3 is depicted in purple (arrow heads). Nuclei were stained using DAPI. The scale bar indicates 100 μm. F: Representative FACS plots showing frequencies of Foxp3-positive cells among cardiac CD4⁺ T cells 5 days post-surgery after administration of an isotype control antibody or CD28-SA to sham-operated mice. (Weirather et al., *Circulation Research*, 2014¹⁶⁸)

In summary, therapeutic T_{reg} cell activation 2 days after MI led to increased T_{reg} cell recruitment into the healing myocardium, associated with increased *de novo* collagen synthesis and, consistently, improved survival due to reduced frequencies of left-ventricular ruptures.

5.10 Therapeutic T_{reg} cell activation induces an M2-like macrophage polarization in the healing myocardium

Since monocytic cells are key players for cardiac wound healing after MI, the absolute number of monocytes/ macrophages within the scar tissue was assessed on day 7 after MI induction. Regarding absolute cell numbers and monocyte subset composition, no difference could be detected between treatment groups (data not shown). However, as monocytic cells exhibit high functional plasticity, the polarization state of monocytes/ macrophages in the healing myocardium was assessed. In the first place, the expression of mediators with capacity to induce healing-promoting M2 cells was determined. In comparison to isotype control Ig-treated mice, mRNA levels of transforming growth factor beta 1 (TGFβ1), interleukin-13 (IL-13) and interleukin-10 (IL-10) were significantly upregulated in the scar tissue of CD28-SA-treated mice on day 5 after MI (Fig. 31A). The increased expression of M2-associated arginase I and CD206 in line with ECM-bracing osteopontin (OPN) and factor XIII (FXIII) indicate that M2 cells were, indeed, present in these hearts (Fig. 31B).

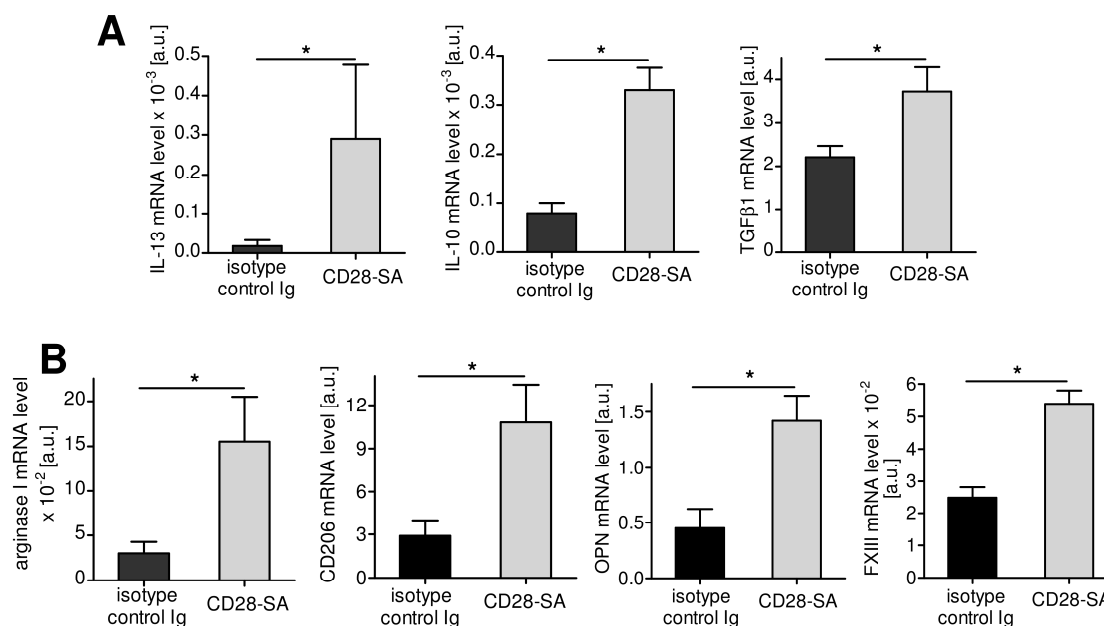


Fig. 31: Expression of M2-associated mediators in scar tissue homogenates in treated mice 5 days after MI. A: mRNA synthesis of M2-inducing IL-13, IL-10 and TGFβ1. B: Real-time RT-PCR analysis of M2-associated arginase I, CD206, osteopontin (OPN) and transglutaminase factor XIII (FXIII) (n=4-7 per group, * $P < 0.05$). (Weirather et al., Circulation Research, 2014¹⁶⁸)

To verify that monocytic cells account for the upregulation of M2 markers in the healing myocardium of CD28-SA-treated mice, CD11b⁺Ly-6G⁻ monocytes/macrophages were sorted from the scar tissue 7 days after MI and, subsequently, analyzed for M1- and M2-prototypic markers (see Fig. 19). In comparison to controls, monocytes/macrophages sorted from the scar of CD28-SA-treated mice showed elevated mRNA levels of the M2-associated markers arginase I, CD206, TGFβ1 and IL-10 in line with a reduced synthesis of M1-associated TNFα message (Fig. 32A, B). However, regarding the expression of the M1 mediators IL-1β and IL-6, no significant differences were identifiable between treatment groups (Fig. 32B).

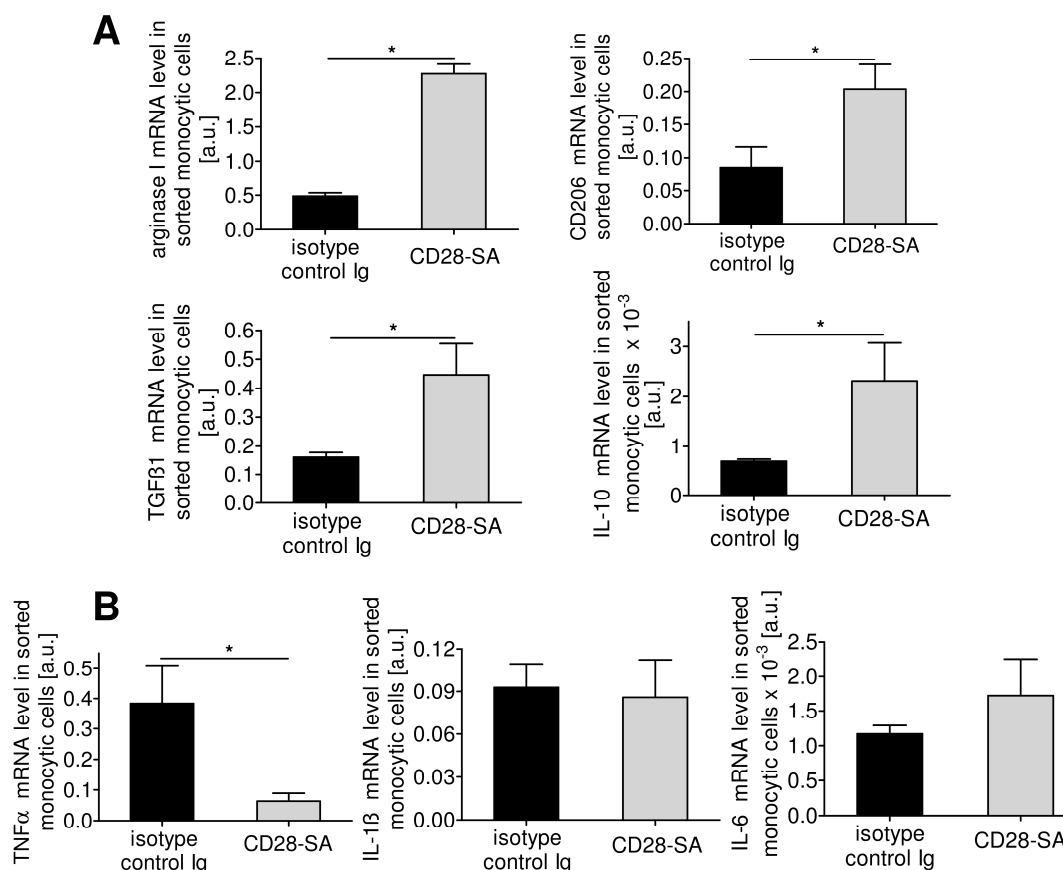


Fig. 32: Monocytes/ macrophages sorted from the healing infarct 7 days after MI. Real-time RT-PCR analysis of M2-associated arginase I, TGFβ1 and IL-10 (A) as well as M1-associated TNFα, IL-1β and IL-6 (B) (n=3-4 per group, *P<0.05). (Weirather et al., Circulation Research, 2014¹⁶⁸)

Conclusively, therapeutic T_{reg} cell activation led to an upregulation of M2-inducing factors in the healing myocardium, correlating with a pronounced M2 transcriptional profile in scar macrophages characterized by an expression of inflammation-resolving and healing-promoting factors.

5.11 T_{reg} cell-derived cytokines drive M2 polarization in monocytic cells *in vitro*

In the healing myocardium of CD28-SA-treated mice, T_{reg} cell numbers were significantly elevated as compared to controls, suggesting that T_{reg} cells might influence macrophage polarization *in situ*. To investigate the potential impact of CD28-SA-activated T_{reg} cells on monocyte/ macrophage differentiation *in vivo*, primary monocytic cells and T cell subsets were cultured *in vitro* in different combinations (Fig. 33).

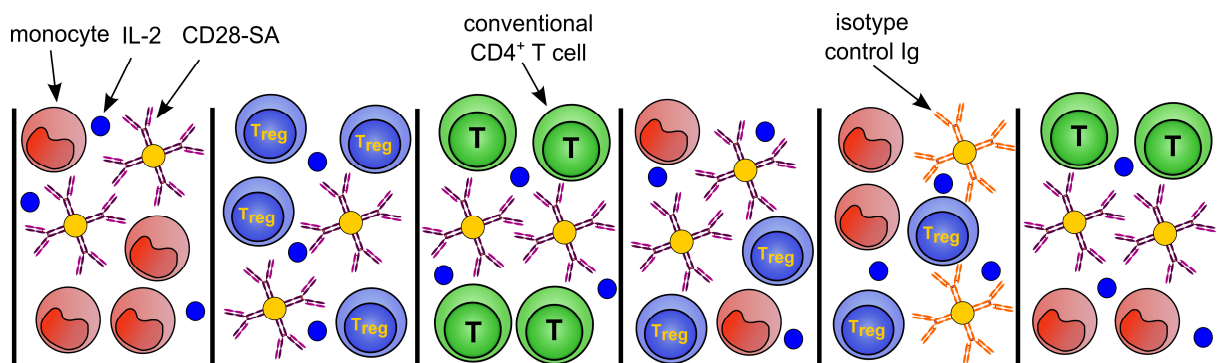


Fig. 33: Experimental setup to evaluate the impact of CD28-SA-activated T_{reg} cells and conventional T cells on monocyte/ macrophage differentiation *in vitro*. Primary monocytes, T_{reg} cells and conventional T cells (T) were cultivated alone or in different combinations in presence of IL-2 and CD28-SA or an isotype control antibody (Ig) of irrelevant specificity. The antibodies were coated on polymer beads before addition to the cell culture. After 4 days of incubation, cell culture supernatants were analyzed for the M2 macrophage-associated mediator osteopontin.

Monocytes/ macrophages were sorted from lymph nodes as well as the spleen and defined as $CD45^+CD11b^{high}Ly-6G^-CD11c^-$. Conventional and regulatory $CD4^+$ T cells were sorted from peripheral lymph nodes and defined as $CD45^+CD4^+CD25^-$ and $CD45^+CD4^+CD25^{high}$, respectively (Fig. 34).

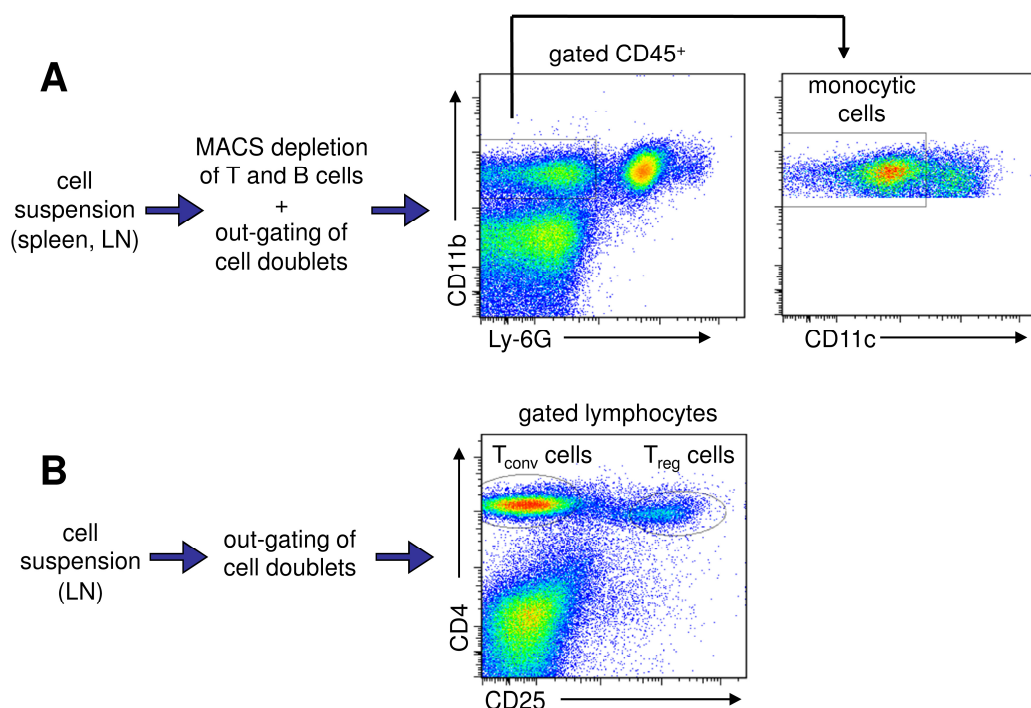


Fig. 34: Sorting strategy to purify primary monocytes/ macrophages (A), conventional $CD4^+$ T cells and regulatory $CD4^+$ T cells (B). A: Monocytic cells were defined as $CD45^+CD11b^+Ly-6G^-CD11c^-$ and sorted from T and B cell-depleted cell suspensions prepared from spleen and lymph nodes. B: Conventional and regulatory $CD4^+$ T cells were sorted from lymph node single cell suspensions and defined as $CD4^+CD25^-$ and $CD4^+CD25^{high}$, respectively. (Weirather et al., Circulation Research, 2014¹⁶⁸)

Post-sort purity of T cell subsets was analyzed on the basis of Foxp3 expression. After 4 days of incubation in presence of IL-2 and either CD28-SA or an isotype control antibody, T cell activation was assessed by an expression analysis of Ki67 that is strictly associated with cellular division (Fig. 35).

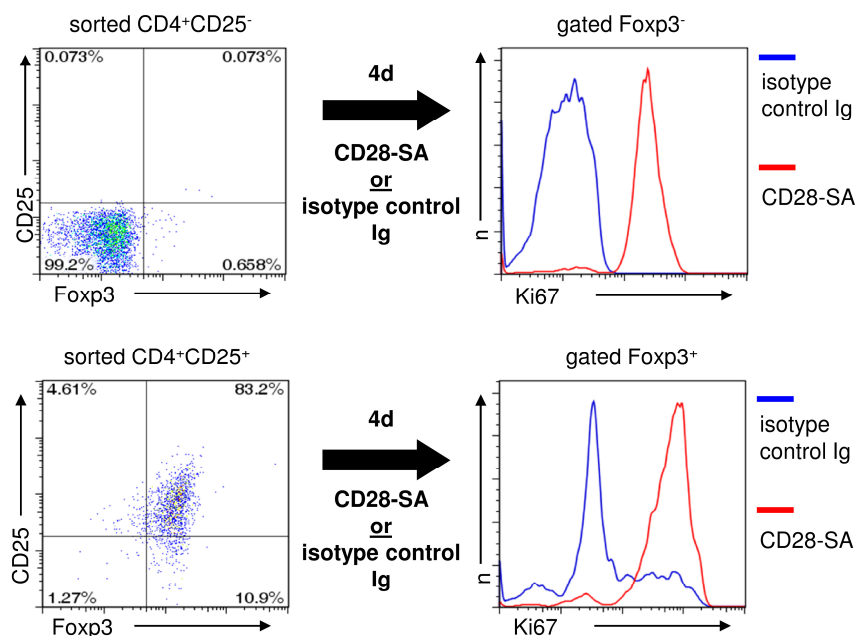


Fig. 35: Evaluation of T cell purity post-sorting and activation state after 4 days of incubation in presence of IL-2 and an isotype control antibody (Ig) or CD28-SA. Conventional CD4⁺ T cells were defined as CD25⁻Foxp3⁻, regulatory T cells as CD25⁺Foxp3⁺. Activation was assessed by an expression analysis of the proliferation marker Ki67. (Weirather et al., Circulation Research, 2014¹⁶⁸)

As OPN represents a prototypical M2 mediator that is crucially involved in postinfarction healing, macrophage M2 polarization was evaluated on the basis of OPN synthesis. Mono-cultures of T_{reg} cells, conventional CD4⁺ T cells and monocytic cells showed minor OPN concentrations in the supernatant after 4 days of incubation in presence of CD28-SA and IL-2 (Fig. 36A). In contrast, co-cultures of T_{reg} cells and monocytic cells showed high OPN secretion after CD28-SA and IL-2 stimulation, but not in presence of IL-2 and an isotype control antibody (Fig. 36A).

T_{reg} cell numbers of 150 cells per mg scar tissue in the infarcted myocardium are considerably low as compared to the predominant fraction of approximately 2000 macrophages per mg tissue¹³⁶. To evaluate whether the unpropitious T_{reg} cell : macrophage ratio of approximately 1:14 can provoke OPN release, T_{reg} cells were

successively titrated from the co-culture system. Even at a T_{reg} cell : monocyte ratio of 1 : 25, OPN concentrations in culture supernatants were still higher as compared to monocytes cultivated alone (Fig. 36B).

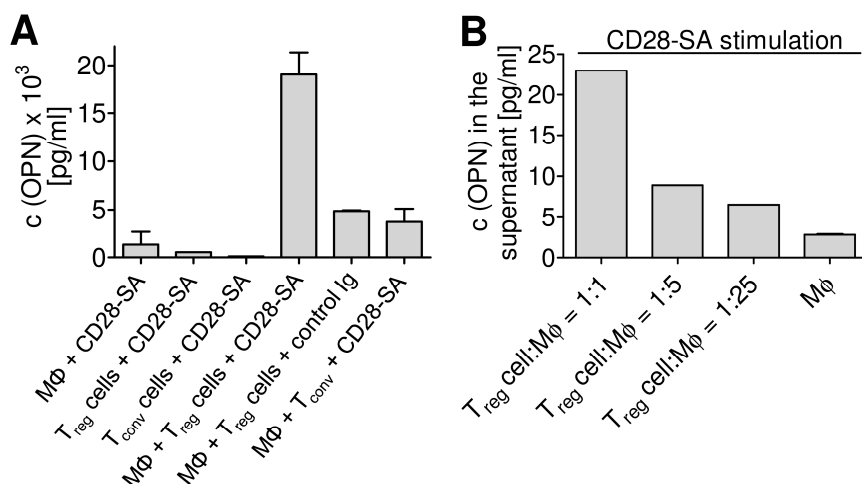


Fig. 36: Osteopontin (OPN) concentrations in cell culture supernatants. A: Monocytic cells (MΦ), regulatory (T_{reg}) and conventional (T_{conv}) $CD4^+$ T cells were cultivated for 4 days alone or in the indicated combinations in presence of CD28-SA or an isotype control antibody (Ig). All cultures were supplemented with IL-2. OPN concentrations were assessed by ELISA (n=3-4 per group). B: OPN concentrations in the supernatant of T_{reg} cell/ monocyte (MΦ) co-cultures cultivated at different ratios. (Weirather et al., Circulation Research, 2014¹⁶⁸)

To investigate whether T_{reg} cells induce OPN secretion from monocytic cells by T_{reg} cell-derived soluble mediators and, moreover, to test whether monocytes/macrophages are indeed responsible for the high OPN concentrations in supernatants of co-culture experiments, T_{reg} cells were activated by CD28-SA and IL-2 *in vitro*. After 4 days of incubation, the supernatant was mixed with culture medium containing freshly purified monocytes/ macrophages at a volume ratio of 1:1. Monocytic cells cultivated in the supernatant of T_{reg} cells that had been cultured in presence of an isotype control antibody and IL-2 were used as reference control. After 3 days of incubation, monocytic cells had released high amounts of OPN in response to mediators in the supernatant of CD28-SA-activated T_{reg} cells, but not in presence of supernatant from non-activated T_{reg} cells (Fig. 37A). OPN release from monocytic cells correlated with CD206 and arginase I mRNA upregulation (Fig. 37B).

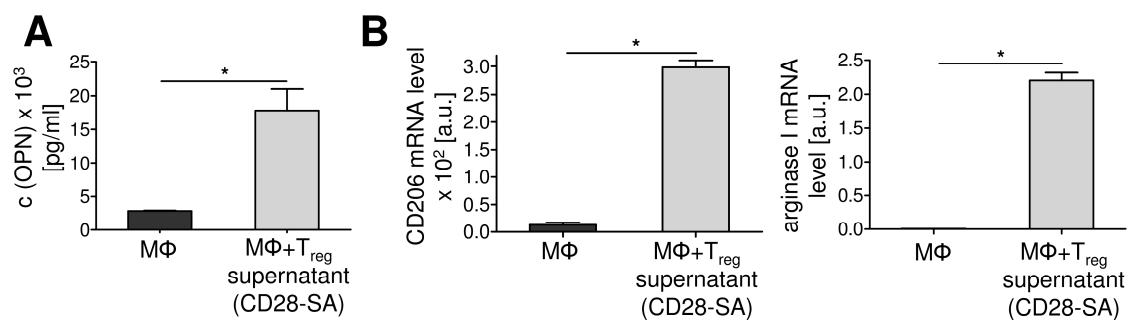


Fig. 37: T_{reg} cell-derived soluble mediators induce osteopontin (OPN) release and expression of M2 marker genes in monocytic cells (MΦ) *in vitro*. A: OPN release from monocytic cells cultivated for 3 days in culture medium alone supplemented with supernatant from unstimulated T_{reg} cells, or culture medium supplemented with supernatant derived from CD28-SA-activated T_{reg} cell cultures. B: Real-time RT-PCR analysis of M2-associated CD206 and arginase I in monocytic cells (MΦ) cultivated alone or in presence of T_{reg} cell supernatant. (Weirather et al., Circulation Research, 2014¹⁶⁸)

Having observed that T_{reg} cell-derived soluble mediators influence monocyte/macrophage differentiation *in vitro*, T_{reg} cell supernatants were analyzed for cytokine composition. In comparison to T_{reg} cells cultivated in presence of an isotype control antibody and IL-2, simultaneous presence of CD28-SA and IL-2 led to a significantly increased secretion of IL-10, IL-13 and TGFβ1, but not IL-2 or IL-4 (Fig. 38). The capacity of IL-10, IL-13 and TGFβ1 to induce OPN release from monocytic cells was further investigated. Supplementation of culture medium with TGFβ1 alone did not reinforce OPN release from monocytic cells *in vitro* (Fig. 38). However, the simultaneous presence of TGFβ1 and IL-10 provoked a strong OPN release from monocytic cells that could be further increased by addition of IL-13. However, neutralization of TGFβ1 dramatically restrained IL-10- and IL-13-driven OPN secretion.

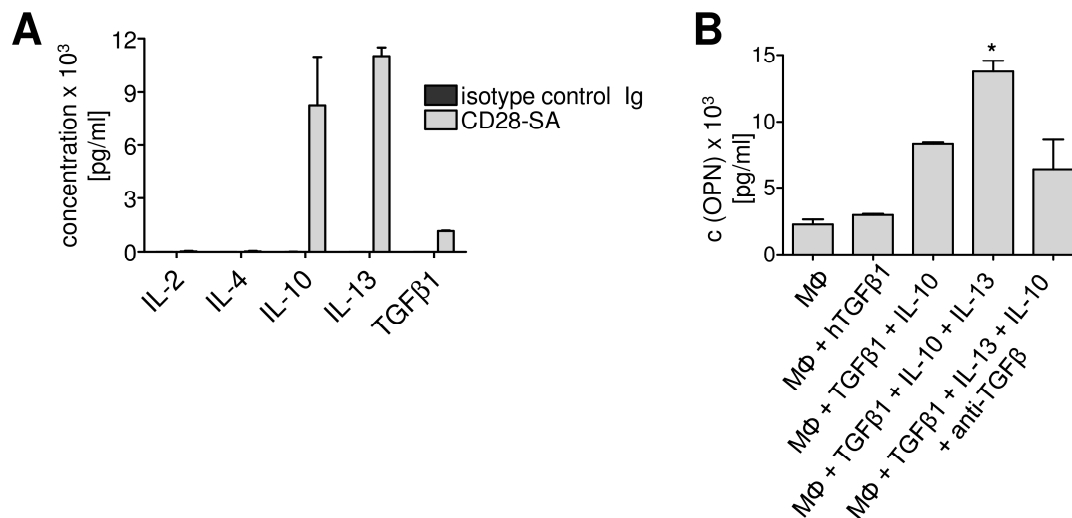


Fig. 38: T_{reg} cell-derived IL-10, IL-13 and TGFβ1 induce osteopontin secretion from monocytic cells *in vitro*. A: Cytokine concentrations in supernatants from T_{reg} cells cultivated for 4 days in presence of CD28-SA or an isotype control antibody (Ig) (n=2 per group). B: Osteopontin (OPN) concentrations in the supernatant of monocytic cells cultivated in presence of the indicated cytokines or a neutralizing anti-TGFβ antibody (n=4 per group, *P<0.05 vs. MΦ+TGFβ1+IL-10). (Weirather et al., Circulation Research, 2014¹⁶⁸)

Conclusively, CD28-SA-stimulated T_{reg} cells released high amounts of IL-10, IL-13 and TGFβ that synergistically drove OPN release and M2 macrophage polarization *in vitro*.

5.12 Therapeutic T_{reg} cell activation by IL-2/ anti-IL-2 monoclonal antibody complexes provokes M2-like macrophage differentiation and accelerates scar tissue formation

Therapeutic T_{reg} cell activation after MI by CD28-SA administration improved survival by reducing the incidence of left-ventricular ruptures. CD28-SA infusion represents therefore a promising modality to treat patients with MI. However, additional strategies to activate T_{reg} cells *in vivo* have been developed, e.g. by administering recombinant human IL-2 at low dosage¹⁷¹. IL-2 in complex with a particular anti-IL-2 monoclonal antibody (IL-2 mAB), hitherto used only experimentally, holds even more clinical potential compared to IL-2 alone by enhancing T_{reg} cell functions on a per cell basis¹⁶⁴. IL-2/ IL-2 mAB complexes were therefore administered to infarcted mice. T_{reg} cell expansion kinetics after IL-2/ IL-2 mAB injection are different from the proliferative behaviour after CD28-SA treatment^{164, 170, 172}. A pilot study was therefore conducted to determine an eligible time point to start the IL-2/ IL-2 mAB treatment of infarcted mice. Principal criteria for an optimal regimen were a supportive induction of

M2 cells and augmented scarring in the reparative phase that did not interfere with the early inflammatory stage of postinfarction healing. IL-2/ IL-2 mAB administration on three consecutive days beginning on day 1 post-MI turned out to represent an adequate regimen that fulfilled the requirements. Compared to animals treated with vehicle solution, IL-2/ IL-2 mAB injection caused increased frequencies of Foxp3-positive cells among CD4⁺ T cells in mediastinal lymph nodes and the infarct zone on day 5 after MI (Fig. 39A). Bulk scar tissue homogenates of IL-2/ IL-2 mAB-treated mice showed a tendency towards an increased expression of M2-inducing IL-10 (Fig. 39B). Similar to CD28-SA-treated mice, IL-13 was significantly upregulated after IL-2/ IL-2 mAB injection as compared to controls, but, however, not TGFβ1 (Fig. 39B). In accordance with upregulated M2-inducing factors, M2-associated arginase I as well as CD206 expression were significantly heightened in hearts of IL-2/ IL-2 mAB-treated mice (Fig. 39C). M2 macrophage differentiation correlated with elevated expression of pro-collagen alpha 1 (III) (Fig. 39D). However, regarding pro-collagen alpha 1 (I) mRNA synthesis, no significant differences were found between the treatment groups (Fig. 39D). In summary, the observation of reinforced M2-like macrophage polarization and augmented scar tissue construction after therapeutic T_{reg} cell activation could be confirmed in an independent approach of T_{reg} cell expansion, i.e. by a therapeutic IL-2/ IL-2 mAB administration.

Conclusively, the results of the present study indicate that therapeutic T_{reg} cell activation after MI generally represents a suitable strategy to improve cardiac infarct healing.

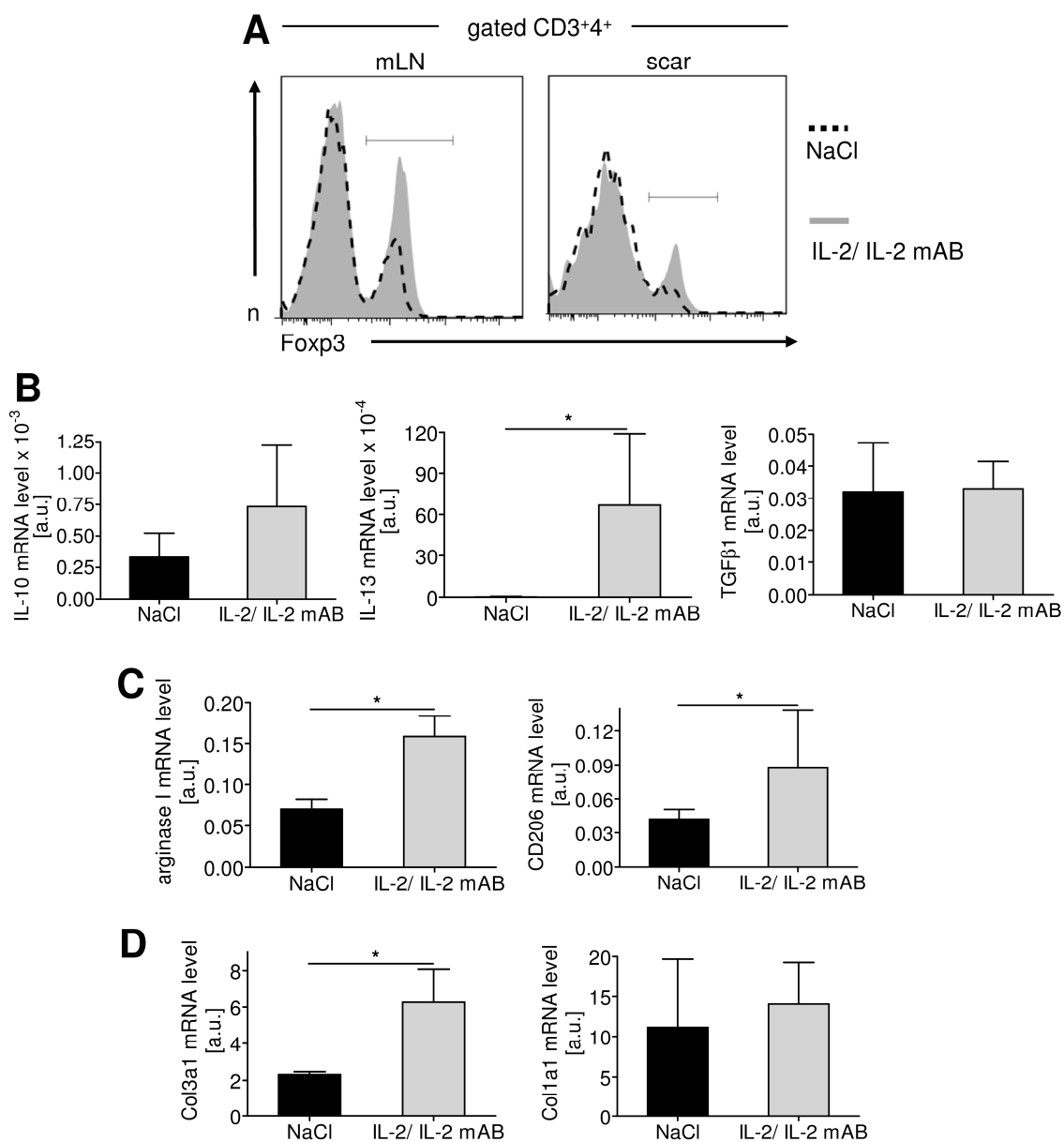


Fig. 39: Therapeutic T_{reg} cell expansion by IL-2/ IL-2 mAB complexes elicits M2-like macrophage polarization and accelerated scar tissue construction evaluated 5 days post-MI. A: Frequency of Foxp3-positive cells among CD4⁺ T cells in heart-draining lymph nodes and scar tissue of treated mice. B: Real-time RT-PCR analysis of the M2-inducing cytokines interleukin (IL)-10, IL-13 and TGF β 1 (n=2-3 per group, * P <0.05). C: mRNA expression of M2-associated arginase I and CD206 (n=2-3 per group, * P <0.05). D: mRNA synthesis of scar-forming collagen alpha 1 (III) (Col3a1) and collagen alpha 1 (I) (Col1a1) (n=2-3 per group, * P <0.05).

6 Discussion

The role of innate immunity in postinfarction cardiac wound healing and remodeling has been studied in great detail. In contrast, the relevance of adaptive immunity in this context has been widely disregarded. The present study focused on the activation of CD4⁺ T cells after MI and systematically addressed their role in cardiac wound healing and remodeling.

6.1 Antigen-dependant CD4⁺ T cell activation post-MI

In terms of adaptive immune reactions, T cell priming by APCs occurs not directly at the location of inflammation, but in lymph nodes that drain the inflammatory site. T cell activation after MI requires therefore passive antigen drainage to lymphoid-resident APCs, or active antigen transport to the lymph nodes by migratory cells such as macrophages or dendritic cells that both reside within the heart during steady state conditions^{115, 173}. Furthermore, a large proportion of macrophages arises from infarct-infiltrating monocytes after MI. A recent study demonstrated that monocyte-derived as well as tissue-resident macrophages mediate cardiomyocyte efferocytosis after angiotensin II-induced cardiac inflammation¹⁷³. Both cardiac macrophage subsets represent potent APCs with capacity to activate T cells *in vitro* suggesting that these myeloid cells might also play a role in T cell priming in the setting of MI¹⁷³.

The fundamental role of APCs in terms of MI is underscored in mice depleted from CD11c⁺ cells comprising dendritic cells and, most likely, also distinct macrophage subsets^{26, 174}. The postinfarction phenotype of CD11c⁺ cell-ablated mice is characterized by an escalated cardiac inflammation along with M1-like macrophage polarization that correlates with deteriorated healing and heart function¹⁷⁵. The observation that depletion of CD11c⁺ APCs aggravates clinical outcome is in line with the interpretation that self-peptide-MHC recognition is crucial for proper T cell activation after MI as OT-II mice in which most CD4⁺ T cells are “blind” for cardiac self-antigens exhibit a fatal postinfarction outcome.

Physiological CD4⁺ T cell expansion kinetics were evaluated in heart-draining lymph nodes where both Foxp3⁻ conventional and Foxp3⁺ regulatory T cells were activated after MI. In contrast to WT animals, heart-draining lymph nodes of OT-II mice did not show an expansion of CD4⁺ T cells indicating that self-antigen recognition constitutes

an indispensable prerequisite for CD4⁺ T cell activation after MI. However, the expansion of T_{reg} cells over concomitantly proliferating conventional CD4⁺ T cells in infarcted wildtype mice closely resembles T cell expansion kinetics in primary immune reactions to foreign pathogen-derived antigens^{176, 177}, implying a release of cardiac self-antigens that are immunologically privileged during steady state conditions. In accordance with this postulation, myocardial self-antigens capable of eliciting CD4⁺ T cell reactions have been described. Heart-specific α -myosin heavy chain (α -MHC), for instance, is not expressed in mTECs of human and mouse thymus resulting in a failure to delete α -MHC-reactive T cells from the repertoire¹⁷⁸. As a consequence, immunization with α -MHC in Complete Freund's Adjuvant provokes the development of severe autoimmune myocarditis in susceptible mouse strains¹⁷⁹. In the context of sterile inflammation post-MI, however, the putative release of α -MHC did not induce a detrimental activation of auto-reactive CD4⁺ T cells in this setting. The MHC haplotype might play a central role for the observation that adverse autoimmunity did not develop in the utilized C57BL/6 mice. Laboratory mouse strains are intentionally homozygous and encode a unique set of MHC alleles termed the MHC haplotype⁶. As each mouse strain encodes a unique set of MHC molecules, the diverse strains exhibit a different capacity to present distinct antigens to T cells^{6, 180}. All experiments in this study were conducted in mice possessing a C57BL/6 background that bear the H-2^b MHC haplotype. Interestingly, this mouse strain is not susceptible to autoimmune myocarditis after α -MHC immunization in contrast to animals of BALB/c background encoding H-2^d. The MHC haplotype and consequently the capacity to present distinct peptides may therefore be decisive for the quality of CD4⁺ T cell reactions in terms of MI and lead to "protective autoimmunity" as observed in infarcted C57BL/6 mice, or, by any chance, result in detrimental autoimmunity as observed in α -MHC-immunized BALB/c animals. However, so far, the influence of genetic MHC predisposition on the outcome after MI has not been systematically addressed.

Thymus-derived T_{reg} cells and conventional T cells show little overlap with respect to their antigen specificity. In terms of thymic development, autoreactive conventional T cells undergo deletion from the repertoire whereas T_{reg} cells become rather selected by self-antigen recognition. In the light of the fact that cardiac-specific α -MHC is absent in mTECs and cTECs, T_{reg} cells specific for α -MHC-derived peptides may not arise during thymopoiesis, implying that α -MHC may not be involved in the priming of

T_{reg} cells post-MI. However, a plethora of potential cardiac self-antigens becomes likely released during ischemic injury. Troponin, for instance, has been reported to provoke the proliferation of $CD4^+$ T cells *in vitro*¹⁵⁷. Furthermore, nasal vaccination with this protein has been reported to improve heart function after myocardial ischemia-reperfusion injury¹⁵⁷ suggesting troponin as a candidate antigen that might be involved in the physiological activation of $CD4^+$ T cells after MI.

6.2 $CD4^+$ T cells facilitate healing post-MI

In order to test the functional relevance of $CD4^+$ T cells in wound healing, MI was induced in two different $CD4^+$ T cell-deficient mouse strains, i.e. MHC II KO mice lacking MHC class II-restricted $CD4^+$ T cells, and OT-II mice harboring $CD4^+$ T cells with restricted (self-) antigen reactivity. Both mouse strains showed a significantly higher mortality during the first week after MI due to a prevalence of left-ventricular ruptures indicating pronounced healing deficits. Both mouse strains were characterized by an attenuated and disarrayed scar tissue construction implying either an impaired myofibroblast function, or a deregulated activation of collagenolytic enzymes in the infarct zone of these mice. The pronounced phenotype of OT-II and MHCII KO mice, however, is most likely the result of both a lack of anti-inflammatory T_{reg} cells in combination with an absence of conventional $CD4^+$ T cells that most likely also directly contribute to the facilitation of postinfarction healing. An array of T cell-derived mediators is capable of fine-tuning the reparative response. IL-13, for instance, has been demonstrated to directly modulate myo-fibroblast function fuelling cell proliferation and collagen deposition^{181, 182}. The impaired scar tissue formation in $CD4^+$ T cell-deficient mice may further represent a consequence of pronounced collagen degradation in these hearts. Dysregulation of collagenolytic MMP-9 constitutes a critical determinant for the development of left-ventricular ruptures^{183, 184}. A lack of T cell-derived IL-10 may have aggravated clinical outcome in OT-II and MHCII KO mice as IL-10 signaling in the infarct zone has been reported to reduce both MMP-9 expression and activity^{185, 186}. Most importantly, macrophage polarization is pivotally influenced by various T cell mediators. It is likely that $CD4^+$ T cell-deficient mice exhibit a disturbed macrophage compartment post-MI that causes impaired scarring and, ultimately, the emergence of left-ventricular ruptures.

6.3 T_{reg} cell depletion deteriorates postinfarction healing due to an impaired macrophage M2 polarization

Healing after MI is characterized by an early pro-inflammatory Ly-6C^{high} monocyte-prevalent phase followed by an M2-like macrophage-dominant reparative stage. As Foxp3⁺ regulatory CD4⁺ T cells have well-known anti-inflammatory characteristics, this T cell subset was implicated to modulate postinfarction healing. To address whether the absence of T_{reg} cells was responsible for the severe phenotype of MHCII KO and OT-II mice lacking the entire functional CD4⁺ T cell compartment, T_{reg} cells were specifically depleted using two different approaches. T_{reg} cell ablation in DEREK mice led to increased infarct sizes, left-ventricular dilatation and deteriorated cardiac function. The adverse phenotype of T_{reg} cell-ablated DEREK mice was reconfirmed in a model of anti-CD25 antibody-mediated T_{reg} cell depletion. Anti-CD25 antibody treatment resulted in aggravated left-ventricular dilatation and, most importantly, to impaired survival rates suggesting that these animals deceased predominantly due to heart failure. The clinical outcome of exacerbated remodeling in T_{reg} cell-depleted mice resembles the postinfarction phenotype of global CCR5 knock-out mice that are characterized by an attenuated T_{reg} cell influx into the infarct zone¹⁸¹. However, as other immune cells such as monocytes also employ CCR5 to infiltrate the healing myocardium, the study could not unambiguously indicate a causal relationship between T_{reg} cell recruitment and outcome.

Neither of the two T_{reg} cell depletion models exhibited a prevalence of left-ventricular ruptures in contrast to MHCII KO and OT-II mice that showed a more severe phenotype characterized by a predisposition to develop ruptures. The attenuated outcome in T_{reg} cell-deficient mice as compared to animals that feature a complete functional lack of CD4⁺ T cells points to a protective role of conventional CD4⁺ T cells in postinfarction healing. Both non-regulatory CD4⁺ and CD8⁺ T cells express significant amounts of the ecto-5'-nucleotidase CD73 that catalyzes a critical step in the synthesis of adenosine¹⁸⁷. In fact, non-regulatory CD4⁺ and CD8⁺ T cells together account for approximately 50% of the synthesized adenosine in the infarcted heart 7 days after MI^{187, 188}. Adenosine signaling has emerged as a critical pathway that mitigates infarct inflammation and, moreover, that fosters scar tissue maturation in the infarct core¹⁸⁸. T_{reg} cell ablation led to an increased expansion of both CD4⁺ and CD8⁺ non-T_{reg} cells that numerously accumulated in the infarcted myocardium. A presumably escalated adenosine synthesis in the infarct zone of T_{reg} cell-deficient

mice may therefore have partially compensated the adverse effects of a maladaptive activation of conventional T cells in these mice characterized by a high synthesis rate of TNF α and IFN γ .

The observation that T_{reg} cell deficiency does not provoke left-ventricular ruptures is, *prima facie*, at odds with the finding that therapeutic T_{reg} cell activation in CD28-SA-treated mice reduces the occurrence of left-ventricular ruptures. However, therapeutic T_{reg} cell activation provoked an escalated synthesis of scar-forming collagens and both TIMP-1 and TIMP-2 in the infarct region indicating that T_{reg} and M2 cells accelerated or even augmented scar tissue construction that likely prevented ruptures. T_{reg} cell depletion, in contrast, did not influence the expression of collagens or collagenolytic enzymes implicating that M1 cells or T_{reg} cell deficiency do not restrain myofibroblast function during scarring.

The phenotypes of both T_{reg} cell depletion models were not entirely congruent with respect to the severity of postinfarction clinical outcome. The significantly impaired survival rate in anti-CD25 antibody-treated mice represents the most striking discrepancy in comparison to DTX-treated DEREK animals. As a limitation of this study, however, one cannot definitely rule out that anti-CD25 or DTX treatments have differentially influenced healing, or the occurrence of fatal cardiac arrhythmias as both treatments are known to be associated with potential off-target or indirect effects to some degree^{189, 190}. DTX administration at the used dose, for instance, has been demonstrated to elicit neutrophilia and monocytosis in mice as early as two days after injection¹⁹¹. As both fractions of myeloid cells influence postinfarction healing, differences in the clinical phenotype between the two depletion models may result from an altered mobilization of monocytes and neutrophils. Furthermore, the anti-CD25 monoclonal antibody may have exerted off-target effects on other CD25-bearing cells besides T_{reg} cells such as activated conventional T cells, dendritic cells, or distinct NK cell subsets that may have also been depleted¹⁹⁰.

Infarcted hearts of both depletion models harbored elevated numbers of pro-inflammatory myeloid cells, i.e. Ly-6C^{high} monocytes, M1 cells and neutrophils. The reinforced influx of myeloid cells into the infarcted heart is in accordance to other models of healing and inflammation. In a rodent model for wound healing after burn injury, T_{reg} cell depletion intensified the infiltration of innate immune cells into the lesion¹⁹². Furthermore, T_{reg} cells can modulate chemokine synthesis at the site of inflammation to regulate the influx of myeloid cells¹⁹³. The enhanced leukocyte

recruitment into hearts of T_{reg} cell-deficient DEREg mice came along with a pronounced accumulation of conventional $CD4^+$ as well as $CD8^+$ T cells contributing to an increased expression of IFN γ and TNF α that are both individually capable of driving M1 differentiation.

In comparison to wildtype littermates, T_{reg} cell ablations prior to MI led to larger infarcts in DEREg mice in line with an exacerbated cardiac remodeling and function in both T_{reg} cell depletion models. Mechanistically, heightened TNF α levels in combination with an M1 macrophage polarization state are likely responsible for the observed maladaptive phenotype. The deleterious impact of TNF α on postinfarction healing and remodeling is underlined in global TNF α knock-out mice that show a preservation of cardiac output post-MI¹⁹⁴ as TNF α abates cardiac contractile function and has been shown to provoke cardiomyocyte apoptosis as well as left-ventricular dilatation^{195, 196}. Aside of TNF α , iNOS-mediated effects are critically involved in cardiac deterioration post-MI. Several independent reports clearly indicate that pharmacological iNOS inhibition or genetic iNOS ablation correlates with a reduction of both infarct size and left-ventricular dilatation^{197, 198, 199, 200}. The detrimental effects of iNOS on postinfarction healing and remodeling are ascribed to the NO-dependant cytotoxicity as NO-derived radicals along with an inactivation of sulphur-iron-centered enzymes lead to the disruption of essential metabolic pathways^{201, 202}. M1-like macrophages in the healing myocardium of T_{reg} cell-deficient DEREg mice showed a significantly increased iNOS expression that likely aggravated remodeling and infarct expansion due to a secondary loss of surviving cardiomyocytes. However, although the mRNA expression of collagenolytic MMP-2 and MMP-9 as well as their respective tissue inhibitors were not different in DEREg mice as compared to controls, an elevated overall collagenase activity cannot be definitely ruled out in these hearts. Secondary collagenase activation by reactive oxygen or nitrogen species at the protein level, for instance, may have further contributed to the exacerbated infarct expansion in DEREg mice²⁰³. In accordance with an elevated iNOS synthesis, monocytic cells in infarcts of T_{reg} cell-deficient mice showed a diminished M2-like macrophage differentiation which has been demonstrated by unrelated reports to correlate with aggravated cardiac remodeling and function^{204, 205}. The attenuated synthesis of scar-stabilizing OPN and FXIII presumably contributed to the cardiac deterioration in T_{reg} cell-deficient mice^{206, 207, 208}. The healing infarct of global OPN KO mice shows both disarrayed collagen deposition and reduced

collagen content indicating a fundamental role of OPN in postinfarction ECM assembly^{206, 209}. Similarly, transglutaminase FXIII is involved in scar tissue construction post-MI as the enzyme promotes cross-linking of ECM components^{207, 210}. Thus, deficits in ECM construction may have contributed to the impairment of cardiac performance in T_{reg} cell-deficient mice. TGF β synthesis in the infarcted myocardium is considered to represent a molecular switch suppressing the early postinfarction inflammation while activating reparative pathways^{208, 211}. Lack of TGF β 1 synthesis by T_{reg} cells in the infarct core of T_{reg} cell-deficient mice, thus, presumably further corrupted healing (Fig. 40).

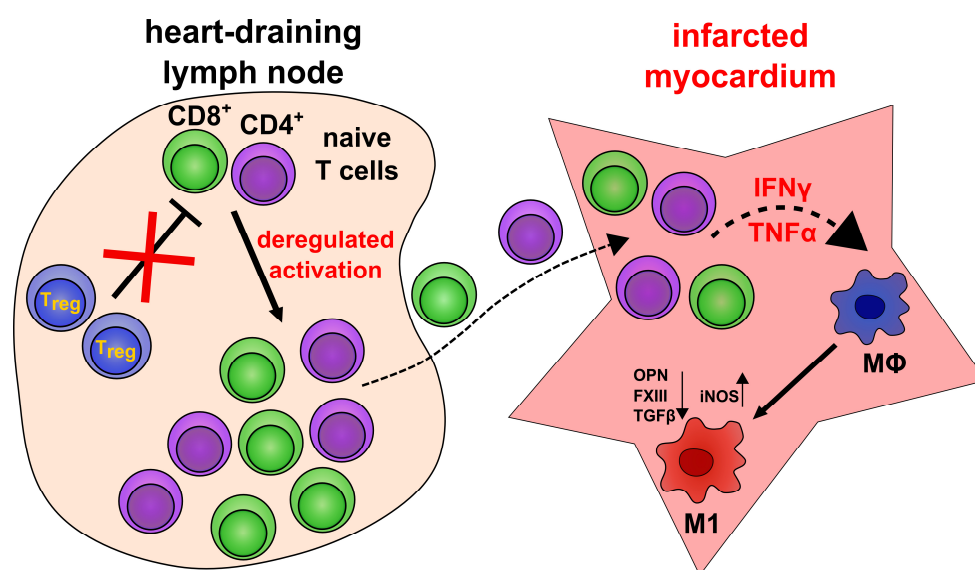


Fig. 40: Proposed model depicting the mechanism for impaired healing in T_{reg} cell-depleted mice. T_{reg} cell depletion provokes an adverse activation and polarization of both CD4⁺ and CD8⁺ non-regulatory T cells in heart-draining lymph nodes of infarcted mice. These non-Treg cells accumulate in the infarcted myocardium and polarize resident macrophages towards an M1-like state by releasing IFN γ and TNF α . The M1 polarization state is characterized by an increased expression of deleterious iNOS in line with a reduced synthesis of healing-promoting osteopontin (OPN), transglutaminase (FXIII) and transforming growth factor beta 1 (TGF β 1).

6.4 Therapeutic T_{reg} cell activation improves postinfarction wound healing by enhancing an M2-like macrophage polarization

The observation that T_{reg} cells facilitate healing after MI suggested that a therapeutic T_{reg} cell activation could further improve the obviously beneficial influence of these cells on postinfarction outcome. The physiological T_{reg} cell activation after MI was amplified by a single CD28-SA injection 2 days after surgery and led to a significantly

improved survival. Echocardiography revealed no significant differences between CD28-SA-treated mice and the respective control group. However, the improved survival of mice with large MI after CD28-SA injection likely explains the fact that no mitigation of adverse left-ventricular dilatation was found in this group as compared to controls.

CD28-SA treatment reinforced the accumulation of T_{reg} cells in the infarct zone 5 days after MI in contrast to conventional $CD4^+$ T cells that did not show an increased influx. The observed T cell mobilization kinetics in treated mice are in line with former reports. Early after CD28-SA-mediated activation, T cells are effectively retained in secondary lymphoid organs²¹². $Foxp3^+$ T_{reg} cells, however, experience a second phase of increased motility post-stimulation facilitating T_{reg} cell homing²¹². The increased T_{reg} cell accumulation in the hearts of CD28-SA-treated mice strengthens the hypothesis that improved healing is attributable to infarct-infiltrating T_{reg} cells that exert their beneficial function directly in the healing myocardium.

M2 macrophages have potent anti-inflammatory characteristics and represent an integral pillar in wound healing processes as M2 cells crucially modulate scar tissue formation^{139, 142, 143}. Consistently, experimental modulation of macrophage polarization towards an M2-like differentiation state has been demonstrated to improve wound healing post-MI^{213, 214}. Alternatively activated or M2-like macrophages differentiate in presence of IL-4, IL-13, IL-10 or $TGF\beta$ ^{139, 144}. T_{reg} cells secreted little $TGF\beta 1$ but considerable amounts of IL-10 and IL-13 upon CD28-SA stimulation *in vitro* which capacitated the cells to induce an M2 polarization state even at the unpropitious T_{reg} cell : monocyte/ macrophage ratio of 1:25 in co-culture experiments. CD28-SA treatment provoked an upregulation of $TGF\beta 1$, IL-10 and IL-13 in scar tissue homogenates implying that T_{reg} cells presumably drove the observed M2-like macrophage differentiation in these hearts. M2 cells, in turn, might have further contributed to the M2-creating milieu by secretion of IL-10 and $TGF\beta$ forming a positive feedback loop. In addition to cytokine release, T_{reg} cells might also modulate macrophage polarization in a contact-dependant manner. However, given the relative low T_{reg} cell : macrophage ratio of approximately 1:14, a contact-mediated mechanism is likely insufficient to polarize a large proportion of myeloid cells towards M2 cells.

6.5 Molecular mediators improving wound healing after therapeutic T_{reg} cell activation

CD28-SA treatment led to an increased amount of collagen in the infarct zone before completion of healing indicating augmented or accelerated scar tissue construction in these mice. TGF β signaling is a prominent driver of collagen deposition by (myo-) fibroblasts^{142, 215} and both T_{reg} and M2 cells likely contributed to the escalated TGF β 1 levels detected in the infarct zone of CD28-SA-treated mice. Moreover, the increased abundance of IL-13 in these hearts presumably further instigated collagen synthesis in a synergistic fashion^{216, 217}.

The matricellular protein OPN is a key player in wound healing and scar tissue formation after MI²⁰⁹. Thus, the observed increase in OPN expression in the infarct zone of CD28-SA-treated mice likely improved the formation of a stable scar.

As OPN favors construction of a mechanically robust scar, an *in vitro* test system was set up to evaluate the contribution of monocytes/ macrophages and T_{reg} cells to the amount of OPN in the healing infarct *in vivo*. CD28-SA-stimulated T_{reg} cells secreted TGF β 1, IL-10 and IL-13 that synergistically elicited OPN release from monocytic cells in line with an M2-like macrophage polarization. Neutralization of TGF β reduced OPN secretion which is in accordance with the observation that M2 differentiation requires TGF β signaling²¹⁸. However, TGF β receptor engagement alone was not sufficient to provoke OPN release from monocytic cells implying that TGF β is necessary to render the cells responsive to IL-10 and IL-13.

Monocytes and macrophages represent the most abundant leukocyte fraction in the reparative phase of postinfarction healing. Therefore, it is likely that the major proportion of OPN in the healing myocardium is derived from monocytic cells. However, other cell types such as myofibroblasts may have additionally contributed to the elevated OPN synthesis²¹⁹.

Aside from OPN, transglutaminase FXIII crucially stabilizes scar tissue integrity by cross-linking ECM components²¹⁰. Global FXIII deficiency in mice and impaired expression in men correlates with a higher incidence of left-ventricular ruptures post-MI^{207, 220}. Consistently, exogenous administration of recombinant FXIII to infarcted mice results in increased collagen density in line with a reduction of rupture frequencies²²⁰. The increased expression of FXIII in the healing myocardium of CD28-SA-treated mice, thus, presumably further improved the scarring process (Fig. 41).

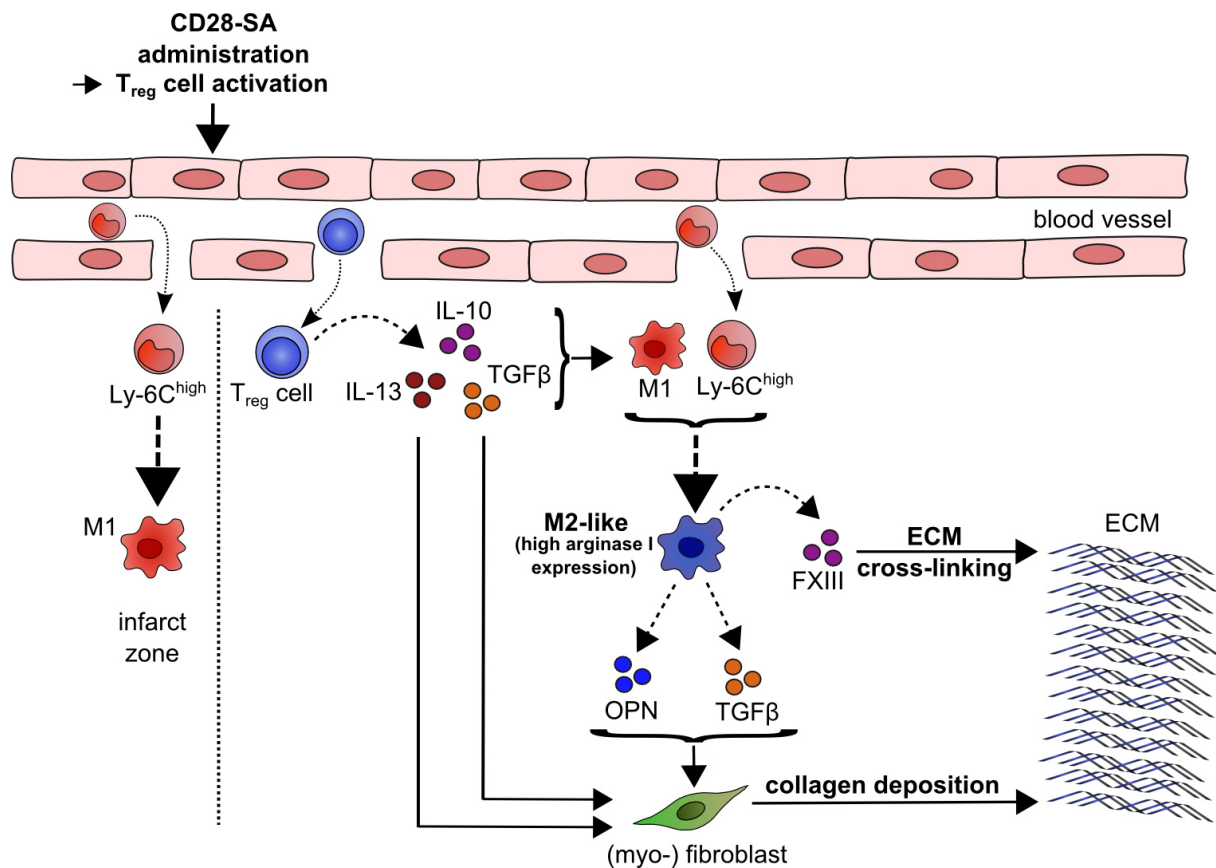


Fig. 41: Model for improved healing after therapeutic CD28-SA administration. During early infarct healing, infiltrating Ly-6C^{high} monocytes and M1 macrophages mediate cardiac inflammation. As healing proceeds, M2-like macrophages emerge in the scar characterized by an inflammation-resolving and healing-promoting transcriptional profile. Therapeutic CD28-SA administration provokes the accumulation of activated T_{reg} cells in the healing myocardium. T_{reg} cell-derived interleukin (IL)-10, IL-13 and transforming growth factor beta (TGFβ) synergistically boost M2-like macrophage polarization resulting in increased synthesis of transglutaminase factor XIII (FXIII), osteopontin (OPN) and transforming growth factor beta 1 (TGFβ1). OPN, TGFβ and T_{reg} cell-derived IL-13 promote collagen deposition by myofibroblasts. FXIII mediates cross-linking of extracellular collagen matrix (ECM) components bracing scar tissue integrity.

6.6 Implications for the treatment of patients with MI

The concept that a deregulated inflammatory reaction exacerbates postinfarction healing is widely accepted and various experimental studies underline that inflammation resolution in the right temporal context is of paramount importance. As T_{reg} cells have well-known anti-inflammatory characteristics, efforts have been taken to harness these cells for the treatment of inflammatory disorders. The present study demonstrated that T_{reg} cells beneficially influence postinfarction wound healing by alleviating inflammation in the healing myocardium. Therapeutic T_{reg} cell activation especially improved the replacement of the irreversibly injured myocardium by a collagenous scar preventing left-ventricular ruptures. Although the incidence of ruptures is relatively low in men as compared to C57BL/6 mice, it seems plausible

that an accelerated healing or improved scarring may attenuate both infarct expansion and adverse left-ventricular dilatation in human patients.

Pro-fibrotic actions in the non-injured remote myocardium represent potential negative effects after CD28-SA treatment that may compromise cardiac function. However, activated T_{reg} cells in CD28-SA-treated mice modulate pro-fibrotic pathways in macrophages and fibroblasts that both accumulate predominantly spatially restricted in the healing infarct core early post-MI. Furthermore, CD28-SA-activated T_{reg} cells did not infiltrate non-injured cardiac parenchyma as sham-operated mice exhibited no accumulation of T_{reg} cells after CD28-SA injection, implying that macrophages and fibroblasts in the remote myocardium of infarcted mice may not have been stimulated to promote fibrosis. The long-term survival of CD28-SA-treated animals further indicates that negative effects were, if at all present, far from annihilating the beneficial effects of CD28-SA administration on postinfarction healing.

In March 2006, a first in-man trial to activate T_{reg} cells utilizing the human CD28-SA TGN1412/ TAB08 yielded a catastrophic result as volunteers experienced a life-threatening cytokine release syndrome^{221, 222}. However, more recently, the same human CD28-SA has been successfully tested in a phase I clinical trial by administration of significantly lower antibody amounts resulting in increased plasma levels of the T_{reg} cell signature mediator IL-10²²². Thus, the usage of CD28-SA to activate T_{reg} cells still holds potential for the treatment of human patients. However, alternative strategies to activate T_{reg} cells *in vivo* have been successfully pursued. Recombinant human IL-2 administered at low dose, for instance, has been successfully used to expand T_{reg} cells over conventional T cells in men¹⁷¹. IL-2/ IL-2 mAB complexes, hitherto used only in experimental settings, bear even more clinical potential as complexed IL-2 further increases suppressive T_{reg} cell functions on a per cell basis as compared to low dose IL-2 treatment¹⁶⁴. Using an experimental mouse model of myocardial infarction, the present study demonstrated that an administration of IL-2/ IL-2 mAB complexes, indeed, was capable of inducing a beneficial M2-like macrophage polarization. Although the expression of M2-inducing cytokines after IL-2/ IL-2 mAB administration was not as pronounced as in hearts of CD28-SA-treated mice, macrophages and myofibroblasts functions were still sufficiently reinforced to promote healing as collagen alpha 1 (III) and, by trend, collagen alpha 1 (I) synthesis was upregulated in the emerging scar.

The results of this study are especially of high clinical relevance since a modulation of T_{reg} cells and, subsequently, the monocyte/ macrophage compartment was conducted in a therapeutic fashion. As healing is considerably slower in men as compared to rodents, there might be a therapeutic window of days to weeks in humans to prevent or attenuate detrimental infarct expansion, left-ventricular remodeling, or even infarct rupture.

7 References

1. Bloom DE, Cafiero, E.T., Jané-Llopis, E., Abrahams-Gessel, S., Bloom, L.R., Fathima, S., Feigl, A.B., Gaziano, T., Mowafi, M., Pandya, A., Prettner, K., Rosenberg, L., Seligman, B., Stein, A., & Weinstein, C. The Global Economic Burden of Non-communicable Diseases. 2001.
2. Dohi T, Daida H. [Change of concept and pathophysiology in acute coronary syndrome]. *Nihon rinsho Japanese journal of clinical medicine* 2010, **68**(4): 592-596.
3. Tsujita K, Kaikita K, Soejima H, Sugiyama S, Ogawa H. [Acute coronary syndrome-initiating factors]. *Nihon rinsho Japanese journal of clinical medicine* 2010, **68**(4): 607-614.
4. Roe MT, Messenger JC, Weintraub WS, Cannon CP, Fonarow GC, Dai D, *et al.* Treatments, Trends, and Outcomes of Acute Myocardial Infarction and Percutaneous Coronary Intervention. *Journal of the American College of Cardiology* 2010, **56**(4): 254-263.
5. Dobaczewski M, Gonzalez-Quesada C, Frangogiannis NG. The extracellular matrix as a modulator of the inflammatory and reparative response following myocardial infarction. *Journal of molecular and cellular cardiology* 2010, **48**(3): 504-511.
6. Janeway C TP, Walport M. *Immunobiology, 7th edn.* Garland Science: New York, 2007.
7. Lichtman A. *Cellular and molecular immunology, 5th edn.* Saunders: Philadelphia, 2003.
8. Medzhitov R, Janeway CA, Jr. Decoding the patterns of self and nonself by the innate immune system. *Science* 2002, **296**(5566): 298-300.
9. Bianchi ME. DAMPs, PAMPs and alarmins: all we need to know about danger. *Journal of leukocyte biology* 2007, **81**(1): 1-5.
10. Park JE, Barbul A. Understanding the role of immune regulation in wound healing. *American journal of surgery* 2004, **187**(5A): 11S-16S.
11. Germain RN. T-cell development and the CD4-CD8 lineage decision. *Nature reviews Immunology* 2002, **2**(5): 309-322.
12. Apostolou I, Sarukhan A, Klein L, von Boehmer H. Origin of regulatory T cells with known specificity for antigen. *Nature immunology* 2002, **3**(8): 756-763.
13. von Boehmer H, Kieselow P. Negative selection of the T-cell repertoire: where and when does it occur? *Immunological reviews* 2006, **209**: 284-289.

14. von Boehmer H, Melchers F. Checkpoints in lymphocyte development and autoimmune disease. *Nature immunology* 2010, **11**(1): 14-20.
15. Girard JP, Moussion C, Forster R. HEVs, lymphatics and homeostatic immune cell trafficking in lymph nodes. *Nature reviews Immunology* 2012, **12**(11): 762-773.
16. Mohan JF, Unanue ER. Unconventional recognition of peptides by T cells and the implications for autoimmunity. *Nature reviews Immunology* 2012, **12**(10): 721-728.
17. Villadangos JA, Schnorrer P. Intrinsic and cooperative antigen-presenting functions of dendritic-cell subsets in vivo. *Nature reviews Immunology* 2007, **7**(7): 543-555.
18. Neefjes J, Jongsma ML, Paul P, Bakke O. Towards a systems understanding of MHC class I and MHC class II antigen presentation. *Nature reviews Immunology* 2011, **11**(12): 823-836.
19. Heath WR, Carbone FR. Cross-presentation in viral immunity and self-tolerance. *Nature reviews Immunology* 2001, **1**(2): 126-134.
20. Traherne JA. Human MHC architecture and evolution: implications for disease association studies. *International journal of immunogenetics* 2008, **35**(3): 179-192.
21. Chen L, Flies DB. Molecular mechanisms of T cell co-stimulation and co-inhibition. *Nature reviews Immunology* 2013, **13**(4): 227-242.
22. Mills KH. TLR-dependent T cell activation in autoimmunity. *Nature reviews Immunology* 2011, **11**(12): 807-822.
23. Rochman Y, Spolski R, Leonard WJ. New insights into the regulation of T cells by gamma(c) family cytokines. *Nature reviews Immunology* 2009, **9**(7): 480-490.
24. von Herrath MG, Harrison LC. Antigen-induced regulatory T cells in autoimmunity. *Nature reviews Immunology* 2003, **3**(3): 223-232.
25. Collin M, Bigley V, Haniffa M, Hambleton S. Human dendritic cell deficiency: the missing ID? *Nature reviews Immunology* 2011, **11**(9): 575-583.
26. Hashimoto D, Miller J, Merad M. Dendritic cell and macrophage heterogeneity in vivo. *Immunity* 2011, **35**(3): 323-335.
27. Geissmann F, Manz MG, Jung S, Sieweke MH, Merad M, Ley K. Development of monocytes, macrophages, and dendritic cells. *Science* 2010, **327**(5966): 656-661.

28. Cheong C, Matos I, Choi JH, Dandamudi DB, Shrestha E, Longhi MP, *et al.* Microbial stimulation fully differentiates monocytes to DC-SIGN/CD209(+) dendritic cells for immune T cell areas. *Cell* 2010, **143**(3): 416-429.
29. Cao C, Lawrence DA, Strickland DK, Zhang L. A specific role of integrin Mac-1 in accelerated macrophage efflux to the lymphatics. *Blood* 2005, **106**(9): 3234-3241.
30. Kirby AC, Coles MC, Kaye PM. Alveolar macrophages transport pathogens to lung draining lymph nodes. *Journal of immunology* 2009, **183**(3): 1983-1989.
31. Randolph GJ, Jakubzick C, Qu C. Antigen presentation by monocytes and monocyte-derived cells. *Current opinion in immunology* 2008, **20**(1): 52-60.
32. Malhotra S, Kovats S, Zhang W, Coggeshall KM. B cell antigen receptor endocytosis and antigen presentation to T cells require Vav and dynamin. *The Journal of biological chemistry* 2009, **284**(36): 24088-24097.
33. Amsen D, Spilianakis CG, Flavell RA. How are T(H)1 and T(H)2 effector cells made? *Current opinion in immunology* 2009, **21**(2): 153-160.
34. Radtke F, MacDonald HR, Tacchini-Cottier F. Regulation of innate and adaptive immunity by Notch. *Nature reviews Immunology* 2013, **13**(6): 427-437.
35. Sun J, Krawczyk CJ, Pearce EJ. Suppression of Th2 cell development by Notch ligands Delta1 and Delta4. *Journal of immunology* 2008, **180**(3): 1655-1661.
36. Amsen D, Antov A, Flavell RA. The different faces of Notch in T-helper-cell differentiation. *Nature reviews Immunology* 2009, **9**(2): 116-124.
37. Amsen D, Antov A, Jankovic D, Sher A, Radtke F, Souabni A, *et al.* Direct regulation of Gata3 expression determines the T helper differentiation potential of Notch. *Immunity* 2007, **27**(1): 89-99.
38. Huang G, Wang Y, Chi H. Regulation of TH17 cell differentiation by innate immune signals. *Cellular & molecular immunology* 2012, **9**(4): 287-295.
39. Lutz MB, Schuler G. Immature, semi-mature and fully mature dendritic cells: which signals induce tolerance or immunity? *Trends in immunology* 2002, **23**(9): 445-449.
40. Harding FA, McArthur JG, Gross JA, Raulet DH, Allison JP. CD28-mediated signalling co-stimulates murine T cells and prevents induction of anergy in T-cell clones. *Nature* 1992, **356**(6370): 607-609.
41. Hawiger D, Inaba K, Dorsett Y, Guo M, Mahnke K, Rivera M, *et al.* Dendritic cells induce peripheral T cell unresponsiveness under steady state conditions in vivo. *The Journal of experimental medicine* 2001, **194**(6): 769-779.

42. Lutz MB. Therapeutic potential of semi-mature dendritic cells for tolerance induction. *Frontiers in immunology* 2012, **3**: 123.
43. Chen L. Co-inhibitory molecules of the B7-CD28 family in the control of T-cell immunity. *Nature reviews Immunology* 2004, **4**(5): 336-347.
44. Bevan MJ. Helping the CD8(+) T-cell response. *Nature reviews Immunology* 2004, **4**(8): 595-602.
45. Zhu J, Paul WE. Peripheral CD4+ T-cell differentiation regulated by networks of cytokines and transcription factors. *Immunological reviews* 2010, **238**(1): 247-262.
46. El-behi M, Rostami A, Ciric B. Current views on the roles of Th1 and Th17 cells in experimental autoimmune encephalomyelitis. *Journal of neuroimmune pharmacology : the official journal of the Society on NeuroImmune Pharmacology* 2010, **5**(2): 189-197.
47. Ma CS, Deenick EK, Batten M, Tangye SG. The origins, function, and regulation of T follicular helper cells. *The Journal of experimental medicine* 2012, **209**(7): 1241-1253.
48. McHeyzer-Williams M, Okitsu S, Wang N, McHeyzer-Williams L. Molecular programming of B cell memory. *Nature reviews Immunology* 2012, **12**(1): 24-34.
49. Vinuesa CG, Sanz I, Cook MC. Dysregulation of germinal centres in autoimmune disease. *Nature reviews Immunology* 2009, **9**(12): 845-857.
50. Staudt V, Bothur E, Klein M, Lingnau K, Reuter S, Grebe N, *et al.* Interferon-regulatory factor 4 is essential for the developmental program of T helper 9 cells. *Immunity* 2010, **33**(2): 192-202.
51. Jelley-Gibbs DM, Strutt TM, McKinstry KK, Swain SL. Influencing the fates of CD4 T cells on the path to memory: lessons from influenza. *Immunology and cell biology* 2008, **86**(4): 343-352.
52. Mills KH. Regulatory T cells: friend or foe in immunity to infection? *Nature reviews Immunology* 2004, **4**(11): 841-855.
53. Hodgson HJ, Wands JR, Isselbacher KJ. Decreased suppressor cell activity in inflammatory bowel disease. *Clinical and experimental immunology* 1978, **32**(3): 451-458.
54. Hardin JA, Chused TM, Steinberg AD. Suppressor cells in the graft vs host reaction. *Journal of immunology* 1973, **111**(2): 650-651.
55. Sakaguchi S, Sakaguchi N, Asano M, Itoh M, Toda M. Immunologic self-tolerance maintained by activated T cells expressing IL-2 receptor alpha-chains (CD25). Breakdown of a single mechanism of self-tolerance causes

- various autoimmune diseases. *Journal of immunology* 1995, **155**(3): 1151-1164.
56. Bluestone JA, Tang Q. How do CD4+CD25+ regulatory T cells control autoimmunity? *Current opinion in immunology* 2005, **17**(6): 638-642.
57. Fontenot JD, Gavin MA, Rudensky AY. Foxp3 programs the development and function of CD4+CD25+ regulatory T cells. *Nature immunology* 2003, **4**(4): 330-336.
58. Liston A, Nutsch KM, Farr AG, Lund JM, Rasmussen JP, Koni PA, *et al.* Differentiation of regulatory Foxp3+ T cells in the thymic cortex. *Proceedings of the National Academy of Sciences of the United States of America* 2008, **105**(33): 11903-11908.
59. Feuerer M, Hill JA, Mathis D, Benoist C. Foxp3+ regulatory T cells: differentiation, specification, subphenotypes. *Nature immunology* 2009, **10**(7): 689-695.
60. Bour-Jordan H, Bluestone JA. Regulating the regulators: costimulatory signals control the homeostasis and function of regulatory T cells. *Immunological reviews* 2009, **229**(1): 41-66.
61. Greenwald RJ, Freeman GJ, Sharpe AH. The B7 family revisited. *Annual review of immunology* 2005, **23**: 515-548.
62. Sharpe AH, Freeman GJ. The B7-CD28 superfamily. *Nature reviews Immunology* 2002, **2**(2): 116-126.
63. Wong J, Obst R, Correia-Neves M, Losyev G, Mathis D, Benoist C. Adaptation of TCR repertoires to self-peptides in regulatory and nonregulatory CD4+ T cells. *Journal of immunology* 2007, **178**(11): 7032-7041.
64. Hsieh CS, Zheng Y, Liang Y, Fontenot JD, Rudensky AY. An intersection between the self-reactive regulatory and nonregulatory T cell receptor repertoires. *Nature immunology* 2006, **7**(4): 401-410.
65. Hsieh CS, Lee HM, Lio CW. Selection of regulatory T cells in the thymus. *Nature reviews Immunology* 2012, **12**(3): 157-167.
66. Jordan MS, Boesteanu A, Reed AJ, Petrone AL, Hohenbeck AE, Lerman MA, *et al.* Thymic selection of CD4+CD25+ regulatory T cells induced by an agonist self-peptide. *Nature immunology* 2001, **2**(4): 301-306.
67. Knoechel B, Lohr J, Kahn E, Bluestone JA, Abbas AK. Sequential development of interleukin 2-dependent effector and regulatory T cells in response to endogenous systemic antigen. *The Journal of experimental medicine* 2005, **202**(10): 1375-1386.
68. Moran AE, Holzapfel KL, Xing Y, Cunningham NR, Maltzman JS, Punt J, *et al.* T cell receptor signal strength in Treg and iNKT cell development

- demonstrated by a novel fluorescent reporter mouse. *The Journal of experimental medicine* 2011, **208**(6): 1279-1289.
69. Killebrew JR, Perdue N, Kwan A, Thornton AM, Shevach EM, Campbell DJ. A self-reactive TCR drives the development of Foxp3+ regulatory T cells that prevent autoimmune disease. *Journal of immunology* 2011, **187**(2): 861-869.
 70. Maloy KJ, Powrie F. Fueling regulation: IL-2 keeps CD4+ Treg cells fit. *Nature immunology* 2005, **6**(11): 1071-1072.
 71. Barron L, Doms H, Hoyer KK, Kuswanto W, Hofmann J, O'Gorman WE, *et al.* Cutting edge: mechanisms of IL-2-dependent maintenance of functional regulatory T cells. *Journal of immunology* 2010, **185**(11): 6426-6430.
 72. Brunkow ME, Jeffery EW, Hjerrild KA, Paepfer B, Clark LB, Yasayko SA, *et al.* Disruption of a new forkhead/winged-helix protein, scurfin, results in the fatal lymphoproliferative disorder of the scurfy mouse. *Nature genetics* 2001, **27**(1): 68-73.
 73. Bennett CL, Christie J, Ramsdell F, Brunkow ME, Ferguson PJ, Whitesell L, *et al.* The immune dysregulation, polyendocrinopathy, enteropathy, X-linked syndrome (IPEX) is caused by mutations of FOXP3. *Nature genetics* 2001, **27**(1): 20-21.
 74. Wildin RS, Ramsdell F, Peake J, Faravelli F, Casanova JL, Buist N, *et al.* X-linked neonatal diabetes mellitus, enteropathy and endocrinopathy syndrome is the human equivalent of mouse scurfy. *Nature genetics* 2001, **27**(1): 18-20.
 75. Lehmann OJ, Sowden JC, Carlsson P, Jordan T, Bhattacharya SS. Fox's in development and disease. *Trends in genetics : TIG* 2003, **19**(6): 339-344.
 76. Ziegler SF. FOXP3: of mice and men. *Annual review of immunology* 2006, **24**: 209-226.
 77. Koh KP, Sundrud MS, Rao A. Domain requirements and sequence specificity of DNA binding for the forkhead transcription factor FOXP3. *PloS one* 2009, **4**(12): e8109.
 78. Song X, Li B, Xiao Y, Chen C, Wang Q, Liu Y, *et al.* Structural and biological features of FOXP3 dimerization relevant to regulatory T cell function. *Cell reports* 2012, **1**(6): 665-675.
 79. Bandukwala HS, Wu Y, Feuerer M, Chen Y, Barboza B, Ghosh S, *et al.* Structure of a domain-swapped FOXP3 dimer on DNA and its function in regulatory T cells. *Immunity* 2011, **34**(4): 479-491.
 80. Mailer RK, Falk K, Rotzschke O. Absence of leucine zipper in the natural FOXP3Delta2Delta7 isoform does not affect dimerization but abrogates suppressive capacity. *PloS one* 2009, **4**(7): e6104.

81. Du J, Huang C, Zhou B, Ziegler SF. Isoform-specific inhibition of ROR alpha-mediated transcriptional activation by human FOXP3. *Journal of immunology* 2008, **180**(7): 4785-4792.
82. Miyao T, Floess S, Setoguchi R, Luche H, Fehling HJ, Waldmann H, *et al.* Plasticity of Foxp3(+) T cells reflects promiscuous Foxp3 expression in conventional T cells but not reprogramming of regulatory T cells. *Immunity* 2012, **36**(2): 262-275.
83. McMurchy AN, Gillies J, Gizzi MC, Riba M, Garcia-Manteiga JM, Cittaro D, *et al.* A novel function for FOXP3 in humans: intrinsic regulation of conventional T cells. *Blood* 2013, **121**(8): 1265-1275.
84. Hill JA, Feuerer M, Tash K, Haxhinasto S, Perez J, Melamed R, *et al.* Foxp3 transcription-factor-dependent and -independent regulation of the regulatory T cell transcriptional signature. *Immunity* 2007, **27**(5): 786-800.
85. Zheng Y, Josefowicz SZ, Kas A, Chu TT, Gavin MA, Rudensky AY. Genome-wide analysis of Foxp3 target genes in developing and mature regulatory T cells. *Nature* 2007, **445**(7130): 936-940.
86. Marson A, Kretschmer K, Frampton GM, Jacobsen ES, Polansky JK, Maclsaac KD, *et al.* Foxp3 occupancy and regulation of key target genes during T-cell stimulation. *Nature* 2007, **445**(7130): 931-935.
87. Li B, Greene MI. FOXP3 actively represses transcription by recruiting the HAT/HDAC complex. *Cell Cycle* 2007, **6**(12): 1432-1436.
88. Xiao Y, Li B, Zhou Z, Hancock WW, Zhang H, Greene MI. Histone acetyltransferase mediated regulation of FOXP3 acetylation and Treg function. *Current opinion in immunology* 2010, **22**(5): 583-591.
89. Chen C, Rowell EA, Thomas RM, Hancock WW, Wells AD. Transcriptional regulation by Foxp3 is associated with direct promoter occupancy and modulation of histone acetylation. *The Journal of biological chemistry* 2006, **281**(48): 36828-36834.
90. Kwon HK, So JS, Lee CG, Sahoo A, Yi HJ, Park JN, *et al.* Foxp3 induces IL-4 gene silencing by affecting nuclear translocation of NFkappaB and chromatin structure. *Molecular immunology* 2008, **45**(11): 3205-3212.
91. Bettelli E, Dastrange M, Oukka M. Foxp3 interacts with nuclear factor of activated T cells and NF-kappa B to repress cytokine gene expression and effector functions of T helper cells. *Proceedings of the National Academy of Sciences of the United States of America* 2005, **102**(14): 5138-5143.
92. Ono M, Yaguchi H, Ohkura N, Kitabayashi I, Nagamura Y, Nomura T, *et al.* Foxp3 controls regulatory T-cell function by interacting with AML1/Runx1. *Nature* 2007, **446**(7136): 685-689.

93. Wu Y, Borde M, Heissmeyer V, Feuerer M, Lapan AD, Stroud JC, *et al.* FOXP3 controls regulatory T cell function through cooperation with NFAT. *Cell* 2006, **126**(2): 375-387.
94. Loizou L, Andersen KG, Betz AG. Foxp3 interacts with c-Rel to mediate NF-kappaB repression. *PloS one* 2011, **6**(4): e18670.
95. Chen W, Jin W, Hardegen N, Lei KJ, Li L, Marinos N, *et al.* Conversion of peripheral CD4⁺CD25⁻ naive T cells to CD4⁺CD25⁺ regulatory T cells by TGF-beta induction of transcription factor Foxp3. *The Journal of experimental medicine* 2003, **198**(12): 1875-1886.
96. Roncarolo MG, Gregori S, Battaglia M, Bacchetta R, Fleischhauer K, Levings MK. Interleukin-10-secreting type 1 regulatory T cells in rodents and humans. *Immunological reviews* 2006, **212**: 28-50.
97. Haribhai D, Williams JB, Jia S, Nickerson D, Schmitt EG, Edwards B, *et al.* A requisite role for induced regulatory T cells in tolerance based on expanding antigen receptor diversity. *Immunity* 2011, **35**(1): 109-122.
98. Horwitz DA, Zheng SG, Gray JD. Natural and TGF-beta-induced Foxp3(+)CD4(+) CD25(+) regulatory T cells are not mirror images of each other. *Trends in immunology* 2008, **29**(9): 429-435.
99. Wu HY, Quintana FJ, da Cunha AP, Dake BT, Koeglsperger T, Starossom SC, *et al.* In Vivo Induction of Tr1 Cells via Mucosal Dendritic Cells and AHR Signaling. *PloS one* 2011, **6**(8).
100. Gottschalk RA, Corse E, Allison JP. TCR ligand density and affinity determine peripheral induction of Foxp3 in vivo. *The Journal of experimental medicine* 2010, **207**(8): 1701-1711.
101. Semple K, Nguyen A, Yu Y, Wang H, Anasetti C, Yu XZ. Strong CD28 costimulation suppresses induction of regulatory T cells from naive precursors through Lck signaling. *Blood* 2011, **117**(11): 3096-3103.
102. Josefowicz SZ, Lu LF, Rudensky AY. Regulatory T cells: mechanisms of differentiation and function. *Annual review of immunology* 2012, **30**: 531-564.
103. Barnes MJ, Griseri T, Johnson AM, Young W, Powrie F, Izcue A. CTLA-4 promotes Foxp3 induction and regulatory T cell accumulation in the intestinal lamina propria. *Mucosal immunology* 2013, **6**(2): 324-334.
104. Sakaguchi S, Wing K, Onishi Y, Prieto-Martin P, Yamaguchi T. Regulatory T cells: how do they suppress immune responses? *International immunology* 2009, **21**(10): 1105-1111.
105. Vignali DA, Collison LW, Workman CJ. How regulatory T cells work. *Nature reviews Immunology* 2008, **8**(7): 523-532.

106. Gu P, Gao JF, D'Souza CA, Kowalczyk A, Chou KY, Zhang L. Trogocytosis of CD80 and CD86 by induced regulatory T cells. *Cellular & molecular immunology* 2012, **9**(2): 136-146.
107. Yamaguchi T, Wing JB, Sakaguchi S. Two modes of immune suppression by Foxp3(+) regulatory T cells under inflammatory or non-inflammatory conditions. *Seminars in immunology* 2011, **23**(6): 424-430.
108. Nahrendorf M, Pittet MJ, Swirski FK. Monocytes: protagonists of infarct inflammation and repair after myocardial infarction. *Circulation* 2010, **121**(22): 2437-2445.
109. Ertl G, Frantz S. Healing after myocardial infarction. *Cardiovascular research* 2005, **66**(1): 22-32.
110. Frantz S, Hofmann U, Fraccarollo D, Schafer A, Kranepuhl S, Hagedorn I, *et al.* Monocytes/macrophages prevent healing defects and left ventricular thrombus formation after myocardial infarction. *FASEB journal : official publication of the Federation of American Societies for Experimental Biology* 2013, **27**(3): 871-881.
111. Sutton MG, Sharpe N. Left ventricular remodeling after myocardial infarction: pathophysiology and therapy. *Circulation* 2000, **101**(25): 2981-2988.
112. Jugdutt BI. Ventricular remodeling after infarction and the extracellular collagen matrix: when is enough enough? *Circulation* 2003, **108**(11): 1395-1403.
113. Czubryt MP. Common threads in cardiac fibrosis, infarct scar formation, and wound healing. *Fibrogenesis & tissue repair* 2012, **5**(1): 19.
114. Pinto AR, Paolicelli R, Salimova E, Gospocic J, Slonimsky E, Bilbao-Cortes D, *et al.* An abundant tissue macrophage population in the adult murine heart with a distinct alternatively-activated macrophage profile. *PloS one* 2012, **7**(5): e36814.
115. Choi JH, Do Y, Cheong C, Koh H, Boscardin SB, Oh YS, *et al.* Identification of antigen-presenting dendritic cells in mouse aorta and cardiac valves. *The Journal of experimental medicine* 2009, **206**(3): 497-505.
116. Swirski FK, Nahrendorf M. Leukocyte behavior in atherosclerosis, myocardial infarction, and heart failure. *Science* 2013, **339**(6116): 161-166.
117. Nahrendorf M, Swirski FK, Aikawa E, Stangenberg L, Wurdinger T, Figueiredo JL, *et al.* The healing myocardium sequentially mobilizes two monocyte subsets with divergent and complementary functions. *The Journal of experimental medicine* 2007, **204**(12): 3037-3047.
118. Frangogiannis NG, Smith CW, Entman ML. The inflammatory response in myocardial infarction. *Cardiovascular research* 2002, **53**(1): 31-47.

119. Wantha S, Alard JE, Megens RT, van der Does AM, Doring Y, Drechsler M, *et al.* Neutrophil-derived cathelicidin promotes adhesion of classical monocytes. *Circulation research* 2013, **112**(5): 792-801.
120. Litt MR, Jeremy RW, Weisman HF, Winkelstein JA, Becker LC. Neutrophil depletion limited to reperfusion reduces myocardial infarct size after 90 minutes of ischemia. Evidence for neutrophil-mediated reperfusion injury. *Circulation* 1989, **80**(6): 1816-1827.
121. Metzler B, Mair J, Lercher A, Schaber C, Hintringer F, Pachinger O, *et al.* Mouse model of myocardial remodelling after ischemia: role of intercellular adhesion molecule-1. *Cardiovascular research* 2001, **49**(2): 399-407.
122. Nahrendorf M, Swirski FK. Monocyte and macrophage heterogeneity in the heart. *Circulation research* 2013, **112**(12): 1624-1633.
123. van Furth R, Cohn ZA. The origin and kinetics of mononuclear phagocytes. *The Journal of experimental medicine* 1968, **128**(3): 415-435.
124. Goodman JW, Hodgson GS. Evidence for stem cells in the peripheral blood of mice. *Blood* 1962, **19**: 702-714.
125. van Furth R, Diesselhoff-den Dulk MM. Dual origin of mouse spleen macrophages. *The Journal of experimental medicine* 1984, **160**(5): 1273-1283.
126. Leuschner F, Rauch PJ, Ueno T, Gorbato R, Marinelli B, Lee WW, *et al.* Rapid monocyte kinetics in acute myocardial infarction are sustained by extramedullary monocytopoiesis. *The Journal of experimental medicine* 2012, **209**(1): 123-137.
127. Schulz C, Gomez Perdiguero E, Chorro L, Szabo-Rogers H, Cagnard N, Kierdorf K, *et al.* A lineage of myeloid cells independent of Myb and hematopoietic stem cells. *Science* 2012, **336**(6077): 86-90.
128. Sieweke MH, Allen JE. Beyond stem cells: self-renewal of differentiated macrophages. *Science* 2013, **342**(6161): 1242974.
129. Tsou CL, Peters W, Si Y, Slaymaker S, Aslanian AM, Weisberg SP, *et al.* Critical roles for CCR2 and MCP-3 in monocyte mobilization from bone marrow and recruitment to inflammatory sites. *The Journal of clinical investigation* 2007, **117**(4): 902-909.
130. Gordon S, Taylor PR. Monocyte and macrophage heterogeneity. *Nature reviews Immunology* 2005, **5**(12): 953-964.
131. Swirski FK, Nahrendorf M, Etzrodt M, Wildgruber M, Cortez-Retamozo V, Panizzi P, *et al.* Identification of splenic reservoir monocytes and their deployment to inflammatory sites. *Science* 2009, **325**(5940): 612-616.

132. Carlin LM, Stamatiades EG, Auffray C, Hanna RN, Glover L, Vizcay-Barrena G, *et al.* Nr4a1-dependent Ly6C(low) monocytes monitor endothelial cells and orchestrate their disposal. *Cell* 2013, **153**(2): 362-375.
133. Yona S, Kim KW, Wolf Y, Mildner A, Varol D, Breker M, *et al.* Fate mapping reveals origins and dynamics of monocytes and tissue macrophages under homeostasis. *Immunity* 2013, **38**(1): 79-91.
134. Varol C, Landsman L, Fogg DK, Greenshtein L, Gildor B, Margalit R, *et al.* Monocytes give rise to mucosal, but not splenic, conventional dendritic cells. *The Journal of experimental medicine* 2007, **204**(1): 171-180.
135. Shi C, Pamer EG. Monocyte recruitment during infection and inflammation. *Nature reviews Immunology* 2011, **11**(11): 762-774.
136. Hilgendorf I, Gerhardt L, Tan TC, Winter C, Holderried TA, Chousterman BG, *et al.* Ly-6Chigh Monocytes Depend on Nr4a1 to Balance both Inflammatory and Reparative Phases in the Infarcted Myocardium. *Circulation research* 2014.
137. Auffray C, Fogg D, Garfa M, Elain G, Join-Lambert O, Kayal S, *et al.* Monitoring of blood vessels and tissues by a population of monocytes with patrolling behavior. *Science* 2007, **317**(5838): 666-670.
138. Lambert JM, Lopez EF, Lindsey ML. Macrophage roles following myocardial infarction. *International journal of cardiology* 2008, **130**(2): 147-158.
139. Mosser DM, Edwards JP. Exploring the full spectrum of macrophage activation. *Nature reviews Immunology* 2008, **8**(12): 958-969.
140. Cordell PA, Kile BT, Standeven KF, Josefsson EC, Pease RJ, Grant PJ. Association of coagulation factor XIII-A with Golgi proteins within monocyte-macrophages: implications for subcellular trafficking and secretion. *Blood* 2010, **115**(13): 2674-2681.
141. Solinas G, Schiarea S, Liguori M, Fabbri M, Pesce S, Zammataro L, *et al.* Tumor-conditioned macrophages secrete migration-stimulating factor: a new marker for M2-polarization, influencing tumor cell motility. *Journal of immunology* 2010, **185**(1): 642-652.
142. Murray PJ, Wynn TA. Protective and pathogenic functions of macrophage subsets. *Nature reviews Immunology* 2011, **11**(11): 723-737.
143. Sica A, Mantovani A. Macrophage plasticity and polarization: in vivo veritas. *The Journal of clinical investigation* 2012, **122**(3): 787-795.
144. Biswas SK, Mantovani A. Macrophage plasticity and interaction with lymphocyte subsets: cancer as a paradigm. *Nature immunology* 2010, **11**(10): 889-896.

145. Arnold L, Henry A, Poron F, Baba-Amer Y, van Rooijen N, Plonquet A, *et al.* Inflammatory monocytes recruited after skeletal muscle injury switch into antiinflammatory macrophages to support myogenesis. *The Journal of experimental medicine* 2007, **204**(5): 1057-1069.
146. Egawa M, Mukai K, Yoshikawa S, Iki M, Mukaida N, Kawano Y, *et al.* Inflammatory monocytes recruited to allergic skin acquire an anti-inflammatory M2 phenotype via basophil-derived interleukin-4. *Immunity* 2013, **38**(3): 570-580.
147. Ramachandran P, Pellicoro A, Vernon MA, Boulter L, Aucott RL, Ali A, *et al.* Differential Ly-6C expression identifies the recruited macrophage phenotype, which orchestrates the regression of murine liver fibrosis. *Proceedings of the National Academy of Sciences of the United States of America* 2012, **109**(46): E3186-3195.
148. Troidl C, Mollmann H, Nef H, Masseli F, Voss S, Szardien S, *et al.* Classically and alternatively activated macrophages contribute to tissue remodelling after myocardial infarction. *Journal of cellular and molecular medicine* 2009, **13**(9B): 3485-3496.
149. Heidt T, Courties G, Dutta P, Sager H, Sebas M, Iwamoto Y, *et al.* Differential Contribution of Monocytes to Heart Macrophages in Steady-State and After Myocardial Infarction. *Circulation research* 2014.
150. Varda-Bloom N, Leor J, Ohad DG, Hasin Y, Amar M, Fixler R, *et al.* Cytotoxic T lymphocytes are activated following myocardial infarction and can recognize and kill healthy myocytes in vitro. *Journal of molecular and cellular cardiology* 2000, **32**(12): 2141-2149.
151. Cheng X, Liao YH, Ge H, Li B, Zhang J, Yuan J, *et al.* TH1/TH2 functional imbalance after acute myocardial infarction: coronary arterial inflammation or myocardial inflammation. *Journal of clinical immunology* 2005, **25**(3): 246-253.
152. Moraru M, Roth A, Keren G, George J. Cellular autoimmunity to cardiac myosin in patients with a recent myocardial infarction. *International journal of cardiology* 2006, **107**(1): 61-66.
153. Abbate A, Bonanno E, Mauriello A, Bussani R, Biondi-Zoccai GG, Liuzzo G, *et al.* Widespread myocardial inflammation and infarct-related artery patency. *Circulation* 2004, **110**(1): 46-50.
154. Hansson GK, Libby P. The immune response in atherosclerosis: a double-edged sword. *Nature reviews Immunology* 2006, **6**(7): 508-519.
155. Libby P, Lichtman AH, Hansson GK. Immune effector mechanisms implicated in atherosclerosis: from mice to humans. *Immunity* 2013, **38**(6): 1092-1104.
156. Liuzzo G, Biasucci LM, Trotta G, Brugaletta S, Pinnelli M, Digianuario G, *et al.* Unusual CD4+CD28null T lymphocytes and recurrence of acute coronary

- events. *Journal of the American College of Cardiology* 2007, **50**(15): 1450-1458.
157. Frenkel D, Pachori AS, Zhang L, Dembinsky-Vaknin A, Farfara D, Petrovic-Stojkovic S, *et al.* Nasal vaccination with troponin reduces troponin specific T-cell responses and improves heart function in myocardial ischemia-reperfusion injury. *International immunology* 2009, **21**(7): 817-829.
158. Yang Z, Day YJ, Toufektsian MC, Xu Y, Ramos SI, Marshall MA, *et al.* Myocardial infarct-sparing effect of adenosine A2A receptor activation is due to its action on CD4+ T lymphocytes. *Circulation* 2006, **114**(19): 2056-2064.
159. Kim JM, Rasmussen JP, Rudensky AY. Regulatory T cells prevent catastrophic autoimmunity throughout the lifespan of mice. *Nature immunology* 2007, **8**(2): 191-197.
160. Setiady YY, Coccia JA, Park PU. In vivo depletion of CD4+FOXP3+ Treg cells by the PC61 anti-CD25 monoclonal antibody is mediated by FcγRIII+ phagocytes. *European journal of immunology* 2010, **40**(3): 780-786.
161. Felonato M, Pina A, de Araujo EF, Loures FV, Bazan SB, Feriotti C, *et al.* Anti-CD25 treatment depletes Treg cells and decreases disease severity in susceptible and resistant mice infected with *Paracoccidioides brasiliensis*. *PloS one* 2012, **7**(11): e51071.
162. Beyersdorf N, Hanke T, Kerkau T, Hunig T. Superagonistic anti-CD28 antibodies: potent activators of regulatory T cells for the therapy of autoimmune diseases. *Annals of the rheumatic diseases* 2005, **64 Suppl 4**: iv91-95.
163. Lin CH, Hunig T. Efficient expansion of regulatory T cells in vitro and in vivo with a CD28 superagonist. *European journal of immunology* 2003, **33**(3): 626-638.
164. Webster KE, Walters S, Kohler RE, Mrkvan T, Boyman O, Surh CD, *et al.* In vivo expansion of T reg cells with IL-2-mAb complexes: induction of resistance to EAE and long-term acceptance of islet allografts without immunosuppression. *The Journal of experimental medicine* 2009, **206**(4): 751-760.
165. Dinh TN, Kyaw TS, Kanellakis P, To K, Tipping P, Toh BH, *et al.* Cytokine therapy with interleukin-2/anti-interleukin-2 monoclonal antibody complexes expands CD4+CD25+Foxp3+ regulatory T cells and attenuates development and progression of atherosclerosis. *Circulation* 2012, **126**(10): 1256-1266.
166. Gao S, Ho D, Vatner DE, Vatner SF. Echocardiography in Mice. *Current protocols in mouse biology* 2011, **1**: 71-83.
167. Whittaker P, Kloner RA, Boughner DR, Pickering JG. Quantitative assessment of myocardial collagen with picrosirius red staining and circularly polarized light. *Basic research in cardiology* 1994, **89**(5): 397-410.

168. Weirather J, Hofmann UD, Beyersdorf N, Ramos GC, Vogel B, Frey A, *et al.* Foxp3+ CD4+ T Cells Improve Healing After Myocardial Infarction by Modulating Monocyte/Macrophage Differentiation. *Circulation research* 2014, **115**(1): 55-67.
169. Hofmann U, Beyersdorf N, Weirather J, Podolskaya A, Bauersachs J, Ertl G, *et al.* Activation of CD4+ T lymphocytes improves wound healing and survival after experimental myocardial infarction in mice. *Circulation* 2012, **125**(13): 1652-1663.
170. Gogishvili T, Langenhorst D, Luhder F, Elias F, Elflein K, Dennehy KM, *et al.* Rapid regulatory T-cell response prevents cytokine storm in CD28 superagonist treated mice. *PloS one* 2009, **4**(2): e4643.
171. Koreth J, Matsuoka K, Kim HT, McDonough SM, Bindra B, Alyea EP, 3rd, *et al.* Interleukin-2 and regulatory T cells in graft-versus-host disease. *The New England journal of medicine* 2011, **365**(22): 2055-2066.
172. Lee SY, Cho ML, Oh HJ, Ryu JG, Park MJ, Jhun JY, *et al.* Interleukin-2/anti-interleukin-2 monoclonal antibody immune complex suppresses collagen-induced arthritis in mice by fortifying interleukin-2/STAT5 signalling pathways. *Immunology* 2012, **137**(4): 305-316.
173. Epelman S, Lavine KJ, Beaudin AE, Sojka DK, Carrero JA, Calderon B, *et al.* Embryonic and adult-derived resident cardiac macrophages are maintained through distinct mechanisms at steady state and during inflammation. *Immunity* 2014, **40**(1): 91-104.
174. Gautier EL, Shay T, Miller J, Greter M, Jakubzick C, Ivanov S, *et al.* Gene-expression profiles and transcriptional regulatory pathways that underlie the identity and diversity of mouse tissue macrophages. *Nature immunology* 2012, **13**(11): 1118-1128.
175. Anzai A, Anzai T, Nagai S, Maekawa Y, Naito K, Kaneko H, *et al.* Regulatory role of dendritic cells in postinfarction healing and left ventricular remodeling. *Circulation* 2012, **125**(10): 1234-1245.
176. Lund JM, Hsing L, Pham TT, Rudensky AY. Coordination of early protective immunity to viral infection by regulatory T cells. *Science* 2008, **320**(5880): 1220-1224.
177. Haribhai D, Lin W, Relland LM, Truong N, Williams CB, Chatila TA. Regulatory T cells dynamically control the primary immune response to foreign antigen. *Journal of immunology* 2007, **178**(5): 2961-2972.
178. Lv H, Havari E, Pinto S, Gottumukkala RV, Cornivelli L, Raddassi K, *et al.* Impaired thymic tolerance to alpha-myosin directs autoimmunity to the heart in mice and humans. *The Journal of clinical investigation* 2011, **121**(4): 1561-1573.

179. Hayward SL, Bautista-Lopez N, Suzuki K, Atrazhev A, Dickie P, Elliott JF. CD4 T cells play major effector role and CD8 T cells initiating role in spontaneous autoimmune myocarditis of HLA-DQ8 transgenic IAb knockout nonobese diabetic mice. *Journal of immunology* 2006, **176**(12): 7715-7725.
180. Kamath AB, Alt J, Debbabi H, Taylor C, Behar SM. The major histocompatibility complex haplotype affects T-cell recognition of mycobacterial antigens but not resistance to Mycobacterium tuberculosis in C3H mice. *Infection and immunity* 2004, **72**(12): 6790-6798.
181. Dobaczewski M, Xia Y, Bujak M, Gonzalez-Quesada C, Frangogiannis NG. CCR5 signaling suppresses inflammation and reduces adverse remodeling of the infarcted heart, mediating recruitment of regulatory T cells. *The American journal of pathology* 2010, **176**(5): 2177-2187.
182. Wynn TA. Cellular and molecular mechanisms of fibrosis. *The Journal of pathology* 2008, **214**(2): 199-210.
183. Creemers EE, Cleutjens JP, Smits JF, Daemen MJ. Matrix metalloproteinase inhibition after myocardial infarction: a new approach to prevent heart failure? *Circulation research* 2001, **89**(3): 201-210.
184. van den Borne SW, Cleutjens JP, Hanemaaijer R, Creemers EE, Smits JF, Daemen MJ, *et al.* Increased matrix metalloproteinase-8 and -9 activity in patients with infarct rupture after myocardial infarction. *Cardiovascular pathology : the official journal of the Society for Cardiovascular Pathology* 2009, **18**(1): 37-43.
185. Krishnamurthy P, Rajasingh J, Lambers E, Qin G, Losordo DW, Kishore R. IL-10 inhibits inflammation and attenuates left ventricular remodeling after myocardial infarction via activation of STAT3 and suppression of HuR. *Circulation research* 2009, **104**(2): e9-18.
186. Mostafa Mtairag E, Chollet-Martin S, Oudghiri M, Laquay N, Jacob MP, Michel JB, *et al.* Effects of interleukin-10 on monocyte/endothelial cell adhesion and MMP-9/TIMP-1 secretion. *Cardiovascular research* 2001, **49**(4): 882-890.
187. Bonner F, Borg N, Burghoff S, Schrader J. Resident cardiac immune cells and expression of the ectonucleotidase enzymes CD39 and CD73 after ischemic injury. *PLoS one* 2012, **7**(4): e34730.
188. Bonner F, Borg N, Jacoby C, Temme S, Ding Z, Fogel U, *et al.* Ecto-5'-nucleotidase on immune cells protects from adverse cardiac remodeling. *Circulation research* 2013, **113**(3): 301-312.
189. van Blijswijk J, Schraml BU, Reis e Sousa C. Advantages and limitations of mouse models to deplete dendritic cells. *European journal of immunology* 2013, **43**(1): 22-26.
190. Wiendl H, Gross CC. Modulation of IL-2Ralpha with daclizumab for treatment of multiple sclerosis. *Nature reviews Neurology* 2013, **9**(7): 394-404.

191. Blankenhaus B, Reitz M, Brenz Y, Eschbach ML, Hartmann W, Haben I, *et al.* Foxp3(+) regulatory T cells delay expulsion of intestinal nematodes by suppression of IL-9-driven mast cell activation in BALB/c but not in C57BL/6 mice. *PLoS pathogens* 2014, **10**(2): e1003913.
192. Murphy TJ, Ni Choileain N, Zang Y, Mannick JA, Lederer JA. CD4+CD25+ regulatory T cells control innate immune reactivity after injury. *Journal of immunology* 2005, **174**(5): 2957-2963.
193. Lee DC, Harker JA, Tregoning JS, Atabani SF, Johansson C, Schwarze J, *et al.* CD25+ natural regulatory T cells are critical in limiting innate and adaptive immunity and resolving disease following respiratory syncytial virus infection. *Journal of virology* 2010, **84**(17): 8790-8798.
194. Sato T, Suzuki H, Shibata M, Kusuyama T, Omori Y, Soda T, *et al.* Tumor-necrosis-factor-alpha-gene-deficient mice have improved cardiac function through reduction of intercellular adhesion molecule-1 in myocardial infarction. *Circulation journal : official journal of the Japanese Circulation Society* 2006, **70**(12): 1635-1642.
195. Horton JW, Maass D, White J, Sanders B. Nitric oxide modulation of TNF-alpha-induced cardiac contractile dysfunction is concentration dependent. *American journal of physiology Heart and circulatory physiology* 2000, **278**(6): H1955-1965.
196. Haudek SB, Taffet GE, Schneider MD, Mann DL. TNF provokes cardiomyocyte apoptosis and cardiac remodeling through activation of multiple cell death pathways. *The Journal of clinical investigation* 2007, **117**(9): 2692-2701.
197. Wang D, Yang XP, Liu YH, Carretero OA, LaPointe MC. Reduction of myocardial infarct size by inhibition of inducible nitric oxide synthase. *American journal of hypertension* 1999, **12**(2 Pt 1): 174-182.
198. Wildhirt SM, Weismueller S, Schulze C, Conrad N, Kornberg A, Reichart B. Inducible nitric oxide synthase activation after ischemia/reperfusion contributes to myocardial dysfunction and extent of infarct size in rabbits: evidence for a late phase of nitric oxide-mediated reperfusion injury. *Cardiovascular research* 1999, **43**(3): 698-711.
199. Feng Q, Lu X, Jones DL, Shen J, Arnold JM. Increased inducible nitric oxide synthase expression contributes to myocardial dysfunction and higher mortality after myocardial infarction in mice. *Circulation* 2001, **104**(6): 700-704.
200. Gilson WD, Epstein FH, Yang Z, Xu Y, Prasad KM, Toufektsian MC, *et al.* Borderzone contractile dysfunction is transiently attenuated and left ventricular structural remodeling is markedly reduced following reperfused myocardial infarction in inducible nitric oxide synthase knockout mice. *Journal of the American College of Cardiology* 2007, **50**(18): 1799-1807.

201. Beckman JS, Beckman TW, Chen J, Marshall PA, Freeman BA. Apparent hydroxyl radical production by peroxynitrite: implications for endothelial injury from nitric oxide and superoxide. *Proceedings of the National Academy of Sciences of the United States of America* 1990, **87**(4): 1620-1624.
202. Geng Y, Hansson GK, Holme E. Interferon-gamma and tumor necrosis factor synergize to induce nitric oxide production and inhibit mitochondrial respiration in vascular smooth muscle cells. *Circulation research* 1992, **71**(5): 1268-1276.
203. Spinale FG. Myocardial matrix remodeling and the matrix metalloproteinases: influence on cardiac form and function. *Physiological reviews* 2007, **87**(4): 1285-1342.
204. Ma Y, Halade GV, Zhang J, Ramirez TA, Levin D, Voorhees A, *et al.* Matrix metalloproteinase-28 deletion exacerbates cardiac dysfunction and rupture after myocardial infarction in mice by inhibiting M2 macrophage activation. *Circulation research* 2013, **112**(4): 675-688.
205. Zamilpa R, Kanakia R, Cigarroa Jt, Dai Q, Escobar GP, Martinez H, *et al.* CC chemokine receptor 5 deletion impairs macrophage activation and induces adverse remodeling following myocardial infarction. *American journal of physiology Heart and circulatory physiology* 2011, **300**(4): H1418-1426.
206. Frangogiannis NG. Matricellular proteins in cardiac adaptation and disease. *Physiological reviews* 2012, **92**(2): 635-688.
207. Nahrendorf M, Hu K, Frantz S, Jaffer FA, Tung CH, Hiller KH, *et al.* Factor XIII deficiency causes cardiac rupture, impairs wound healing, and aggravates cardiac remodeling in mice with myocardial infarction. *Circulation* 2006, **113**(9): 1196-1202.
208. Ikeuchi M, Tsutsui H, Shiomi T, Matsusaka H, Matsushima S, Wen J, *et al.* Inhibition of TGF-beta signaling exacerbates early cardiac dysfunction but prevents late remodeling after infarction. *Cardiovascular research* 2004, **64**(3): 526-535.
209. Singh M, Foster CR, Dalal S, Singh K. Osteopontin: role in extracellular matrix deposition and myocardial remodeling post-MI. *Journal of molecular and cellular cardiology* 2010, **48**(3): 538-543.
210. Tsujimoto I, Moriya K, Sakai K, Dickneite G, Sakai T. Critical role of factor XIII in the initial stages of carbon tetrachloride-induced adult liver remodeling. *The American journal of pathology* 2011, **179**(6): 3011-3019.
211. Frangogiannis NG. Regulation of the inflammatory response in cardiac repair. *Circulation research* 2012, **110**(1): 159-173.
212. Muller N, van den Brandt J, Odoardi F, Tischner D, Herath J, Flugel A, *et al.* A CD28 superagonistic antibody elicits 2 functionally distinct waves of T cell activation in rats. *The Journal of clinical investigation* 2008, **118**(4): 1405-1416.

-
213. Harel-Adar T, Ben Mordechai T, Amsalem Y, Feinberg MS, Leor J, Cohen S. Modulation of cardiac macrophages by phosphatidylserine-presenting liposomes improves infarct repair. *Proceedings of the National Academy of Sciences of the United States of America* 2011, **108**(5): 1827-1832.
214. Courties G, Heidt T, Sebas M, Iwamoto Y, Jeon D, Truelove J, *et al.* In Vivo Silencing of the Transcription Factor IRF5 Reprograms the Macrophage Phenotype and Improves Infarct Healing. *Journal of the American College of Cardiology* 2014, **63**(15): 1556-1566.
215. Wynn TA. Fibrotic disease and the T(H)1/T(H)2 paradigm. *Nature reviews Immunology* 2004, **4**(8): 583-594.
216. Chiamonte MG, Donaldson DD, Cheever AW, Wynn TA. An IL-13 inhibitor blocks the development of hepatic fibrosis during a T-helper type 2-dominated inflammatory response. *The Journal of clinical investigation* 1999, **104**(6): 777-785.
217. Oriente A, Fedarko NS, Pacocha SE, Huang SK, Lichtenstein LM, Essayan DM. Interleukin-13 modulates collagen homeostasis in human skin and keloid fibroblasts. *The Journal of pharmacology and experimental therapeutics* 2000, **292**(3): 988-994.
218. Gong D, Shi W, Yi SJ, Chen H, Groffen J, Heisterkamp N. TGFbeta signaling plays a critical role in promoting alternative macrophage activation. *BMC immunology* 2012, **13**: 31.
219. Ashizawa N, Graf K, Do YS, Nunohiro T, Giachelli CM, Meehan WP, *et al.* Osteopontin is produced by rat cardiac fibroblasts and mediates A(II)-induced DNA synthesis and collagen gel contraction. *The Journal of clinical investigation* 1996, **98**(10): 2218-2227.
220. Nahrendorf M, Aikawa E, Figueiredo JL, Stangenberg L, van den Borne SW, Blankesteijn WM, *et al.* Transglutaminase activity in acute infarcts predicts healing outcome and left ventricular remodelling: implications for FXIII therapy and antithrombin use in myocardial infarction. *European heart journal* 2008, **29**(4): 445-454.
221. Suntharalingam G, Perry MR, Ward S, Brett SJ, Castello-Cortes A, Brunner MD, *et al.* Cytokine storm in a phase 1 trial of the anti-CD28 monoclonal antibody TGN1412. *The New England journal of medicine* 2006, **355**(10): 1018-1028.
222. Tabares P, Berr S, Romer PS, Chuvpilo S, Matskevich AA, Tyrsin D, *et al.* Human regulatory T cells are selectively activated by low-dose application of the CD28 superagonist TGN1412/TAB08. *European journal of immunology* 2014, **44**(4): 1225-1236.

8 Appendix

8.1 Abbreviations

A	ampere
ADP	adenosine diphosphate
α -SMA	alpha smooth muscle actin
APC	antigen presenting cell
APS	ammonium peroxydisulphate
ATP	adenosine triphosphate
BSA	bovine serum albumin
$^{\circ}\text{C}$	Degree Celsius
Ca^{2+}	calcium
CD	cluster of differentiation
DAMP	danger-associated molecular pattern
ddH ₂ O	double-desalted water
DTR	diphtheria toxin receptor
DTX	diphtheria toxin
ECL	enhanced chemiluminescence
ECM	extracellular matrix
EDTA	ethylenediaminetetraacetic acid
ELISA	enzyme-linked immunosorbance assay
et al.	et aliter
FCS	fetal calf (bovine) serum
Fig.	figure
FACS	fluorescence-activated cell sorting
FITC	fluorescein isothiocyanate
Foxp3	Forkhead-Box-Protein P3
FSC	forward scatter
FXIII	transglutaminase factor XIII
g	gram
h	hour(s)
HCl	hydrogen chloride
HRP	horseradish peroxidase
H ₂ O	water
Ig	immunoglobulin
IL	interleukin
IFN γ	interferon gamma
iNOS	induced NO synthase
IU	international units
kDa	kilo Dalton
KO	knock-out
Ly-6C	lymphocyte antigen 6C
Ly-6G	lymphocyte antigen 6G
M	molar
MI	myocardial infarction
MFI	mean fluorescence intensity
mg	milligram
min	minute(s)

ml	milliliter
mLN	mediastinal lymph nodes
μ	micro
Mφ	macrophage
NaCl	sodium chloride
NaOH	sodium hydroxide
OPN	osteopontin
PAMP	pathogen-associated molecular pattern
pg	picogramm
PBS	phosphate buffered saline
PerCP	Peridinin chlorophyl
PCR	polymerase chain reaction
PE	phycoerythrin
PRR	pathogen recognition receptor
rpm	rounds per minute
RT	room temperature
SE	standard error
SDS	sodium dodecyl sulfate
SDS-PAGE	sodium dodecyl sulfate polyacrylamide gel electrophoresis
SSC	sideward scatter
TGFβ	transforming growth factor beta
TNFα	tumor necrosis factor-α
T _{reg} cell	regulatory T cell
TRIS	trishydroxymethylaminomethane
V	Volt
vWF	von Willebrand factor
wt	wildtype

8.2 Acknowledgements

The work presented here was conducted at the Center for Experimental Molecular Medicine, the University Hospital Wuerzburg, the Comprehensive Heart Failure Center and the Institute for Virology and Immunobiology Wuerzburg. During this period, many people supported me and without this help this doctoral thesis would not have been possible. I want to express my gratitude to the following people:

- My supervisor, Prof. Dr. Stefan Frantz, for giving me the chance to work in his laboratory and his support. Especially, I want to thank him for giving me the freedom to realize own ideas and for providing me the opportunity to visit impressive international conferences.
- PD Dr. Ulrich Hofmann for his constant support, helpful discussions and his excellent ideas that significantly helped to advance my doctoral research studies.
- PD Dr. Thomas Kerkau for carefully reviewing my thesis, for his permanent support, fruitful discussions, and the pleasant time in his laboratory.
- PD Dr. Ingolf Berberich for supervising my doctoral studies, for reviewing my thesis and for helpful discussions.
- PD Dr. Niklas Beyersdorf for reviewing my thesis and precious advice concerning technical and immunological issues.
- Prof. Dr. Thomas Hünig for helpful advice and the outstanding education in the seminars at the Institute for Virology and Immunobiology as well as in the Graduate College 520 *Immunomodulation*.
- The technical assistants Charlotte Dienesch, Helga Wagner, Sandra Umbenhauer, Gabriele Riehl, Andrea Leupold, Lisa Bauer, Barbara Bayer, Susanne Knorr, Sandra Werner, and Nelli Wolf for their everyday support.
- All past and present members of the Frantz and Kerkau group that have not been mentioned by name.
- Finally, but most importantly, I want to thank my family: My parents Hannelore and Josef, my sister Stefanie, and my girlfriend Franziska who have always encouraged me in my professional and private life.

8.3 Publications

Weirather J, Hofmann UD, Beyersdorf N, Ramos GC, Vogel B, Frey A, Ertl G, Kerkau T, Frantz S. Foxp3⁺ CD4⁺ T cells improve healing after myocardial infarction by modulating monocyte/macrophage differentiation. *Circulation research* 2014, **115**(1): 55-67.

Weirather J, Frantz S. *Altara & Blankesteyn - Inflammation in Heart Failure*, Chapter: Role of the innate immune system in ischemic heart failure. Philadelphia: Elsevier, 2014 (in press).

Li X, Bauer W, Israel I, Kreissl MC, **Weirather J**, Richter D, Bauer E, Herold V, Jakob P, Buck A, Frantz S, Samnick S. Targeting P-selectin by Gallium-68-labeled fucoidan positron emission tomography for noninvasive characterization of vulnerable plaques: correlation with in vivo 17.6T MRI. *Arteriosclerosis, thrombosis, and vascular biology* 2014 (in press).

Hofmann U, Knorr S, Vogel B, **Weirather J**, Frey A, Ertl G, Frantz S. Interleukin-13 deficiency aggravates healing and remodeling in male mice after experimental myocardial infarction. *Circulation Heart failure* 2014 (in press).

Mathes D, **Weirather J**, Arias P, Vogel B, Pachel C, Sparwasser T, Ertl G, Kerkau T, Beyersdorf N, Frantz S, Hofmann U. CD4⁺ Foxp3⁺ regulatory T cells promote murine myocardial reperfusion injury by MHC class II-restricted T cell receptor signaling. (Manuscript in revision).

Li X, Bauer W, Kreissl MC, **Weirather J**, Bauer E, Israel I, Richter D, Riehl G, Buck A, Samnick S. Specific somatostatin receptor II expression in arterial plaque: (68)Ga-DOTATATE autoradiographic, immunohistochemical and flow cytometric studies in apoE-deficient mice. *Atherosclerosis* 2013, **230**(1): 33-39.

Hofmann U, Beyersdorf N, **Weirather J**, Podolskaya A, Bauersachs J, Ertl G, Kerkau T, Frantz S. Activation of CD4⁺ T lymphocytes improves wound healing and survival after experimental myocardial infarction in mice. *Circulation* 2012, **125**(13): 1652-1663.

8.4 Oral presentations

Foxp3⁺CD4⁺ regulatory T cells improve healing after experimental myocardial infarction in mice. Third retreat of the Comprehensive Heart Failure Center, December 2013, Pommersfelden (Germany).

Die Rolle von T-Zellen in der kardialen Ischämie. First retreat of the Comprehensive Heart Failure Center, December 2011, Bad Brückenau (Germany).

CD4⁺ T-Lymphocytes Have an Impact on Wound Healing after Experimental Myocardial Infarction in Mice. 6th Network Meeting of the DFG graduate schools GK520, GK592 and GK794, June 2011, Neresheim (Germany).

8.5 Poster presentations

Foxp3⁺ Regulatory T cells Modulate Wound Healing After Experimental Myocardial Infarction in Mice by Modulating Monocyte/ Macrophage Differentiation. Keystone Symposium: Molecular Cell Biology of Macrophages in Human Diseases, February 2014, Santa Fe (USA).

Bedeutung von Foxp3⁺CD4⁺ regulatorischer T-Zellen für die kardiale Wundheilung nach Myokardinfarkt. Second retreat of the Comprehensive Heart Failure Center, December 2012, Bad Staffelstein (Germany).

CD4⁺CD25⁺FoxP3⁺ T-Lymphocytes Modulate Wound Healing and Influence Survival after Experimental Myocardial Infarction in Mice. 7th Network Meeting of the DFG graduate schools GK520, GK592 and GK794, July 2012, Schöntal (Germany).

Immunomodulation by CD4⁺CD25⁺Foxp3⁺ regulatory T-lymphocytes crucially influences wound healing and survival after experimental myocardial infarction in mice. World Immune Regulation Meeting VI, March 2012, Davos (Switzerland).

CD4⁺CD25⁺Foxp3⁺ regulatory T-lymphocytes get activated and modulate wound healing after experimental myocardial infarction in mice. World Immune Regulation Meeting V, March 2011, Davos (Switzerland).

Role of CD4⁺ T cells in wound healing after experimental myocardial infarction in mice. 5th Network Meeting of the DFG graduate schools GK520, GK592 and GK794, November 2010, Schöntal (Germany).

8.6 Curriculum Vitae

Personal information

- Date of birth June 29, 1985
- Place of birth Memmingen, Germany

Education

- Sept 2004 – Nov 2009 Diploma in Biology
Diploma thesis at the Institute for Virology and Immunobiology: “Establishment of a minigenome replication system for measles virus”
Supervision: Prof. Dr. Jürgen Schneider-Schaulies
University of Wuerzburg, Germany
- Sept 1995 – June 2004 Abitur
Bernhard-Strigel Gymnasium in Memmingen,
Germany

Würzburg
Date Signature

8.7 Affidavit

I hereby confirm that my thesis entitled “Role of CD4⁺ T lymphocytes in cardiac wound healing and remodeling after experimental myocardial infarction in mice” is the result of my own work. I did not receive any help or support from commercial consultants. All sources and/ or materials applied are listed and specified in the thesis.

Furthermore, I confirm that this thesis has not yet been submitted as part of another examination process neither in identical nor in similar form.

Würzburg
Date Signature

Eidesstattliche Erklärung

Hiermit erkläre ich an Eides statt, die Dissertation „Die Bedeutung von CD4⁺ T-Lymphozyten für die kardiale Wundheilung und Remodeling nach experimentellem Herzinfarkt im Mausmodell“ eigenständig, d.h. insbesondere selbständig und ohne Hilfe eines kommerziellen Promotionsberaters, angefertigt und keine anderen als die von mir angegebenen Quellen und Hilfsmittel verwendet zu haben.

Ich erkläre außerdem, dass die Dissertation weder in gleicher noch in ähnlicher Form bereits in einem anderen Prüfungsverfahren vorgelegen hat.

Würzburg
Datum Unterschrift